# Ice Melt, Sea Level Rise and Superstorms: Evidence from Paleoclimate Data, Climate Modeling, and Modern Observations that 2°C Global Warming is Highly Dangerous

James Hansen[1], Makiko Sato[1], Paul Hearty[2], Reto Ruedy[3,4], Maxwell Kelley[3,4], Valerie Masson-Delmotte[5], Gary Russell[4], George Tselioudis[4], Junji Cao[6], Eric Rignot[7,8], Isabella Velicogna[8,7], Evgeniya Kandiano[9], Karina von Schuckmann[10], Pushker Kharecha[1,4], Allegra N. Legrande[4], Michael Bauer[11,4], Kwak-Wai Lo[3,4]

**Abstract.** There is evidence of ice melt, sea level rise to +5-9 meters, and extreme storms in the prior interglacial period that was less than 1°C warmer than today. Human-made climate forcing is stronger and more rapid than paleo forcings, but much can be learned by combining insights from paleoclimate, climate modeling, and on-going observations. We argue that ice sheets in contact with the ocean are vulnerable to non-linear disintegration in response to ocean warming, and we posit that ice sheet mass loss can be approximated by a doubling time up to sea level rise of at least several meters. Doubling times of 10, 20 or 40 years yield sea level rise of several meters in 50, 100 or 200 years. Paleoclimate data reveal that subsurface ocean warming causes ice shelf melt and ice sheet discharge. Our climate model exposes amplifying feedbacks in the Southern Ocean that slow Antarctic bottom water formation and increase ocean temperature near ice shelf grounding lines, while cooling the surface ocean and increasing sea ice cover and water column stability. Ocean surface cooling, in the North Atlantic as well as the Southern Ocean, increases tropospheric horizontal temperature gradients, eddy kinetic energy and baroclinicity, which drive more powerful storms. We focus attention on the Southern Ocean's role in affecting atmospheric $CO_2$ amount, which in turn is a tight control knob on global climate. The millennial (500-2000 year) time scale of deep ocean ventilation affects the time scale for natural $CO_2$ change, thus the time scale for paleo global climate, ice sheet and sea level changes. This millennial carbon cycle time scale should not be misinterpreted as the ice sheet time scale for response to a rapid human-made climate forcing. Recent ice sheet melt rates have a doubling time near the lower end of the 10-40 year range. We conclude that 2°C global warming above the preindustrial level, which would spur more ice shelf melt, is highly dangerous. Earth's energy imbalance, which must be eliminated to stabilize climate, provides a crucial metric.

## 1 Introduction

Humanity is rapidly extracting and burning fossil fuels without full understanding of the consequences. Current assessments place emphasis on practical effects such as increasing extremes of heat waves, droughts, heavy rainfall, floods, and encroaching seas (IPCC, 2014; USNCA, 2014). These assessments and our recent study (Hansen et al., 2013a) conclude that there is an urgency to slow carbon dioxide ($CO_2$) emissions, because the longevity of the carbon

[1] Climate Science, Awareness and Solutions, Columbia University Earth Institute, New York, NY 10115, USA
[2] Department of Environmental Studies, University of North Carolina at Wilmington, North Carolina 28403, USA
[3] Trinnovium LLC, New York, NY 10025, USA
[4] NASA Goddard Institute for Space Studies, 2880 Broadway, New York, NY 10025, USA
[5] Institut Pierre Simon Laplace, Laboratoire des Sciences du Climat et de l'Environnement (CEA-CNRS-UVSQ), Gif-sur-Yvette, France
[6] Key Lab of Aerosol Chemistry & Physics, Institute of Earth Environment, Chinese Academy of Sciences, Xi'an 710075, China
[7] Jet Propulsion Laboratory, California Institute of Technology, Pasadena, California, 91109, USA
[8] Department of Earth System Science, University of California, Irvine, California, 92697, USA
[9] GEOMAR, Helmholtz Centre for Ocean Research, Wischhofstrasse 1-3, Kiel 24148, Germany
[10] Mediterranean Institut of Oceanography, University of Toulon, La Garde, France
[11] Department of Applied Physics and Applied Mathematics, Columbia University, New York, NY, 10027, USA

in the climate system (Archer, 2005) and persistence of the induced warming (Solomon et al., 2010) may lock in unavoidable highly undesirable consequences.

Despite these warnings, global $CO_2$ emissions continue to increase as fossil fuels remain the primary energy source. The argument is made that it is economically and morally responsible to continue fossil fuel use for the sake of raising living standards, with expectation that humanity can adapt to climate change and find ways to minimize effects via advanced technologies.

We suggest that this viewpoint fails to appreciate the nature of the threat posed by ice sheet instability and sea level rise. If the ocean continues to accumulate heat and increase melting of marine-terminating ice shelves of Antarctica and Greenland, a point will be reached at which it is impossible to avoid large scale ice sheet disintegration with sea level rise of at least several meters. The economic and social cost of losing functionality of all coastal cities is practically incalculable. We suggest that a strategic approach relying on adaptation to such consequences is unacceptable to most of humanity, so it is important to understand this threat as soon as possible.

We examine events late in the last interglacial period warmer than today, called Marine Isotope Stage (MIS) 5e in studies of ocean sediment cores, Eemian in European climate studies, and sometimes Sangamonian in American literature (see Sec. 5 for timescale diagram of Marine Isotope Stages). Accurately known changes of Earth's astronomical configuration altered the seasonal and geographical distribution of incoming radiation during the Eemian. Resulting global warming was due to feedbacks that amplified the orbital forcing. While the Eemian is not an analog of future warming, it is useful for investigating climate feedbacks, the response of polar ice sheets to polar warming, and the interplay between ocean circulation and ice sheet melt.

Our study relies on a large body of research by the scientific community. After introducing evidence concerning late Eemian climate change, we analyze relevant climate processes in three stages. First we carry our IPCC-like climate simulations, but with growing freshwater sources in the North Atlantic and Southern Oceans. Second we use paleoclimate data to extract information on key processes identified by the modeling. Third we use modern data to show that these processes are already spurring climate change today.

## 2 Evidence concerning Eemian climate

We first discuss geologic evidence of late-Eemian sea level rise and storms. We then discuss ocean core data that help define a rapid cooling event in the North Atlantic that marks the initial descent from interglacial conditions toward global ice age conditions. This rapid end-Eemian cooling occurs at ~118 ky b2k in ocean cores with uncertainty ~2 ky, and is identified by Chapman and Shackleton (1999) as cold event C26.

C26 is the cold phase of Dansgaard-Oeschger climate oscillation D-O 26 in the NGRIP (North Greenland Ice Core Project) ice core (NGRIP, 2004). C26 begins with a sharp cooling at 119.14 ky b2k on the GICC05modelext time scale (Rasmussen et al., 2014). The GICC05 time scale is based on annual layer counting in Greenland ice cores for the last 60 ky and on an ice flow-model extension for earlier times. An alternative time scale is provided by Antarctic ice core chronology AICC2012 (Bazin et al., 2013; Veres et al., 2013) on which Greenland ice core records have been synchronized via global markers such as oscillations of atmospheric $CH_4$ amount. C26 on Greenland is at 116.72 ky b2k on the AICC2012 time scale. Fig. S1 shows the difference between GICC05 and AICC2012 times scales versus time.

This age uncertainty for C26 is consistent with the ice core $2\sigma$ error estimate of 3.2 ky at Eemian time (Bazin et al., 2013). Despite this absolute age uncertainty, we can use Greenland data synchronized to the AICC2012 time scale to determine the relative timing of Greenland and Antarctic climate changes (Section 5) to an accuracy of a few decades (Bazin et al., 2013).

## 2.1 Eemian sea level

Eemian sea level is of special interest because Eemian climate was at most ~2ºC warmer than pre-industrial climate, thus at most ~1ºC warmer than today. Indeed, based on multiple data and model sources Masson-Delmotte et al. (2013) suggest that peak Eemian temperature was only a few tenths of a degree warmer than today. The Eemian period thus provides an indication of sea level change that can be expected if global temperature reaches and maintains a level moderately higher than today. Eemian sea level reached heights several meters above today's level (Chen et al., 1991; Neumann and Hearty, 1996; Hearty et al., 2007; Kopp et al., 2009; Dutton and Lambeck, 2012; O'Leary et al., 2013). Although climate forcings were weak and changed slowly during the Eemian, there were probably instances in the Eemian with sea level change of the order of 1 m/century (Rohling et al., 2008; W. Thompson et al., 2011; Blanchon et al., 2009).

Hearty et al. (2007) used shoreline stratigraphy, field information, and geochronological data from 15 sites around the world to construct a composite curve of Eemian sea level change. Their reconstruction has sea level rising in the early Eemian to +2-3 m ("+" indicates above today's sea level). Mid-Eemian sea level may have fallen a few meters to a level near today's sea level. Sea level rose rapidly in the late Eemian when it cut multiple bioerosional notches in older limestone in the Bahamas and elsewhere at +6-9 m. These brief upward shifts of sea level were interpreted as evidence of rapid ice melt events.

This sea level behavior may be surprising at first glance, and it is easy to question specific details because of the difficulties in sea level reconstructions, including the effect of regional glacio-isostatic adjustment (GIA) of Earth's crust as ice sheets grow and decay. Indeed, rapid late-Eemian sea level rise is unexpected, because seasonal insolation anomalies favored growth of Northern Hemisphere ice at that time. However, the basic conclusion that arises from global studies is a sea level elevation difference of 3-5 m between late and early Eemian. We will show in the remainder of this paper that there is now substantial supporting evidence for these sea level change features and a rational interpretation.

Assessed chronology of sea level change depends on ages estimated for fossil corals. The analytic uncertainty of uranium radioactive decay (U-series) ages is about 1 ky (Edwards et al., 2003; Scholz and Mangini, 2007), but often undetectable diagenetic effects can increase the error (Bard et al., 1992; Thompson and Goldstein, 2005). The growth position of corals is a good, though not comprehensive, indicator of sea level, because sea level had to be higher than the reef at the time of coral growth. However, some corals grow at a range of depths, which adds uncertainty. Furthermore, if sea level rises too fast, corals tend to "give up" or founder, only recording minimum sea level (Neumann and MacIntyre, 1985), and if sea level falls corals are exposed, die, and thus stop recording sea level. Mobile carbonate sediments that mantle limestone platforms such as Bermuda and the Bahamas record rapid sea level change effectively, because the sediments respond and cement quickly, thus preserving sea level change evidence.

Hearty and Kindler (1993), White et al. (1998) and Wilson et al. (1998) describe evidence in fossil Bahamian reefs of a mid-Eemian regressive-transgressive cycle (sea level fall and rise). They estimated a sea level fall from +4 m to approximately today's level, and then a rise to at least +6 m. U-series dating defined the period of fall and rise as a maximum of 1500 years covering ~ 125 to 124 ky b2k, and the high stand lasting until ~119 ky b2k. Such rapid sea level change requires ice sheet growth and melt, regional lithospheric adjustment, or both.

Blanchon et al. (2009) used a sequence of coral reef crests from northeast Yucatan peninsula, Mexico, to investigate sea level change with a higher temporal precision than possible with U-series dating alone. They used coral reef "back-stepping", i.e., the fact that the location of coral reef building moves shoreward as sea level rises, to infer sea level change. They found that in the latter half of the Eemian there was a point at which sea level jumped by 2-3 m within an

"ecological" period, i.e., within several decades. From U-series dating they estimated that this period of rapid sea level rise occurred at about 121 ky b2k. W. Thompson et al. (2011) reexamined Eemian coral reef data from the Bahamas with a method that corrected uranium-thorium ages for diagenic disturbances. They confirmed a mid-Eemian sea level minimum, putting sea level at +4 m at 123 ky b2k, at +6 m at 119 ky b2k, and at 0 m at some time in between, again noting that coral reefs only record minimum sea level.

Despite general consistency among these studies, considerable uncertainty remains about details of Eemian sea level change. Sources of uncertainty include post-depositional effects of GIA and local tectonics. Global models of GIA of Earth's crust to loading and unloading of ice sheets are used increasingly to improve assessments of past sea level change. Although GIA models contain uncertain parameters, they provide a useful indication of possible displacement of geological sea level indicators. O'Leary et al. (2013) provide a new perspective on Eemian sea level change using over 100 well-dated U-series coral reefs at 28 sites along the 1400 km west coast of Australia and incorporating GIA corrections on regional sea level. In agreement with Hearty et al. (2007), their analyses suggest that sea level was relatively stable at 3-4 m in most of the Eemian, followed by a rapid (<1000 yr) late-Eemian sea level rise to about +9 m. U-series dating of the corals has the sea level rise begin at 119 ky b2k and peak sea level at 118.1 ± 1.4 ky b2k. This dating of peak sea level is consistent with the estimate of Hearty and Neumann (2001) of ~118 ky b2k as the time of rapid climate changes and extreme storminess.

End-Eemian sea level rise would seem to be a paradox, because orbital forcing then favored growth of Northern Hemisphere ice sheets. We will find evidence, however, that the sea level rise and increased storminess are consistent, and likely related to events in the Southern Ocean.

### 2.2 Evidence of end-Eemian storms in Bahamas and Bermuda

Late-Eemian sea level rise was followed by rapid sea level fall at the end of MIS 5e (Neumann and Hearty, 1996; Stirling et al., 1998; McCulloch and Esat, 2000; Lambeck and Chappell, 2001; Lea et al., 2002). Geologic data suggest that this sea level oscillation was accompanied by increased temperature gradients and storminess in the North Atlantic region. Here we summarize evidence for end-Eemian storminess, based mainly on geological studies of Neumann and Hearty (1996), Hearty (1997), Hearty et al. (1998), Hearty and Neumann (2001) and Hearty et al. (2007) in Bermuda and the Bahamas. In following sections we examine data from ocean sediment cores relevant to climate events in this period and then make global climate simulations, which help us suggest causal connections among end-Eemian events.

The Bahama Banks are low-lying carbonate platforms that are exposed during glacials and largely flooded during interglacial high stands. From a tectonic perspective, the platforms are relatively stable, but may have experienced minor GIA effects. When flooded during MIS 5e sea level rise, enormous volumes of aragonitic oolitic grains were generated across the shallow high energy banks, shoals, ridges, and dunes, where storm deposits indurated rapidly upon subaerial exposure, preserving rock evidence of brief, high-energy events. The preserved stratigraphic, sedimentary and geomorphic features attest to the energy of the late-Eemian Atlantic Ocean and point to a turbulent end-Eemian transition.

In the Bahama Islands, extensive oolitic sand ridges with a distinctive landward-pointing V-shape are common, each standing in relief across several kilometers of low area (Hearty et al., 1998). Termed ''chevron ridges'' from their characteristic V-shape, these beach ridges are found on broad, low lying platforms or ramps throughout the Atlantic-facing, deep-water margins of the Bahamas. Hearty et al. (1998) examined 35 areas with chevron ridges across the Bahamas, which all point in a southwest direction (S65ºW) with no apparent relation to the variable configuration of the coastline.

**Fig. 1.** Two boulders (#1 and #2 of Hearty, 1997) on coastal ridge of North Eleuthera Island, Bahamas. Scale: person in both photos = 1.6 m. Estimated weight of largest boulder (#1, on left) is ~ 2300 tons.

The lightly indurated ooid sand ridges are several kilometers long and appear to have originated from the action of long-period waves from a northeasterly Atlantic source. The chevron ridges contain bands of beach fenestrae, formed by air bubbles trapped in fine ooid sand inundated by water and quickly indurated. The internal sedimentary structures including the beach fenestrae and scour structures (Tormey, 2015) show that the chevrons were rapidly emplaced by water rather than wind (Hearty et al., 1998). These landforms were deposited near the end of a sea level high stand, when sea level was just beginning to fall, otherwise they would have been reworked subsequently by stable or rising seas. Some chevrons contain multiple smaller ridges "nested" in a seaward direction (Hearty et al., 1998), providing further evidence that sea level was falling fast enough to strand and preserve older chevrons as distinct landforms.

Fine-grained carbonate ooids cement rapidly, sometimes within decades to a century, if left immobile (Taft et al., 1968; Curran et al., 2008). Additional evidence of the rapid emplacement of the sand ridges is inferred from burial of large trees and fronds in living positions (Neumann and Hearty, 1996; Hearty and Olson, 2011). Fenestrae are abundant primarily in the youngest 5e beds throughout the eastern margin of the Bahamas.

Older ridges adjacent to the chevron ridges have wave runup deposits that reach heights nearly 40 m above present sea level, far above the reach of a quiescent 5e sea surface. Such elevated beach fenestrae are considered to result from runup of very large waves (Wanless and Dravis, 1989). These stratigraphically youngest deposits on the shore-parallel ridges are 1-5 m thick fenestrae-filled seaward-sloping tabular beds of stage 5e age that mantle older MIS 5e dune deposits (Neumann and Moore, 1975; Chen at al., 1991; Neumann and Hearty, 1996; Tormey, 2015). Runup beds reach more than a kilometer from the present coast, mantling the eastern flanks of stage 5e ridges (Hearty et al., 1998). Bain and Kindler (1994) suggested the fenestrae could be rain-generated, but the fenestrae at high elevations are widespread and exclusive to the late 5e deposits. They are not commonly found in older dune ridges (Hearty et al., 1998).

Enormous boulders tossed onto an older Pleistocene landscape (Hearty, 1997; Hearty et al., 1998; Hearty and Neumann, 2001) provide a metric of powerful waves at the end of stage 5e. Giant displaced boulders (Fig. 1) were deposited in north Eleuthera, Bahamas near chevron ridges and runup deposits (Hearty, 1997). The boulders are composed of recrystallized oolitic-peloidal limestone of MIS 9 or 11 age (300-400 ky; Kindler and Hearty, 1996; Hearty, 1998). The boulders rest on oolitic sediments and fossils typical of MIS 5e, and thus were deposited after most of the interglacial had passed. The maximum age of boulder emplacement is ~115-120 ky based on their stratigraphy and association with regressive stage 5e marine, eolian and fossil land snail (*Cerion*) deposits (Hearty, 1997; Hearty et al., 1998). Hearty (1997) reasoned that the

boulders were emplaced during the latest substage 5e highstand, while sea level remained high, because even larger waves would have been required at times of lower sea level during MIS substages 5c and 5a in order to lift the boulders over the cliffs.

The boulders must have been transported to their present position by waves, as two of the largest ones (Fig. 1) are located on the crest of the island's ridge, eliminating the possibility that they were moved downward by gravity (Hearty, 1998) or are the karstic remnants of some ancient landscape. A tsunami conceivably deposited the boulders, but the area is not near a tectonic plate boundary. The coincidence of a tsunami at the end-Eemian moment is improbable given the absence of evidence of tsunamis at other times in the Bahamas and the lack of evidence of tsunamis on the Atlantic Coastal Plain of the United States. The proximity of run-up deposits and nested chevron ridges across a broad front of Bahamian islands is clear evidence of a sustained series of high-energy wave events.

The remarkable size of the boulders in north Eleuthera becomes more comprehensible upon realization that numerous boulders larger than 10 $m^3$ have been thrown up on Eleuthera Island by storms during the Holocene (Hearty, 1997). The mass and volume of the Holocene boulders (the largest ~90 $m^3$, Table 4 of Hearty, 1997) are about 10× smaller than the MIS 5e boulders (Table 2 of Hearty, 1997). Hearty (1998) notes that the large 5e and Holocene boulders are all located at the apex of a narrowing horseshoe-shaped submerged embayment (Fig. 2 of Hearty, 1997). Long period ocean waves are funneled into this embayment, generating huge surge and splash even today as they impact the cliffs near the Glass Window Bridge.

Movement of these sediments, including chevrons, run-up deposits and boulders, required a potent sustained energy source. Anticipating our interpretation in terms of powerful storms driven by an unusually warm tropical ocean and strong zonal temperature gradients in the North Atlantic, we must ask whether there should not be evidence of comparable end-Eemian storms in Bermuda. Indeed, there are seaward sloping planar beds rising to about +20 m along several kilometers of the north coast of Bermuda (Land et al., 1967; Vacher and Rowe, 1997; Hearty et al., 1998). These beds, from the latest stage 5e, are filled with beach fenestrae in platy grains and thick air-filled laminations, in marked contrast to older stage 5 sedimentary structures that underlie them (Hearty et al., 1998). Meter-scale, subtidal cross beds comprise the seaward facies of the elevated beach beds, reflecting an interval of exceptional wave energy on the normally tranquil, shallow and broad north shore platform of Bermuda.

Given the geologic evidence of high seas and storminess from Bermuda and the Bahamas, Hearty and Neumann (2001) suggested "Steeper pressure, temperature, and moisture gradients adjacent to warm tropical waters could presumably spawn larger and more frequent cyclonic storms in the North Atlantic than those seen today." We now seek further evidence related to the question of whether powerful end-Eemian storms in the North Atlantic may have dispersed long-period, well-organized waves to the southwest.

### 2.3 End-Eemian evidence from North Atlantic sediment cores

Sediment cores from multiple locations provide information not only on ocean temperature and circulation changes (Fig. 2), but also changes on ice sheet destabilization inferred from ice rafted debris. Comparison of data from different sites is affected by inaccuracy in absolute dating and use of different age models. Dating of sediments is usually based on tuning to the time scale of Earth orbital variations (Martinson et al., 1987) or "wiggle-matching" to another record (Sirocko et al., 2005), which limits accuracy to several ky. Temporal resolution is limited by bioturbation of sediments; thus resolution varies with core location and climate (Keigwin and Jones, 1994). For example, high deposition rates during ice ages at the Bermuda Rise yield a resolution of a few decades, but low sedimentation rates during the Eemian yield a resolution of

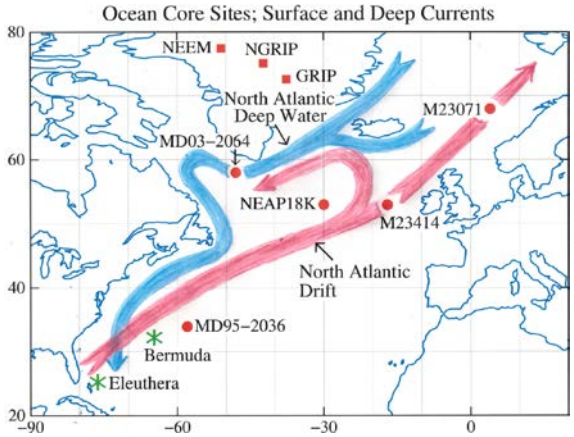


**Fig. 2.** Ocean and ice core sites and simplified sketch of upper ocean North Atlantic Current and North Atlantic Deep Water return flow. In interglacial periods the North Atlantic Current extends further north, allowing the Greenland-Iceland-Norwegian Sea to become an important source of deepwater formation.

a few centuries (Lehman et al., 2002). Lateral transport of sedimentary material prior to deposition complicates data interpretation and can introduce uncertainty, as argued specifically regarding data from the Bermuda Rise (Ohkouchi et al., 2002; Engelbrecht and Sachs, 2005).

Adkins et al. (1997) analyzed sediment core (MD95-2036, 34°N,58°W) from the Bermuda Rise using an age model based on Martinson et al. (1987) orbital tuning with the MIS stage 5/6 transition set at 131 ky b2k and the stage 5d/5e transition at 114 ky b2k. They found that oxygen isotope $\delta^{18}O$ of planktonic (near-surface dwelling) foraminifera and benthic (deep ocean) foraminifera both attain full interglacial values at ~128 ky b2k and remain nearly constant for ~10 ky (their Fig. 2). Adkins et al. (1997) infer that: "Late within isotope stage 5e (~118 ky b2k), there is a rapid shift in oceanic conditions in the western North Atlantic…" They find in the sediments at that point an abrupt increase of clays indicative of enhanced land-based glacier melt and an increase of high nutrient "southern source waters". The latter change implies a shutdown or diminution of NADW formation that allows Antarctic Bottom Water (AABW) to push into the deep North Atlantic Ocean (Duplessy et al., 1988; Govin et al., 2009). Adkins et al. (1997) continue: "The rapid deep and surface hydrographic changes found in this core mark the end of the peak interglacial and the beginning of climate deterioration towards the semi-glacial stage 5d. Before and immediately after this event, signaling the impeding end of stage 5e, deep-water chemistry is similar to modern NADW." This last sentence refers to a temporary rebound to near interglacial conditions. In Section 5 we use accurately synchronized Greenland and Antarctic ice cores, which also reveal this temporary end-Eemian climate rebound, to interpret the glacial inception and its relation to ice melt and late-Eemian sea level rise.

Ice rafted debris (IRD) found in ocean cores provides a useful climate diagnostic tool (Heinrich, 1988; Hemming, 2004). Massive ice rafting ("Heinrich") events are often associated with decreased NADW production and shutdown or slowdown of the Atlantic Meridional Overturning Circulation (AMOC) (Broecker, 2002; Barrieiro et al., 2008; Srokosz et al., 2012). However, ice rafting occurs on a continuum of scales, and significant IRD is found in the cold phase of all the 24 Dansgaard-Oeschger (D-O) climate oscillations first identified in Greenland ice cores (Dansgaard et al., 1993). D-O events exhibit rapid warming on Greenland of at least several degrees within a few decades or less, followed by cooling over a longer period. Chapman and Shackleton (1999) found IRD events in the NEAP18K core for all D-O events (C19-C24) within the core interval that they studied, and they also labeled two additional events (C25 and C26). C26 did not produce identifiable IRD at the NEAP18K site, but it was added to the series because of its strong surface cooling.

Lehman et al. (2002) quantify the C26 cooling event using the same Bermuda Rise core (MD95-2036) and age model as Adkins et al. (1997). Based on the alkenone paleo-temperature technique (Sachs and Lehman, 1999), Lehman et al. (2002) find a sharp sea surface temperature (SST) decrease of ~3ºC (their Fig. 1) at ~118 ky BP, coinciding with the end-Eemian shoulder of the benthic $\delta^{18}O$ plateau that defines stage 5e in the deep ocean. The SST partially recovered after several centuries, but C26 marked the start of a long slide into the depths of stage 5d cold, as ice sheets grew and sea level fell ~50 m in 10 ky (Lambeck and Chappell, 2001; Rohling et al., 2009). Lehman et al. (2002) wiggle-match the MD95-2036 and NEAP18K cores, finding a simple adjustment to the age model of Chapman and Shackleton (1999) that maximizes correlation of the benthic $\delta^{18}O$ records with the Adkins et al. (1997) $\delta^{18}O$ record. Specifically, they adjust the NEAP time scale by +4 ky before the MIS 5b $\delta^{18}O$ minimum and by +2 ky after it, which places C26 cooling at 118 ky b2k in both records. They give preference to the Adkins et al. (1997) age scale because it employs a $^{230}Th$-based time scale between 100 and 130 ky b2k.

We do not assert that the end-Eemian C-26 cooling was necessarily at 118 ky b2k, but we suggest that the strong rapid cooling observed in several sediment cores in this region of the subtropical and midlatitude North Atlantic Drift at about this time were all probably the same event. Such a large cooling lasting for centuries would not likely be confined to a small region. The dating models in several other studies place the date of the end-Eemian shoulder of the deep ocean $\delta^{18}O$ and an accompanying surface cooling event in the range 116-118 ky b2k.

Kandiano et al. (2004) and Bauch and Kandiano (2007) analyze core M23414 (53°N,17°W), west of Ireland, finding a major SST end-Eemian cooling that they identify as C26 and place at 117 ky b2k. The 1 ky change in the timing of this event compared with Lehman et al. (2002), is due to a minor change in the age model, specifically, Bauch and Kandiano say: "The original age model of MD95-2036 (Lehman et al., 2002) has been adjusted to our core M23414 by alignment of the 4 per mil level in the benthic $\delta^{18}O$ records (at 130 ka in M23414) and the prominent C24 event in both cores." Bauch and Erlenkeuser (2008) and H. Bauch et al. (2012) examine ocean cores along the North Atlantic Current including its continuation into the Nordic seas. They find that in the Greenland-Iceland-Norwegian (GIN) Sea, unlike middle latitudes, the Eemian was warmest near the end of the interglacial period. The age model employed by Bauch and Erlenkeuser (2008) has the Eemian about 2 ky younger than the Adkins et al. (1997) age model, Bauch and Erlenkeuser (2008) having the benthic $\delta^{18}O$ plateau at ~ 116-124 ky BP (their Fig. 6). Rapid cooling they illustrate there at ~ 116.6 ky BP for core M23071 on the Voring Plateau (67°N,3°E) likely corresponds to the C26 end-Eemian cooling event.

Identification of end-Eemian cooling in ocean cores is hampered by the fact that Eemian North Atlantic climate was more variable than in the Holocene (Fronval and Jansen, 1996). There were at least three cooling events within the Eemian, each with minor increases in IRD, which are labeled C27, C27a and C27b by Oppo et al. (2006); see their Fig. 2 for core site ODP-980 in the eastern North Atlantic (55°N,15°W) near Ireland. High (sub-centennial) resolution cores in the Eirik drift region (MD03-2664, 57°N,49°W) near the southern tip of Greenland reveal an event with rapid cooling accompanied by reduction in NADW production (Irvali et al., 2012; Galaasen et al., 2014), which they place at ~117 ky b2k. However, their age scale has the benthic $\delta^{18}O$ shoulder at ~115 ky b2k (Fig. S1, Galaasen et al., 2014), so that event may have been C27b with C26 being stronger cooling that occurred thereafter.

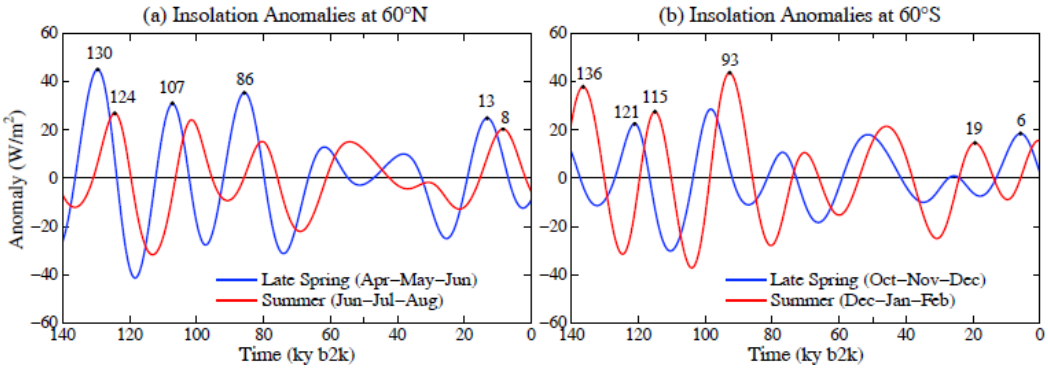


**Fig. 3.** Summer (Jun-Jul-Aug) and late spring (Apr-May-Jun) insolation anomalies at 60ºN and summer (Dec-Jan-Feb) and late spring (Oct-Nov-Dec) anomalies at 60ºS.

### 2.4 Eemian timing consistency with insolation anomalies

Glacial-interglacial climate cycles are affected by insolation change, as shown persuasively by Hays et al. (1976) and discussed in Sec. 5.1. Each "termination" (Broecker, 1984) of glacial conditions in the past several hundred thousand years coincided with a large positive warm-season insolation anomaly at the latitude of North American and Eurasian ice sheets (Raymo, 1997; Paillard, 2001). The explanation is that positive summer insolation anomalies (negative in winter) favor increased summer melting and reduced winter snowfall, thus shrinking ice sheets.

Termination timing is predicted better by high Northern Hemisphere late spring (April-May-June) insolation than by summer anomalies. For example, Raymo (1997) places Terminations I and II (preceding the Holocene and Eemian) midpoints at 13.5 and 128-131 ky b2k. Late spring insolation maxima are at 13.2 and 129.5 ky b2k (Fig. 4a). The AICC2012 ice core chronology (Bazin et al., 2013) places Termination II at 128.5 ky b2k, with 2σ uncertainty 3.2 ky. Late spring irradiance maximizes warm-season ice melt by producing the earliest feasible warm-season ice sheet darkening via snow melt and snow recrystallization (Hansen et al., 2007b).

Late Eemian sea level rise is seemingly a paradox, because glacial-interglacial sea level change is mainly a result of the growth and decay of Northern Hemisphere ice sheets. Northern warm-season insolation anomalies were negative and declining in the latter part of the Eemian (Fig. 3a), so Northern Hemisphere ice sheets should have been growing. We suggest that the explanation for a mid-Eemian sea level minimum is a substantial late-Eemian collapse of the Antarctic ice sheet facilitated by the positive warm-season insolation anomaly on Antarctica and the Southern Ocean during the late Eemian (Fig. 3b).

Persuasive presentation of this interpretation requires analysis of relevant climate mechanisms with a global model as well as a detailed discussion of paleoclimate data. We will show that these analyses in turn help to explain ongoing climate change today, with implications for continuing climate change this century.

## 3 Simulations of 1850-2300 climate change

We make simulations for 1850-2300 with radiative forcings that were used for IPCC (2007, 2013) studies. This allows comparison with simulations made for prior studies.

### 3.1 Climate model

Simulations are made with an improved version of a coarse-resolution model that allows long runs at low cost, GISS (Goddard Institute for Space Studies) model E-R. The atmosphere model is the documented modelE (Schmidt et al., 2006). The ocean is based on the Russell et al. (1995) model that conserves water and salt mass, has a free surface with divergent flow, uses a linear upstream scheme for advection, allows flow through 12 sub-resolution straits, has background diffusivity 0.3 $cm^2/s$, 4°×5° resolution and 13 layers that increase in thickness with depth.

However, the ocean model includes simple but significant changes, compared with the version documented in simulations by Miller et al. (2014). First, an error in the calculation of neutral surfaces in the Gent-McWilliams (GM, Gent and McWilliams, 1990) mesoscale eddy parameterization was corrected; the resulting increased slope of neutral surfaces provides proper leverage to the restratification process and correctly orients eddy stirring along those surfaces.

Second, the calculation of eddy diffusivity $K_{meso}$ for GM following Visbeck et al. (1997) was simplified to use a length scale independent of the density structure (J. Marshall, pers. comm.):

$$K_{meso} = C/[T_{eady} \times f(\text{latitude})] \quad (1)$$

where $C = (27.9\ km)^2$, Eady growth rate $1/T_{eady} = \{|S \times N|\}$, S is the neutral surface slope, N the Brunt-Vaisala frequency, { } signifies averaging over the upper D meters of ocean depth, D = min(max(depth, 400 m), 1000 m), and f(latitude) = max(0.1, sin(|latitude|)) to qualitatively mimic the larger values of the Rossby radius of deformation at low latitudes. These choices for $K_{meso}$, whose simplicity is congruent with the use of a depth-independent eddy diffusivity and the use of $1/T_{eady}$ as a metric of eddy energy, result in the zonal average diffusivity shown in Fig. 4.

Third, the so-called nonlocal terms in the KPP mixing parameterization (Large et al., 1994) were activated. All of these modifications tend to increase the ocean stratification, and in particular the Southern Ocean state is improved by the GM modifications. However, as is apparent in Fig. 4, drift in the Southern Ocean state leads to a modest reduction of the eddy diffusivities over the first 500 years of spin-up. Overall realism of the ocean circulation is improved, but significant model deficiencies remain, as we will describe.

The simulated Atlantic Meridional Overturning Circulation (AMOC) has maximum flux that varies within the range ~14-18 Sv in the model control run (Figs. 5 and 6). AMOC strength in recent observations is 17.5 ± 1.6 Sv (Baringer et al., 2013; Srokosz et al., 2012), based on eight years (2004-2011) data for an in situ mooring array (Rayner et al., 2011; Johns et al., 2011).

Ocean model control run initial conditions are climatology for temperature and salinity (Levitus and Boyer, 1994; Levitus et al., 1994); atmospheric composition is that of 1880 (Hansen et al., 2011). Overall model drift from control run initial conditions is moderate (see Fig. S2 for planetary energy imbalance and global temperature), but there is drift in the North Atlantic circulation. The AMOC circulation cell initially is confined to the upper 3 km at all latitudes (1st century in Figs. 5 and 6), but by the 5th century the cell reaches deeper at high latitudes.

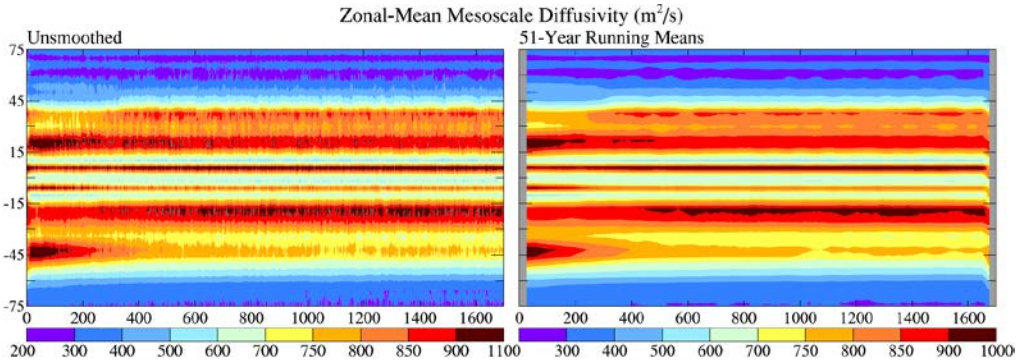


**Fig. 4.** Control run zonal-mean mesoscale diffusivity versus time in 1700-year control run.

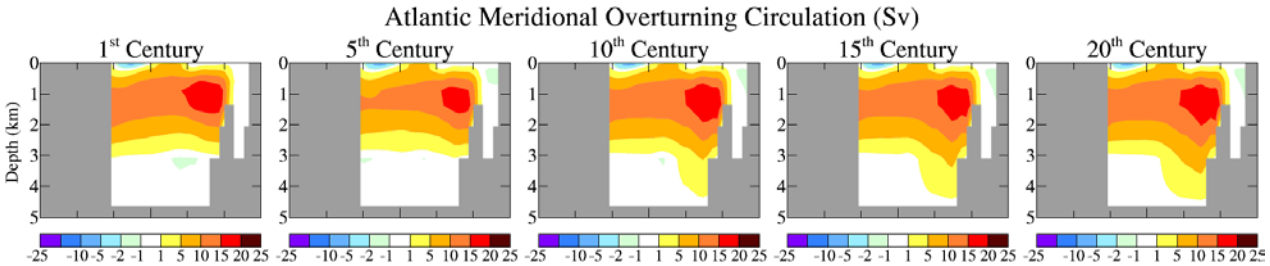


**Fig. 5.** Atlantic Ocean mass stream function for the control run in its 1st, 5th, 10th, 15th and 20th centuries.

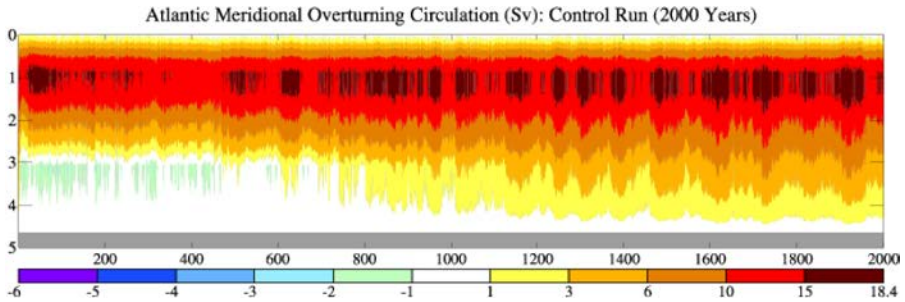


**Fig. 6.** Annual mean Atlantic Ocean mass stream function at 28N in the model control run.

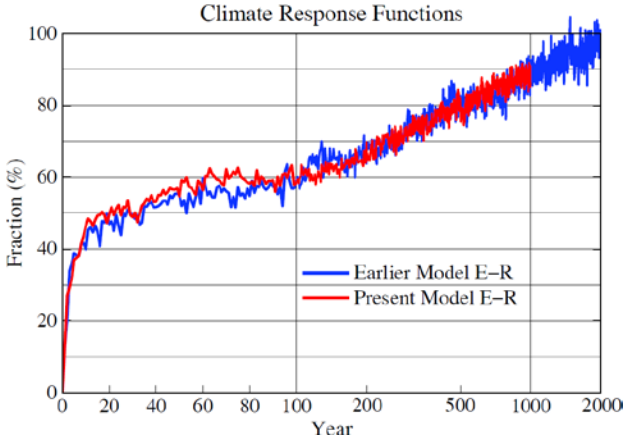


**Fig. 7.** Climate response function, R(t), i.e., the fraction of equilibriums surface temperature response for GISS model E-R based on a 2000 year control run (Hansen et al., 2007a). Forcing was instant $CO_2$ doubling with fixed ice sheets, vegetation distribution, and other long-lived GHGs.

Atmospheric and surface climate in the present model is similar to the documented modelE-R, but because of changes to the ocean model we provide several diagnostics in the Supplement. A notable flaw in the simulated surface climate is the unrealistic double precipitation maximum in the tropical Pacific (Fig. S3). This double ITCZ (intertropical convergence zone) occurs in many models and is related to the difficulty of producing realistic stratus clouds in the Eastern Tropical Pacific. Another flaw is unrealistic hemispheric sea ice, with too much sea ice in the Northern Hemisphere and too little in the Southern Hemisphere (Figs. S4 and S5). Excessive Northern Hemisphere sea ice might be caused by deficient poleward heat transport in the Atlantic Ocean (Fig. S6). However, the AMOC has realistic strength and Atlantic meridional heat transport is only slightly below observations at high latitudes (Fig. S6). Thus we suspect that the problem may lie in sea ice parameterizations or deficient dynamical transport of ice out of the Arctic. The deficient Southern Hemisphere sea ice, at least in part, is likely related to excessive poleward (southward) transport of heat by the simulated global ocean (Fig. S6), which is related to deficient northward transport of heat in the modeled Atlantic Ocean (Fig. S6).

A key characteristic of the model and the real world is the response time: how fast does the surface temperature adjust to a climate forcing, i.e., an imposed perturbation of the planet's energy balance? ModelE-R response is about 40% in five years (Fig. 7) and 60% in 100 years, with the remainder requiring many centuries. Hansen et al. (2011) concluded that most ocean models, including modelE-R, mix a surface temperature perturbation downward too efficiently and thus have a slower surface response than the real world. The basis for this conclusion was empirical analysis using climate response functions, with 50%, 75% and 90% response at year 100 for climate simulations (Hansen et al., 2011). Earth's measured energy imbalance in recent years and global temperature change in the past century revealed that the response function with 75% response in 100 years provided a much better fit with observations than the other choices. Durack et al. (2012) compared observations of how rapidly surface salinity changes are mixed into the deeper ocean with the large number of global models in the CMIP3 (Climate Model Intercomparison Project), reaching a similar conclusion, that the models mix too rapidly.

Our present ocean model has a faster response on 10-75 year time scales than the old model (Fig. 7), but the change is small. Although the climate response time in our model is comparable to that in many other ocean models (Hansen et al., 2011), we believe that it is likely slower than the response in the real world on time scales of a few decades and longer. A too slow surface response could result from excessive small scale mixing. We will suggest, after the studies below, that excessive mixing has other consequences, e.g., causing the effect of freshwater stratification on slowing AABW formation and growth of Antarctic sea ice cover to occur 1-2 decades later than in the real world. Similarly, excessive mixing may make the AMOC in the model less sensitive to freshwater forcing than the real world AMOC.

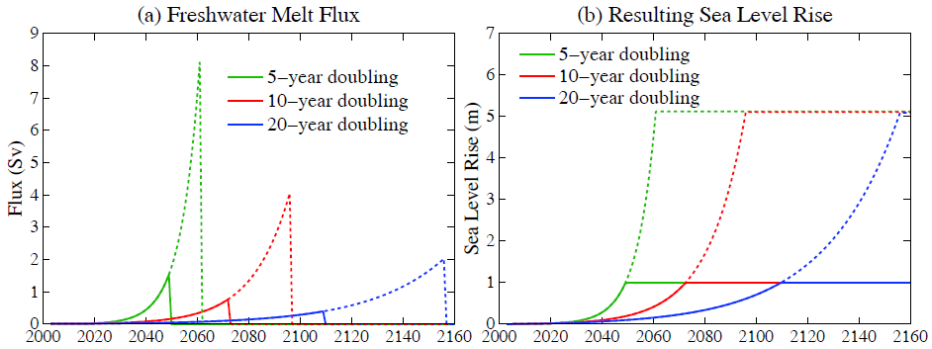


**Fig. 8. (a)** total fresh water flux added in North Atlantic and Southern Oceans, **(b)** resulting sea level rise. Solid lines for 1 m sea level rise, dotted for 5 m. One Sverdrup (Sv) is $10^6$ $m^3/s$, which is ~$3\times10^4$ Gt/year.

### 3.2 Experiment definition: exponentially increasing fresh water

Freshwater injection is specified as 360 Gt/yr (1 mm sea level) in 2003-2015, then growing with 5, 10 or 20 year doubling time (Fig. 8). Injection ends when input to global sea level reaches 1m or 5m. The sharp cut-off aids separation of immediate forcing effects and feedbacks.

We do not argue for this specific input function, but we suggest that rapid meltwater increase is likely if GHGs continue to grow rapidly. Greenland and Antarctica have outlet glaciers occupying canyons with bedrock below sea level well back into the ice sheet (Fretwell et al., 2013; Morlighem et al., 2014; Pollard et al., 2015). Feedbacks, including ice sheet darkening due to surface melt (Hansen et al., 2007b; Robinson et al., 2012; Tedesco et al., 2012; Box et al., 2012) and lowering and thus warming of the near-coastal ice sheet surface, make increasing ice melt likely. Paleoclimate data reveal instances of sea level rise of several meters in a century (Fairbanks, 1989; Deschamps et al., 2012). Those cases involved ice sheets at lower latitudes, but 21st century climate forcing is larger and increasing much more rapidly.

Radiative forcings are those of Hansen et al. (2007c), based on data through 2003 and IPCC scenario A1B for later GHGs. A1B is an intermediate IPCC scenario over the century, but on the high side early this century (Fig. 2, Hansen et al., 2007c). We add freshwater to the North Atlantic (ocean area within 52°N-72°N and 15°E-65°N) or Southern Ocean (ocean south of 60°S), or equally divided between the two oceans. Ice sheet discharge (icebergs plus meltwater) is mixed as fresh water with mean temperature -15°C into top three ocean layers (Fig. S7).

### 3.3 Simulated surface temperature and energy balance

We present surface temperature and planetary energy balance first, thus providing a global overview. Then we examine changes in ocean circulation and compare results with prior studies.

Temperature change in 2065, 2080 and 2096 for 10-year doubling time (Fig. 9) should be thought of as results when sea level rise reaches 0.6, 1.7 and 5 m, because the dates depend on initial freshwater flux. Actual current freshwater flux may be about a factor of four higher than assumed in these initial runs, as we will discuss, and thus effects may occur ~20 years earlier. A sea level rise of 5 m in a century is about the most extreme in the paleo record (Fairbanks, 1989; Deschamps et al., 2012), but the assumed 21st century climate forcing is also more rapidly growing than any known natural forcing.

Meltwater injected on the North Atlantic has larger initial impact, but Southern Hemisphere ice melt has a greater global effect for larger melt as the effectiveness of more meltwater in the North Atlantic begins to decline. The global effect is large long before sea level rise of 5 m is reached. Meltwater reduces global warming about half by the time sea level rise reaches 1.7 m. Cooling due to ice melt more than eliminates A1B warming in large areas of the globe.

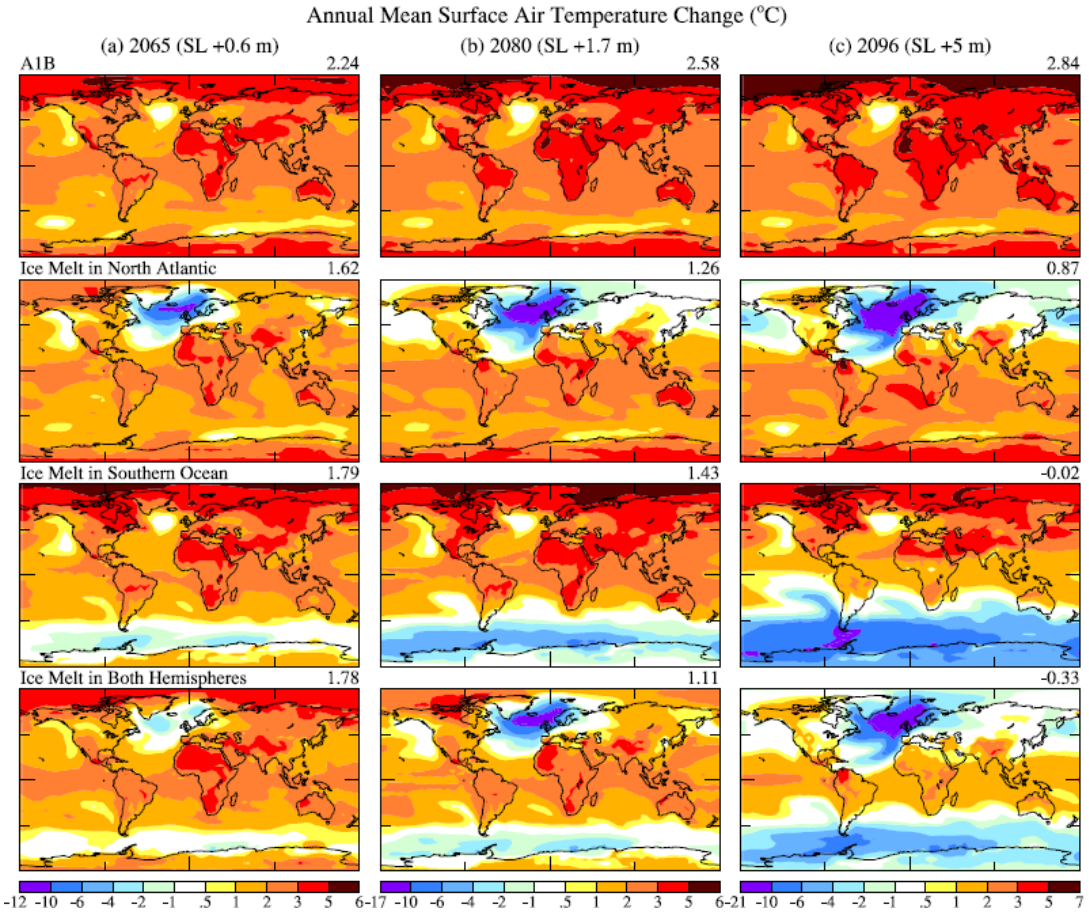


**Fig. 9.** Surface air temperature relative to 1880-1920 in **(a)** 2065, **(b)** 2080, and **(c)** 2096. Top row is IPCC scenario A1B. Ice melt with 10-year doubling is added in other scenarios.

The large cooling effect of ice melt does not decrease much as the ice melting rate varies between doubling times of 5, 10 or 20 years (Fig. 10a). In other words, the cumulative ice sheet melt, rather than the rate of ice melt, largely determines the climate impact for the range of melt rates covered by 5, 10 and 20 year doubling times. Thus if ice sheet loss occurs even to an extent of 1.7 m sea level rise (Fig. 10b), a large impact on climate and climate change is predicted.

Greater global cooling occurs for freshwater injected on the Southern Ocean, but the cooling lasts much longer for North Atlantic injection (Fig. 10a). That persistent cooling, mainly at Northern Hemisphere middle and high latitudes (Fig. S8), is a consequence of the sensitivity, hysteresis effects, and long recovery time of the AMOC (Stocker and Wright, 1991; Rahmstorf, 1995 and earlier studies referenced therein). AMOC changes are described below.

When freshwater injection on the Southern Ocean is halted, global temperature jumps back within two decades to the value it would have had without any freshwater addition (Fig. 10a). Quick recovery is consistent with the Southern Ocean-centric picture of the global overturning circulation (Fig. 4, Talley, 2013), as the Southern Meridional Overturning Circulation (SMOC), driven by AABW formation, responds to change of the vertical stability of the ocean column near Antarctica (see Sec. 4) and the ocean mixed layer and sea ice have limited thermal inertia.

Global cooling due to ice melt causes a large increase in Earth's energy imbalance (Fig. 10b), adding about +2 W/m$^2$, which is larger than the imbalance caused by increasing GHGs. Thus, although the cold fresh water from ice sheet disintegration provides a negative feedback on regional and global surface temperature, it increases the planet's energy imbalance, thus providing more energy for ice melt (Hansen, 2005). This added energy is pumped into the ocean.

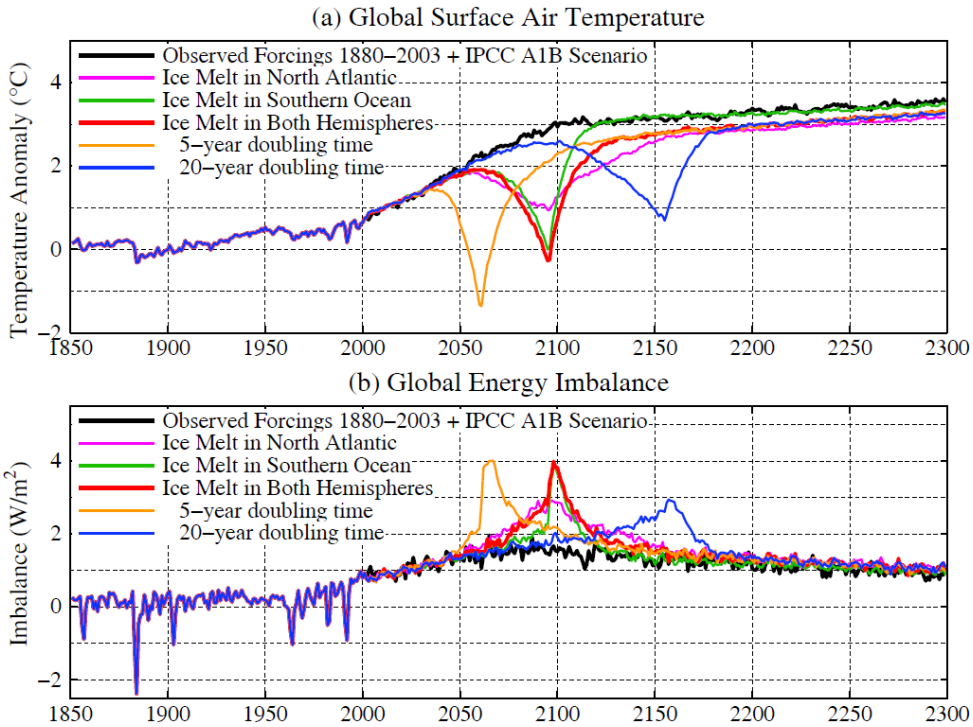


**Fig. 10.** (a) Surface air temperature relative to 1880-1920 for several scenarios. (b) Global energy imbalance for the same scenarios.

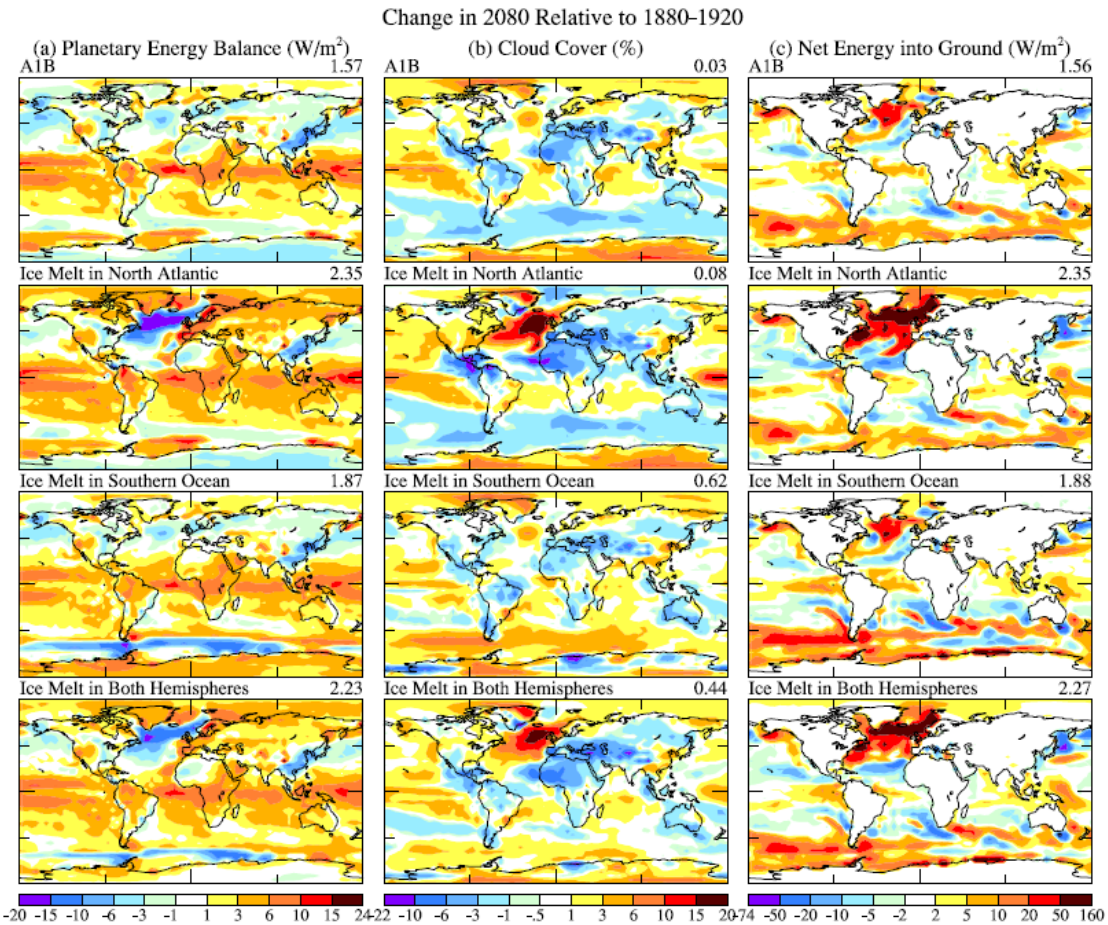


**Fig. 11.** Change in 2078-2082, relative to 1880-1920, of the annual mean **(a)** planetary energy balance, **(b)** cloud cover, and **(c)** net energy into the ground, for the same four scenarios as in Fig. 9.

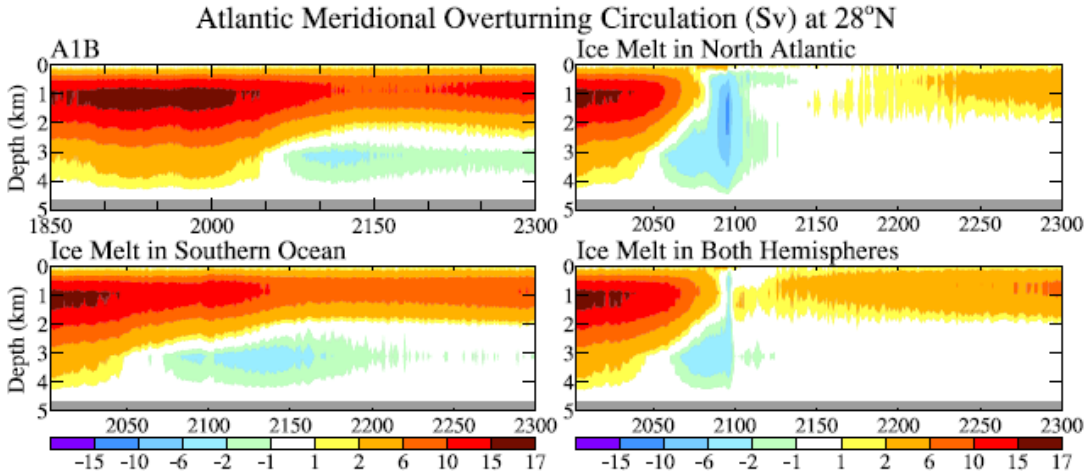


**Fig. 12.** Ensemble-mean AMOC at 28N versus time for the same four scenarios as in Fig. 9, with ice melt reaching 5 m at the end of the 21st century in the three experiments with ice melt.

Increased downward energy flux at the top of the atmosphere is not located in the regions cooled by ice melt. On the contrary, those regions suffer a large reduction of net incoming energy (Fig. 11a). The regional energy reduction is a consequence of increased cloud cover (Fig. 11b) in response to the colder ocean surface. However, the colder ocean surface reduces upward radiative, sensible and latent heat fluxes, thus causing a large (~50 W/m$^2$) increase of energy into the North Atlantic and a substantial but smaller flux into the Southern Ocean (Fig. 11c).

Below we conclude that the principal mechanism by which this ocean heat increases ice melt is via its effect on ice shelves. Discussion requires examination of how the freshwater injections alter the ocean circulation and internal ocean temperature.

### 3.4 Simulated AMOC

Broecker's articulation of likely effects of freshwater outbursts in the North Atlantic on ocean circulation and global climate (Broecker, 1990; Broecker et al., 1990) spurred quantitative studies with idealized ocean models (Stocker and Wright, 1991) and global atmosphere-ocean models (Manabe and Stouffer, 1995; Rahmstorf 1995, 1996). Scores of modeling studies have since been carried out, many reviewed by Barreiro et al. (2008), and observing systems are being developed to monitor modern changes in the AMOC (Carton and Hakkinen, 2011).

Our climate simulations in this section are 5-member ensembles of runs initiated at 25-year intervals at years 901-1001 of the control run. We chose this part of the control run because the planet is then in energy balance (Fig. S2), although by that time model drift had altered the slow deep ocean circulation. Some model drift away from initial climatological conditions is inevitable, as all models are imperfect, and we carry out the experiments with cognizance of model limitations. However, there is strong incentive to seek basic improvements in representation of physical processes to reduce drift in future versions of the model.

GHGs alone (scenario A1B) slow AMOC by the early 21st century (Fig. 12), but variability among individual runs (Fig. S9) would make definitive detection difficult at present. Freshwater injected onto the North Atlantic or in both hemispheres shuts down the AMOC (Fig. 12 right side). GHG amounts are fixed after 2100 and ice melt is zero, but after two centuries of stable climate forcing the AMOC has not recovered to its earlier state. This slow recovery was found in the earliest simulations by Manabe and Stouffer (1994) and Rahmstorf (1995, 1996).

Freshwater injection already has a large impact when ice melt is a fraction of 1 m of sea level. By the time sea level rise reaches 59 cm (2065 in the present scenarios), when fresh water flux is 0.48 Sv, the impact on AMOC is already large, consistent with the substantial surface cooling in the North Atlantic (Fig. 9).

### 3.5 Comparison with prior simulations

AMOC sensitivity to GHG forcing has been examined extensively based on IPCC studies. Schmittner et al. (2005) found that AMOC weakened 25±25% by the end of the 21st century in 28 simulations of 9 different models forced by the A1B emission scenario. Gregory et al. (2005) found 10-50% AMOC weakening in 11 models for $CO_2$ quadrupling (1%/year increase for 140 years), with largest decreases in models with strong AMOCs. Weaver et al. (2007) found a 15-31% AMOC weakening for $CO_2$ quadrupling in a single model for 17 climate states differing in initial GHG amount. AMOC in our model weakens 30% between 1990-2000 and 2090-2100, the period used by Schmittner et al (2005), for A1B forcing (Fig. S9). Thus our model is more sensitive than the average, but within the range of other models, a conclusion that continues to be valid in comparison with 10 CMIP5 models (Cheng et al., 2013).

AMOC sensitivity to freshwater forcing has not been compared as systematically among models. Several studies find little impact of Greenland melt on AMOC (Huybrechts et al., 2002; Jungclaus et al., 2006; Vizcaino et al., 2008) while others find substantial North Atlantic cooling (Fichefet et al., 2003; Swingedouw et al., 2007; Hu et al., 2009, 2011). Studies with little impact calculated or assumed small ice sheet melt rates, e.g., Greenland contributed only 4 cm of sea level rise in the 21st century in the ice sheet model of Huybrechts et al. (2002). Fichefet et al. (2003), using nearly the same atmosphere-ocean model as Huybrechts et al. (2002) but a more responsive ice sheet model, found AMOC weakening from 20 to 13 Sv late in the 21st century, but separate contributions of ice melt and GHGs to AMOC slowdown were not defined.

Hu et al. (2009, 2011) use the A1B scenario and freshwater from Greenland starting at 1 mm sea level per year increasing 7%/year, similar to our 10-year doubling case. Hu et al. keep the melt rate constant after it reaches 0.3 Sv (in 2050), yielding 1.65 m sea level rise in 2100 and 4.2 m in 2200. Global warming found by Hu et al. for scenario A1B resembles our result but is 20-30% smaller [compare Fig. 2b of Hu et al. (2009) to our Fig. 9], and cooling they obtain from the freshwater flux is moderately less than that in our model. AMOC is slowed about one-third by the latter 21st century in the Hu et al. (2011) 7%/year experiment, comparable to our result.

General consistency holds for other quantities, such as changes of precipitation. Our model yields southward shifting of the Inter-Tropical Convergence Zone (ITCZ) and intensification of the subtropical dry region with increasing GHGs (Fig. S10), as has been reported in modeling studies of Swingedouw et al. (2007, 2009) and others (IPCC, 2013). These effects are intensified by ice melt and cooling in the North Atlantic region (Fig. S10).

A recent 5-model study (Swingedouw et al., 2014) finds a small effect on AMOC for 0.1 Sv Greenland freshwater flux added in 2050 to simulations with a strong GHG forcing. Our larger response is likely due, at least in part, to our freshwater flux reaching several tenths of a Sv.

Freshwater sensitivity in our model is similar to an earlier version of the model used to simulate the 8.2 ky b2k freshwater event associated with demise of the Hudson Bay ice dome (LeGrande et al., 2006). The ~50% AMOC slowdown in that model, in response to forcings of 2.5-5 Sv years indicated by geologic and paleohydraulic studies (e.g., Clarke et al, 2004), is consistent with indications from isotope-enabled analyses of the 8.2 ky event (LeGrande and Schmidt, 2008) and sediment records from the northwest Atlantic (Kleiven et al., 2008). The 1-2 century AMOC recovery time in numerical experiments (LeGrande and Schmidt, 2008) seems consistent with the 160-year duration of the 8.2 ky cooling event (Rasmussen et al., 2013).

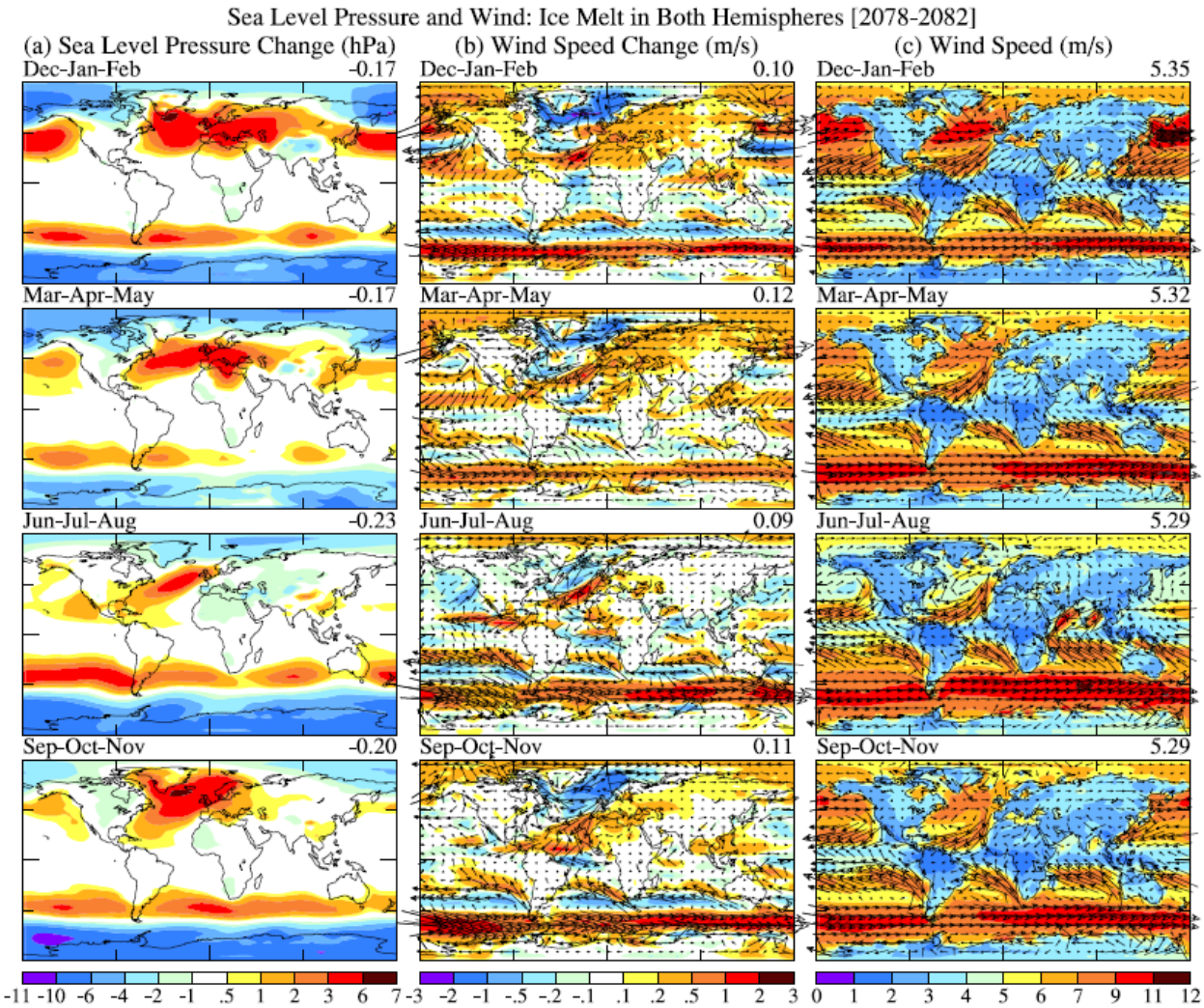


**Fig. 13.** Change of seasonal mean **(a)** sea level pressure and **(b)** wind speed in 2078-2082 relative to 1880-1920, and **(c)** the wind speed itself, all for the scenario with ice melt in both hemispheres.

### 3.6 Storm-related model diagnostics

Ice melt in the North Atlantic creates a substantial increment toward higher sea level pressure in the North Atlantic region in all seasons (Fig. 13). In the summer the added surface pressure strengthens and moves northward the Bermuda high pressure system (Fig. S3). Circulation around the high pressure creates strong prevailing northeasterly winds in the North Atlantic at the latitudes of Bermuda and the Bahamas. A1B climate forcing alone (top row of Fig. S11) has only a small impact on the winds, but cold meltwater in the North Atlantic causes a strengthening and poleward shift of the high pressure.

The high pressure in the model is located further east than appropriate for producing the fastest possible winds at the Bahamas. Our coarse resolution (4°×5°) model, which slightly misplaces the pressure maximum for today's climate, may be partly responsible for the displacement. However, the location of high pressure also depends meltwater placement, which we spread uniformly over all longitudes in the North Atlantic between 65°W and 15°E and on specific location of ocean currents and surface temperature during the Eemian.

Our results at least imply that strong cooling in the North Atlantic from AMOC shutdown does create higher wind speed. It would be useful to carry out more detailed studies with higher resolution climate models including the most realistic possible distribution of meltwater.

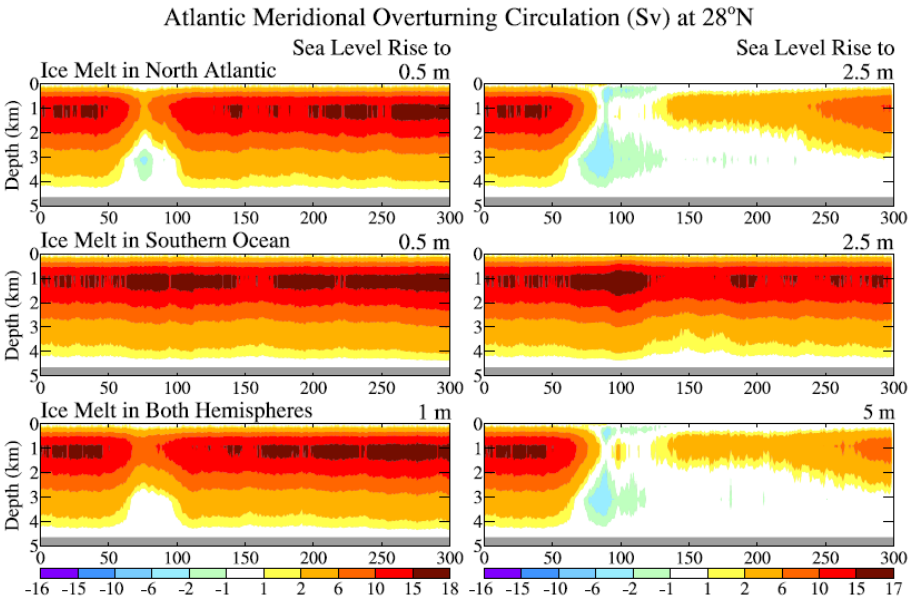


**Fig. 14.** Ensemble-mean AMOC at 28°N versus time for six pure freshwater forcing experiments.

The increment in seasonal mean wind speed of the northeasterlies relative to preindustrial conditions is as much as 10-20%. Such a percentage increase of wind speed in a storm translates into an increase of storm power dissipation by a factor ~1.4-2, because wind power dissipation is proportional to the cube of wind speed (Emanuel, 1987, 2005). However, our simulated changes refer to seasonal mean winds averaged over large grid-boxes, not individual storms.

A blocking high pressure system in the North Atlantic creating consistent strong northeasterly flow would provide wave action that may have contributed to the chevron ridge formation in the Bahamas and Bermuda. This blocking high pressure system could contribute to powerful storm impacts in another way. In combination with the warm tropical conditions that existed in the late Eemian (Cortijo et al., 1999), and are expected in the future if GHGs continue to increase, this blocking high pressure could create a preferred alley for tropical storm tracks.

We assumed, in discussing the relevance of these experiments to Eemian climate, that effects of freshwater injection dominate over changing GHG amount, as seems likely because of the large freshwater effect on SSTs and sea level pressure. However, Eemian $CO_2$ was actually almost constant at ~275 ppm (Luthi et al., 2008). Thus, to isolate effects better, we now carry out simulations with fixed GHG amount, which helps clarify important feedback processes.

### 3.7 Pure freshwater experiments

Our pure freshwater experiments are 5-member ensembles starting at years 1001, 1101, 1201, 1301, and 1401 of the control run. Each experiment ran 300 years. Freshwater flux in the initial decade averaged 180 $km^3$/year (0.5 mm sea level) in the hemisphere with ice melt and increased with a 10-year doubling time. Freshwater input is terminated when it reaches 0.5 m sea level rise per hemisphere for three 5-member ensembles: two ensembles with injection in the individual hemispheres and one ensemble with input in both hemispheres (1 m total sea level rise). Three additional ensembles were obtained by continuing freshwater injection until hemispheric sea level contributions reached 2.5 m. Here we provide a few model diagnostics central to discussions that follow. Additional results are provided in Figs. S12-S14.

The AMOC shuts down for Northern Hemisphere freshwater input yielding 2.5 m sea level rise (Fig. 14). By year 300, more than 200 years after cessation of all freshwater input, AMOC is still far from full recovery for this large freshwater input. On the other hand, freshwater input of 0.5 m does not cause full shutdown, and AMOC recovery occurs in less than a century.

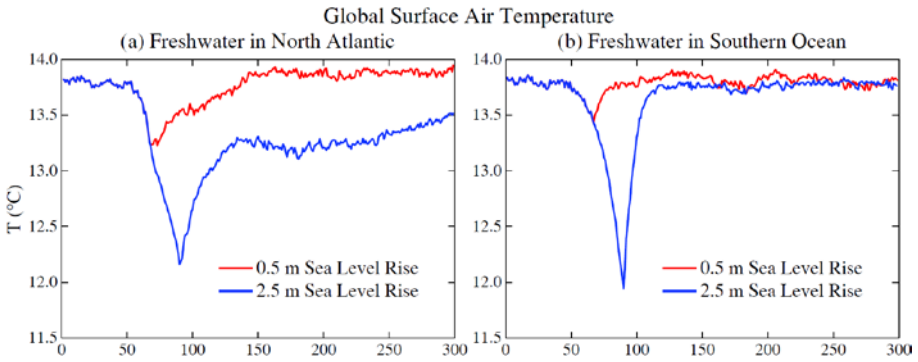


**Fig. 15.** Ensemble-mean global surface air temperature for experiments (years on x-axis) with freshwater forcing in either the North Atlantic Ocean (left) or the Southern Ocean (right).

Global temperature change (Fig. 15) reflects the fundamentally different impact of freshwater forcings of 0.5 m and 2.5 m. The response also differs greatly depending on the hemisphere of the freshwater input. The case with freshwater forcing in both hemispheres is shown only in the Supplement because, to a good approximation, the response is simply the sum of the responses to the individual hemispheric forcings (see Figs. S12-S14). The sum of responses to hemispheric forcings moderately exceeds the response to global forcing.

Global cooling continues for centuries for the case with freshwater forcing sufficient to shut down the AMOC (Fig. 15). If the forcing is only 0.5 m of sea level, the temperature recovers in a few decades. However, the freshwater forcing required to reach the tipping point of AMOC shutdown may be less in the real world than in our model, as discussed below. Global cooling due to freshwater input on the Southern Ocean recovers in a few years after freshwater input ceases (Fig. 15), for both the smaller (0.5 m of sea level) and larger (2.5 m) freshwater forcings.

Injection of a large amount of surface freshwater in either hemisphere has a notable impact on heat uptake by the ocean and the internal ocean heat distribution (Fig. 16). Despite continuous injection of a large amount of very cold (-15°C) water in these pure freshwater experiments, substantial portions of the ocean interior become warmer. Tropical and Southern Hemisphere warming is the well-known effect of reduced heat transport to northern latitudes in response to the AMOC shutdown (Rahmstorf, 1996; Barreiro et al., 2008).

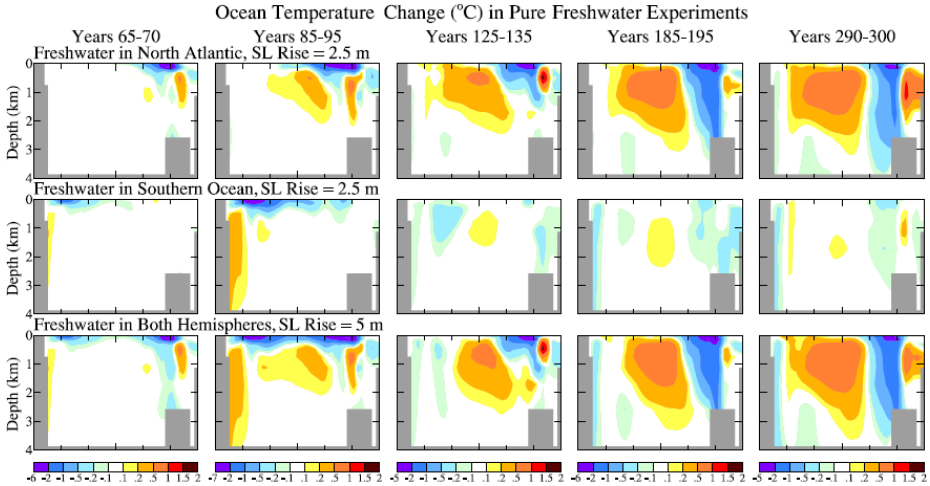


**Fig. 16.** Change of ocean temperature relative to control run due to freshwater input that reaches 2.5 m of global sea level in a hemisphere (thus 5 m sea level rise in the bottom row).

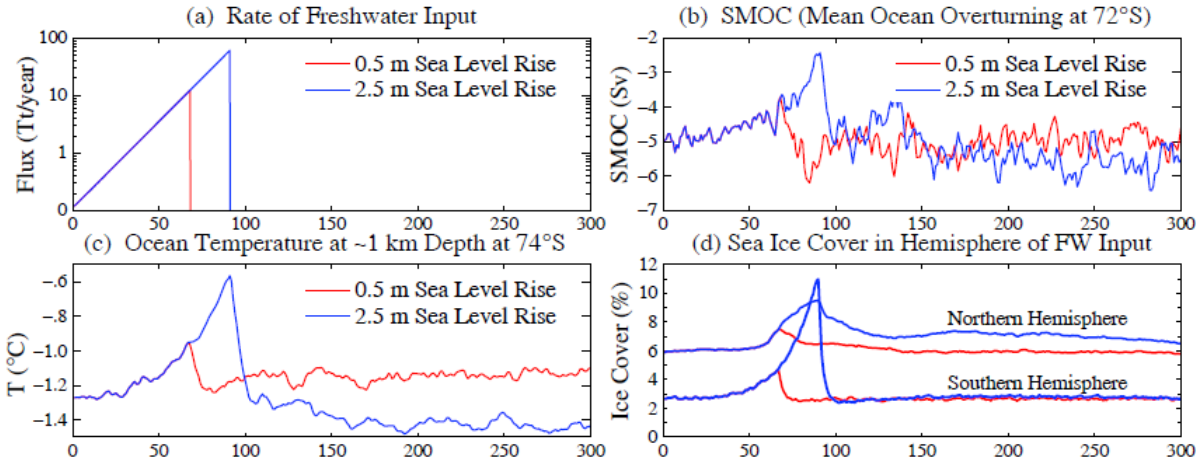


**Fig. 17.** (a) Freshwater input to Southern Ocean (1 Tt = 1000 km$^3$/year). (b, c, d) Simulated overturning strength (Sv) of AABW cell at 72°S, temperature at depth 1.13 km at 74S, and hemispheric sea ice cover.

However, deep warming in the Southern Ocean may have greater consequences. Warming is maximum at grounding line depths (~1-2 km) of Antarctic ice shelves (Rignot and Jacobs, 2002). Ice shelves near their grounding lines (Fig. 13 of Jenkins and Doake, 1991) are sensitive to temperature of the proximate ocean, with ice shelf melting increasing 1 meter per year for each 0.1°C temperature increase (Rignot and Jacobs, 2002). The foot of an ice shelf provides most of the restraining force that ice shelves exert on landward ice (Fig. 14 of Jenkins and Doake, 1991), making ice near the grounding line the buttress of the buttress. Pritchard et al. (2012) deduce from satellite altimetry that ice shelf melt has primary control of Antarctic ice sheet mass loss.

Thus we examine our simulations in more detail (Fig. 17). The pure freshwater experiments add 5 mm sea level in the first decade (requiring an initial 0.346 mm/year for 10-year doubling), 10 mm in the second decade, and so on (Fig. 17a). Cumulative freshwater injection reaches 0.5 m in year 68 and 2.5 m in year 90.

AABW formation is reduced ~20% by year 68 and ~50% by year 90 (Fig. 17b). When freshwater injection ceases, AABW formation rapidly regains full strength, in contrast to the long delay in reestablishing NADW formation after AMOC shutdown. The response time of the Southern Ocean mixed layer dictates the recovery time for AABW formation. Thus rapid recovery also applies to ocean temperature at depths of ice shelf grounding lines (Fig. 17c).

The rapid response of the SMOC (within a decade) to a change of the density of the Southern Ocean mixed layer implies that the rate of freshwater addition to the mixed layer is the driving factor. We will argue below that our model, because of excessive small scale mixing, probably understates the mixed layer and SMOC sensitivities to freshwater flux change, and in a later section we present evidence that the real world is responding more quickly than the model.

Sea ice cover, accurately monitored from satellites since the late 1970s, is a key diagnostic of the ocean surface layer. Increasing sea ice cover, we show below, is a powerful feedback that amplifies ice shelf melt. Freshwater flux has little effect on our simulated Northern Hemisphere sea ice until the 7$^{th}$ decade of freshwater growth (Fig. 17d), but Southern Hemisphere sea ice is more sensitive, with substantial response in the 5$^{th}$ decade and large response in the 6$^{th}$ decade.

Is 5$^{th}$ decade freshwater flux (2880 Gt/year) of relevance to today's world? Yes, we will conclude, the Southern Ocean is already experiencing at least "5$^{th}$ decade" freshwater forcing. We explain the basis of that conclusion below, and then make a climate simulation for the 21$^{st}$ century with more realistic forcings than in our prior simulations.

## 4 Simulations to 2100 with modified (more realistic) forcings

Recent data imply that current ice melt is larger than assumed in our 1850-2300 climate simulations. Thus we make an additional simulation and use the opportunity to make minor improvements in the radiative forcing.

### 4.1 Advanced (earlier) freshwater injection

Atmosphere-ocean climate models, including ours, commonly include a fixed freshwater flux from the Greenland and Antarctic ice sheets to the ocean. This flux is chosen to balance snow accumulation in the model's control run, with the rationale that approximate balance is expected between net accumulation and mass loss including icebergs and ice shelf melting. Global warming creates a mass imbalance that we want to investigate. Ice sheet models can calculate the imbalance, but it is unclear how reliably ice sheet models simulate ice sheet disintegration. We forgo ice sheet modeling, instead adding a growing freshwater amount to polar oceans with alternative growth rates and initial freshwater amount estimated from available data.

Change of freshwater flux on the ocean in a warming world with shrinking ice sheets consists of two terms, Term 1 being net ice melt and Term 2 being change of P-E (precipitation minus evaporation) over the relevant ocean. Term 1 includes land based ice mass loss, which can be detected by satellite gravity measurements, loss of ice shelves, and net sea ice mass change. Term 2 is calculated in a climate model forced by changing atmospheric composition, but it is not included in our pure freshwater experiments that have no global warming.

IPCC (2013, Chapter 4) estimated land ice loss in Antarctica that increased from 30 Gt/year in 1992-2001 to 147 Gt/year in 2002-2011 and in Greenland from 34 Gt/year to 215 Gt/year, with uncertainties discussed by IPCC (2013). Gravity satellite data suggest Greenland ice sheet mass loss ~300-400 Gt/year in the past few years (Barletta et al., 2013). A newer analysis of gravity data for 2003-2013 (Velicogna et al., 2014), discussed in more detail in section 6, finds a Greenland mass loss 280 ± 58 Gt/yr and Antarctic mass loss 67 ± 44 Gt/year.

One estimate of net ice loss from Antarctica, including ice shelves, is obtained by surveying and adding the mass flux from all ice shelves and comparing this freshwater mass loss with the freshwater mass gain from the continental surface mass budget. Rignot et al. (2013) and Depoorter et al. (2013) independently assessed the freshwater mass fluxes from Antarctic ice shelves. Their respective estimates for the basal melt are 1500 ±237 Gt/year and 1454 ±174 Gt/year. Their respective estimates for calving are 1265 ± 139 Gt/year and 1321 ± 144 Gt/year.

This estimated freshwater loss via the ice shelves (~2800 Gt/year) is larger than freshwater gain by the Antarctic surface. Vaughan et al. (1999) estimated the net surface mass balance of the continent as +1811 Gt/year and +2288 Gt/year including precipitation on ice shelves. IPCC (2013) estimates the net Antarctic surface mass balance as +1983 ± 122 Gt/year excluding ice shelves. Thus comparison of continental freshwater input with ice shelf output suggests a net export of freshwater to the Southern Ocean of several hundred Gt/year in recent years. However, substantial uncertainty exists in the difference between these two large numbers.

A remarkable independent evaluation has recently been achieved by Rye et al. (2014) using satellite measured changes of sea level around Antarctica in the period 1992-2011. Sea level along the Antarctic coast rose 2 mm/year faster than the regional mean sea level rise in the Southern Ocean south of 50°S, an effect that they conclude is almost entirely a steric adjustment caused by accelerating freshwater discharge from Antarctica. They conclude that an excess freshwater input of 430 ± 230 Gt/year, above the rate needed to maintain a steady ocean salinity, is required. Rye et al. (2014) note that these values constitute a lower bound for the actual excess discharge above a "steady salinity" rate, because numerous in situ data, discussed below, indicate that freshening began earlier than 1992.

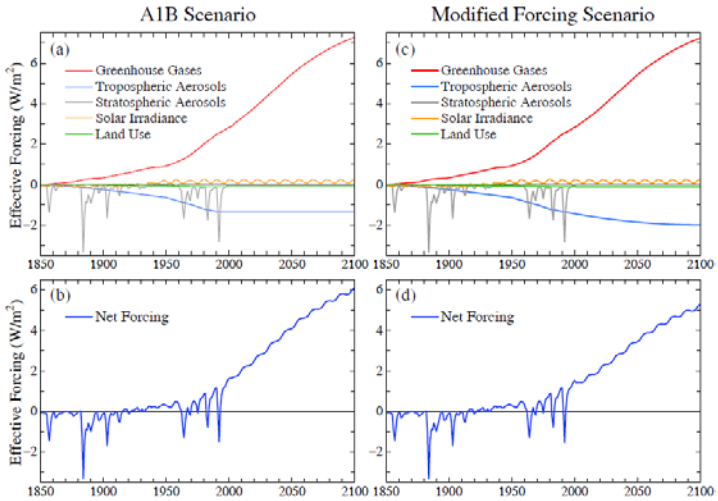


**Fig. 18.** Effective global climate forcings in our climate simulations relative to values in 1850.

Term 2, change of P-E over the Southern Ocean relative to its pre-industrial amount, is large in all climate simulations (IPCC, 2013). In our ensemble of runs (using observed GHGs for 1850-2003 and scenario A1B thereafter) the increase of P-E in the decade 2011-2020, relative to the control run, was in the range 3500 to 4000 Gt/year, as mean precipitation over the Southern Ocean increased ~35 mm/year and evaporation decreased ~3 mm/year.

Increasing ice melt and increasing P-E are climate feedbacks, their growth in recent decades driven by global warming. Our pure freshwater simulations indicate that their sum, at least 4000 Gt/year, is sufficient to affect ocean circulation, sea ice cover, and surface temperature, which can spur other climate feedbacks. We investigate these feedbacks via climate simulations using improved estimates of freshwater flux from ice melt. P-E is computed by the model.

We take freshwater injection to be 720 Gt/year from Antarctica and 360 Gt/year in the North Atlantic in 2011, with injection rates at earlier and later times defined by assumption of a 10-year doubling time. Resulting mean freshwater injection around Antarctica in 1992-2011 is ~400 Gt/year, similar to the estimate of Rye et al. (2014). A recent estimate of 310 ±74 $km^3$ volume loss of floating Antarctic ice shelves in 2003-2012 (Paolo et al., 2015) is not inconsistent, as the radar altimeter data employed for ice shelves does not include contributions from the ice sheet or fast ice tongues at the ice shelf grounding line. Greenland ice sheet mass loss provides most of the assumed 360 Gt/year freshwater, and this would be supplemented by shrinking ice shelves (Rignot and Steffen, 2008) and small ice caps in the North Atlantic and west of Greenland (Ohmura, 2009) that are losing mass (Abdalati et al., 2004; Bahr et al., 2009).

We add the freshwater around Antarctica at coastal grid boxes (Fig. S15) guided by the data of Rignot et al. (2013) and Depoorter et al. (2013), the flux in the western hemisphere from the Weddell Sea to the Ross Sea being about three times larger than for the rest of the coastline. Specified freshwater flux around Greenland is similar on the east and west coasts, and small along the north coast (Fig. S15).

### 4.2 Modified radiative forcings

Actual GHG forcing has grown slower than scenario A1B, because growth of $CH_4$ and minor gases declined after IPCC scenarios were defined (Fig. 5, Hansen et al., 2013c, update at http://www.columbia.edu/~mhs119/GHGs/). As a simple improvement we decreased the A1B $CH_4$ scenario during 2003-2013 such that subsequent $CH_4$ is reduced 100 ppb, thus decreasing the radiative forcing ~0.05 $W/m^2$.

Stratospheric aerosol forcing to 2014 uses the data set of Sato et al. (1993) as updated at http://www.columbia.edu/~mhs119/StratAer/. Future years have constant aerosol optical depth

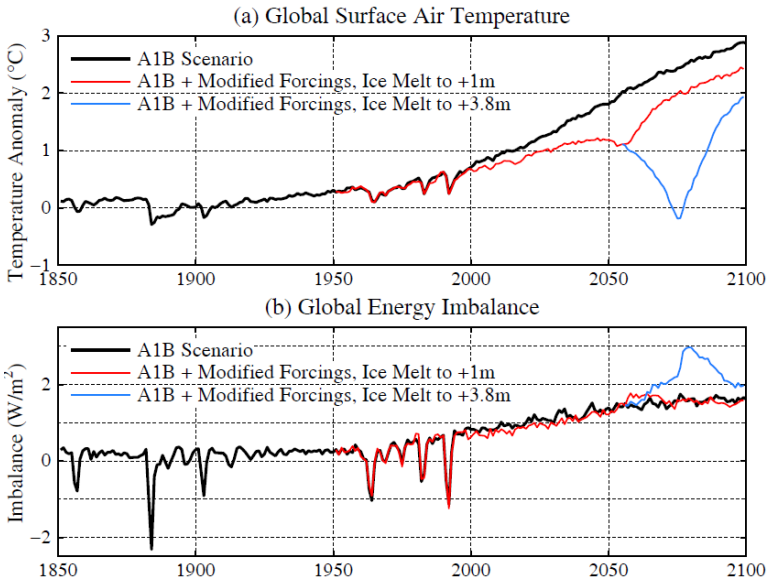


**Fig. 19.** Surface air temperature change relative to 1880-1920 (a) and global energy imbalance (b) for the modified forcing scenario including cases with global ice melt allowed to reach 1 m and 3.8 m.

0.0052 yielding effective forcing -0.12 W/m$^2$, implemented by using fixed 1997 aerosol data. Tropospheric aerosol growth is assumed to slow smoothly, leveling out at -2 W/m$^2$ in 2100. Future solar forcing is assumed to have an 11-year cycle with amplitude 0.25 W/m$^2$. Net forcing exceeds 5 W/m$^2$ by the end of the 21$^{st}$ century, about three times the current forcing (Fig. 18).

### 4.3 Climate simulations with modified forcings

Global temperature has a peak at +1.2°C in the 2040s for the modified forcings (Fig. 19). Ice melt cooling is advanced as global ice melt reaches 1 m of sea level in 2060, 1/3 from Greenland and 2/3 from Antarctica. Actual sea level rise could be less than 1 m, depending on the portion of melt from ice shelves (which has little effect on sea level), but contributions from ocean thermal expansion and mountain glacier melt would probably make global mean sea level rise at least of the order of 1 m.

Global temperature rise resumes in the 2060s after total cessation of the freshwater injection. However, termination of freshwater injection is imposed only for the sake of analyzing climate mechanisms, not with expectation that a sudden halt of ice sheet disintegration is realistic.

Global temperature becomes an unreliable diagnostic of planetary condition as the ice melt rate increases. Global energy imbalance (Fig. 19b) is a more meaningful measure of planetary status as well as an estimate of the climate forcing change required to stabilize climate. Our calculated present energy imbalance of ~0.8 W/m$^2$ (Fig. 19b) is larger than the observed 0.58 ± 0.15 W/m$^2$ during 2005-2010 (Hansen et al., 2011). The discrepancy is likely accounted for by excessive ocean heat uptake at low latitudes in our model, a problem related to the model's slow surface response time (Fig. 7) that may be caused by excessive small scale ocean mixing.

Large scale regional cooling occurs in the North Atlantic and Southern Oceans by mid-century (Fig. 20) for 10-year doubling of freshwater injection. A 20-year doubling places similar cooling near the end of this century, 40 years earlier than in our prior simulations (Fig. 10), as the factor of four increase of current freshwater from Antarctica is a 40-year advance.

The critical issue is whether human-spurred ice sheet mass loss can be approximated as an exponential process during the next few decades. Such nonlinear behavior depends upon amplifying feedbacks, which, indeed, our climate simulations reveal in the Southern Ocean.

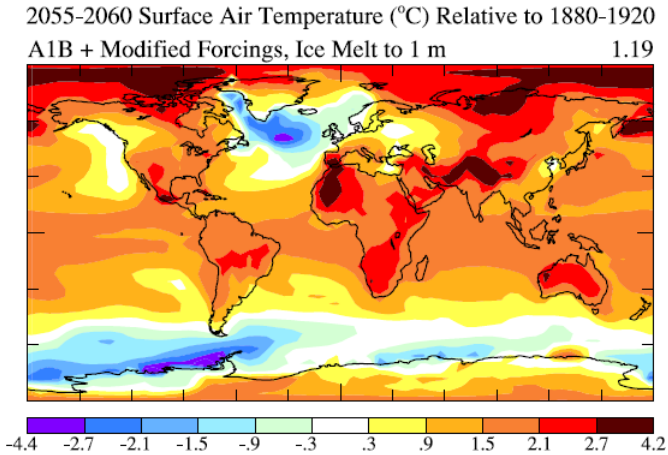


**Fig. 20.** Surface air temperature change relative to 1880-1920 in 2055-2060 with the modified forcings.

### 4.4 Southern Ocean feedbacks

Amplifying feedbacks in the Southern Ocean and atmosphere contribute to dramatic climate change in our simulations (Fig. 20). We first summarize the feedbacks to identify processes that must be simulated well to draw valid conclusions. While recognizing the complexity of the global ocean circulation (Lozier, 2012; Lumpkin and Speer, 2007; Marshall and Speer, 2012; Munk and Wunsch, 1998; Orsi et al., 1999; Sheen et al., 2014; Talley, 2013; Wunsch and Ferrari, 2004), we use a simple two-dimensional representation to discuss the feedbacks.

Climate change includes slowdown of AABW formation, indeed shutdown by midcentury if freshwater injection increases with a doubling time as short as 10 years (Fig. 21). Implications of AABW shutdown are so great that we must ask whether the mechanisms are simulated with sufficient realism in our climate model, which has coarse resolution and relevant deficiencies that we have noted. After discussing the feedbacks here, we examine how well the processes are included in our model (Sec. 4.5). Paleoclimate data (Sec. 5) provides much insight about these processes and modern observations (Sec. 7) show that these feedbacks are already underway.

Large-scale climate processes affecting ice sheets are sketched in Fig. 22. The role of the ocean circulation in the global energy and carbon cycles is captured to a useful extent by the two-dimensional (zonal mean) overturning circulation featuring deep water (NADW) and bottom water (AABW) formation in the polar regions. Marshall and Speer (2012) discuss the circulation based in part on tracer data and analyses by Lumpkin and Speer (2007). Talley (2013) extends the discussion with diagrams clarifying the role of the Pacific and Indian Oceans.

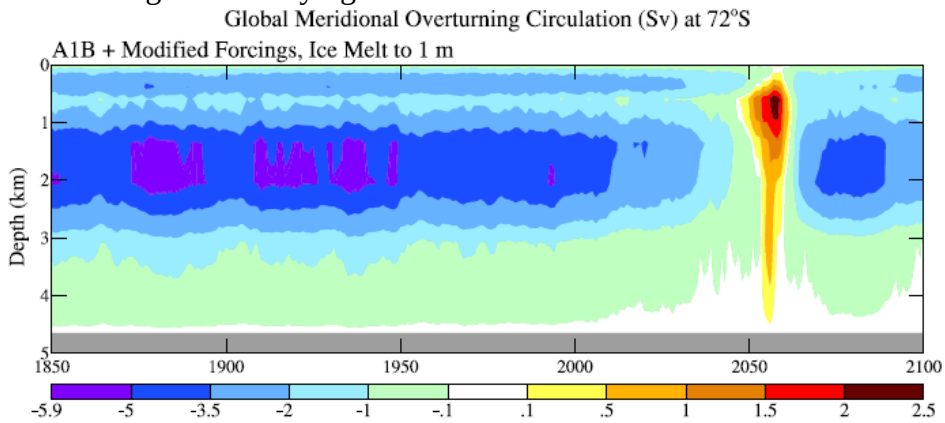


**Fig. 21.** SMOC, ocean overturning strength at 72°S., including only the mean (Eularian) transport (section 4.5). This is the average of a 5-member model ensemble for the modified forcing including advanced ice melt (720 Gt/year from Antarctica in 2011) and 10-year doubling.

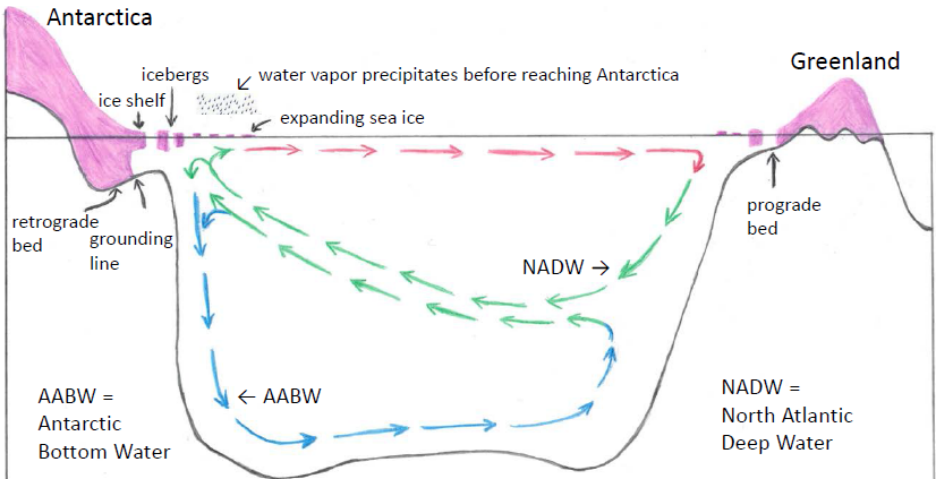


**Fig. 22.** Schematic of stratification and precipitation amplifying feedbacks. Stratification: increased freshwater/iceberg flux increases ocean vertical stratification, reduces AABW formation, traps NADW heat, thus increasing ice shelf melting. Precipitation: increased freshwater/iceberg flux cools ocean mixed layer, increases sea ice area, causing increase of precipitation that falls before it reaches Antarctica, adding to ocean surface freshening and reducing ice sheet growth. A substantial amount of ice in West Antarctica and the Wilkes Basin, East Antarctica is vulnerable because of the reduced stability of retrograde beds.

Wunsch (2002) emphasizes that the ocean circulation is driven primarily by atmospheric winds and secondarily by tidal stirring. The energy drawing deep water toward the surface in the Southern Ocean (Fig. 22) is provided by strong circumpolar westerly winds. This complex global thermohaline circulation can be altered by natural and human-made forcings, including freshwater injection from ice sheets, which stimulate powerful feedback processes.

A key feedback concerns the effect of cold freshwater injection on ocean temperature at ice shelf grounding lines. In our "pure freshwater" simulations the freshwater added to the Southern Ocean acts as a lid that reduces ventilation of ocean heat to the atmosphere and space. Warming is largest at depths near ice shelf grounding lines, the portion of the ice shelf that provides most of the restraining force that limits the rate of ice sheet discharge to the ocean (Fig. 14 of Jenkins and Doake, 1991). Melting at ice shelf grounding lines in West Antarctica and Wilkes Basin in East Antarctica has potential to result in rapid, nonlinear sea level rise because these basins have retrograde beds (beds sloping inland), a configuration with potential for unstable grounding line retreat and substantial ice sheet disintegration (Mercer, 1978), as discussed further below. Multiple submarine valleys make much of the Greenland ice sheet vulnerable to thermal forcing by a warming ocean (Morlighem et al., 2014), but with a few exceptions (Khan et al., 2014) the valleys are prograde and thus rapid nonlinear growth of ice melt is not likely.

Another feedback occurs via the effect of surface and atmospheric cooling on precipitation and evaporation over the Southern Ocean. In climate simulations that do not include increasing freshwater injection in the Southern Ocean (IPCC, 2013), it is found that snowfall on Antarctica increases substantially in the 21$^{st}$ century, thus providing a negative term to sea level change. Frieler et al. (2015) assert that 35 global climate models are consistent in showing that a warming climate will yield increasing Antarctic snow accumulation, but this paleo "affirmation" refers to slowly changing climate in quasi-equilibrium with ocean boundary conditions. In our experiments with growing freshwater injection the increasing sea ice cover and cooling of the Southern Ocean surface and atmosphere cause the increased precipitation to occur over the Southern Ocean, rather than over Antarctica. This feedback not only reduces any increase of snowfall over Antarctica, it also provides a large freshening term to the surface of the Southern Ocean, thus magnifying the direct freshening effect from increasing ice sheet melt.

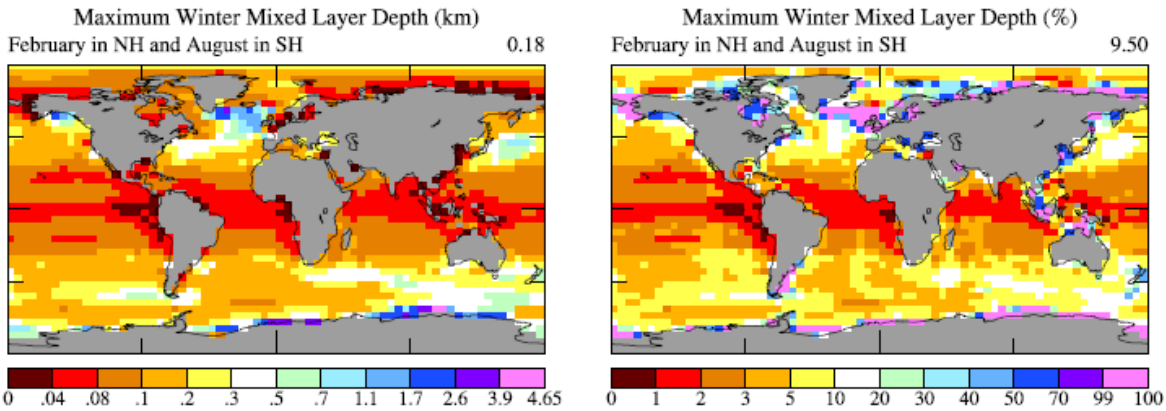


**Fig. 23.** Maximum mixed layer depth (in km, left, and % of ocean depth, right) in February (Northern Hemisphere) and August (Southern Hemisphere) using the mixed layer definition of Heuze et al. (2013).

### 4.5 Model's ability to simulate these feedbacks

Realistic representation of these feedbacks places requirements on both the atmosphere and ocean components of our climate model. We discuss first the atmosphere, then the ocean.

There are two main requirements on the atmospheric model. First, it must simulate well P-E and changes of P-E, because of its importance for ocean circulation and the amplifying feedback in the Southern Ocean. Precise verification of P-E is difficult to attain, but the ultimate model requirement is that it produce realistic sea surface salinity (SSS) patterns and ongoing changes.

Simulated P-E (Fig. S16b) agrees well with meteorological reanalysis (Fig. 3.4b, IPCC, 2013). Simulated global sea surface salinity (SSS) patterns (Fig. S16a) agree well with global ocean surface salinity patterns (Antonov et al., 2010 and Fig. 3.4a, IPCC, 2013). SSS trends in our simulation (Fig. S16c), with the Pacific on average becoming fresher while most of the Atlantic and the subtropics in the Southern Hemisphere become saltier, are consistent with observed salinity trends (Durack and Wijffels, 2010). Recent freshening of the Southern Ocean in our simulation is somewhat less than in observed data (IPCC, Fig. 3.4c and 3.4d), implying that the amplifying feedback may be underestimated in our simulation. A likely reason for that is discussed below in conjunction with observed sea ice change.

The second requirement is that the atmospheric model simulate well winds and their changes, because these drive the ocean. Thus the model must simulate well atmospheric pressure patterns and changes in response to climate forcings. A test is provided by observed changes of the Southern Annular Mode (SAM), with a decrease of surface pressure near Antarctica and a small increase at mid-latitudes (Marshall, 2003) that D. Thompson et al. (2011) relate to stratospheric ozone loss and increasing GHGs. Our climate forcing (Fig. 18) includes ozone change (Fig. 2, Hansen et al., 2007a) with stratospheric ozone depletion in 1979-1997 and constant ozone thereafter. Our model produces a trend toward the high index polarity of SAM (Fig. S17) similar to observations, although perhaps a slightly smaller change than observed (compare Fig. S17 with Fig. 3 of Marshall, 2003). SAM continues to increase in our model after ozone stabilizes (Fig. S17), suggesting that GHGs may provide a larger portion of the SAM response in our model than in the model study of D. Thompson et al. (2011). It would not be surprising if the stratospheric dynamical response to ozone change were weak in our model, given the coarse resolution and simplified representation of atmospheric drag and dynamical effects in the stratosphere (Hansen et al., 2007a), but that is not a major concern for our present purposes.

The ocean model must be able to simulate realistically the ocean's overturning circulation and its response to forcings including freshwater additions. Heuze et al. (2013, 2015) point out that simulated deep convection in the Southern Ocean is unrealistic in most models, with AABW formation occurring in the open ocean where it rarely occurs in nature. Our present ocean model

contains significant improvements (see Sec. 3.1) compared to the GISS E2-R model that Heuze et al. include in their comparisons. Thus we show (Fig. 23) the maximum mixed layer depth in winter (February in the Northern Hemisphere and August in the Southern Hemisphere) using the same criterion as Heuze et al. to define the mixed layer depth, i.e., the layers with a density difference from the ocean surface layer less than 0.03 kg/m$^3$.

Southern Ocean mixing in the model reaches a depth of ~500 m in a wide belt near 60°S stretching west from the southern tip of South America, with similar depths south of Australia. These open ocean mixed layer depths compare favorably with observations shown in Fig. 2a of Heuze et al. (2015), based on data of de Boyer Montegut et al. (2004). There is no open ocean deep convection in our model.

Deep convection occurs only along the coast of Antarctica (Fig. 23). Coastal grid boxes on the continental shelf are a realistic location for AABW formation. Orsi et al. (1999) suggest that most AABW is formed on shelves around the Weddell-Enderby Basin (60%) and shelves of the Adelie-Wilkes Coast and Ross Sea (40%). Our model produces mixing down to the shelf in those locations (Fig. 23b), but also on the Amery Ice Shelf near the location where Ohshima et al. (2013) identified AABW production, which they term Cape Darnley Bottom Water.

However, with our coarse 4°×5° stair step to the ocean bottom the AABW cannot readily slide down the slope to the ocean floor. As a result, the denser water from the shelf mixes into the open ocean grid boxes, making our modeled Southern Ocean less stratified than the real world (cf. temporal drift of Southern Ocean salinity in Fig. S18), because the denser water must move several degrees of latitude horizontally before it can move deeper. Nevertheless, our Southern Ocean is sufficiently stratified to avoid the unrealistic open ocean convection that infects many models (Heuze et al., 2013).

Orsi et al. (1999) estimate the AABW formation rate in several ways, obtaining values in the range 8-12 Sv, larger than our modeled 5-6 Sv (Fig. 21). However, as in most models (Heuze et al., 2015) our SMOC diagnostic (Fig. 21) is the mean (Eulerian) circulation, i.e., excluding eddy-induced transport. Rerun of a 20-year segment of our control run to save eddy-induced changes reveals an increase of SMOC at 72°S by 1-2 Sv, with negligible change at middle and low latitudes, making our simulated transport close to the range estimated by Orsi et al. (1999).

We conclude that the climate model can potentially simulate Southern Ocean feedbacks that magnify the effect of freshwater injection onto the Southern Ocean: the P-E feedback that wrenches global-warming-enhanced water vapor from the air before it reaches the Antarctic continent and the AABW slowdown that traps deep ocean heat, leaving that heat at levels where it accelerates ice shelf melting. Indeed, we will argue that both of these feedbacks are probably underestimated in our current model.

The model seems less capable in Northern Hemisphere polar regions. Deep convection today is believed to occur mainly in the Greenland-Iceland-Norwegian (GIN) Sea and at the southern end of Baffin Bay (Fig. 2b, Heuze et al., 2015). In our model, perhaps because of excessive sea ice in those regions, open ocean deep convection occurs to the southeast of the southern tip of Greenland and at less deep grid boxes between that location and the United Kingdom (Fig. 23). Mixing reaching the ocean floor on the Siberian Coast in our model (Fig. 23) may be realistic, as coastal polynya are observed on the Siberian continental shelf (D. Bauch et al., 2012). However, the winter mixed layer on the Alaska south coast is unrealistically deep (Fig. 23). These model limitations must be kept in mind in interpreting simulated Northern Hemisphere climate change.

## 5 Implications of paleoclimate data

Paleoclimate data are essential for understanding the major climate feedbacks. Processes of special importance are: (1) the role of the Southern Ocean in ventilating the deep ocean, affecting $CO_2$ control of global temperature, and (2) the role of subsurface ocean warming in ice shelf melt, affecting ice sheet disintegration and sea level rise.

### 5.1 Paleoclimate context

Major glacial-interglacial climate oscillations are spurred by periodic variation of seasonal and geographical insolation (Hays et al., 1976). Insolation anomalies are caused by slow changes of the eccentricity of Earth's orbit, tilt of Earth's spin axis, and precession of the equinoxes, thus the day of year at which Earth is closest to the Sun, with dominant periodicities near 100,000, 40,000 and 20,000 years (Berger, 1978). These periods emerge in long climate records, yet a large fraction of climate variability at any site is stochastic (Wunsch, 2004; Lisiecki and Raymo, 2005). Such behavior is expected for a weakly-forced system characterized by amplifying feedbacks, complex dynamics, and multiple sources of inertia with a range of time scales.

Large glacial-interglacial climate change and stochastic variability are a result of two strong amplifying feedbacks, surface albedo and atmospheric $CO_2$. Orbit-induced insolation anomalies, per se, cause a climate forcing, i.e., an Earth energy imbalance, only of order 0.1 W/m$^2$, but the persistent regional insolation anomalies spur changes of ice sheet size and GHGs. The albedo and GHG changes arise as slow climate feedbacks, but they are the forcings that maintain a quasi-equilibrium climate state nearly in global radiative balance. Glacial-interglacial albedo and greenhouse forcings are each ~3 W/m$^2$ (Fig. 24e,f)[12]. These forcings fully account for glacial-interglacial global temperature change with a climate sensitivity 0.5-1°C per W/m$^2$ (Hansen et al., 2008; Masson-Delmotte et al., 2010; Palaeosens, 2012).

The insolation anomaly peaking at 129.5 ky b2k (Fig. 24a) succeeded in removing ice sheets from North America and Eurasia and in driving atmospheric $CO_2$ up to ~285 ppm, as discussed below. However, smaller climate oscillations within the last glacial cycle are also instructive about ice feedbacks. Some of these oscillations are related to weak insolation anomalies and all are affected by predominately amplifying climate feedbacks.

Insolation anomalies peaking at 107 and 86 ky b2k (Fig. 24a) led to ~40 m sea level rises at rates exceeding 1 m/century (Stirling et al., 1998; Cutler et al., 2003) in early MIS 5c and 5a (Fig. 24f), but $CO_2$ did not rise above 250 ppm and interglacial status was not achieved. $CO_2$ then continued on a 100 ky decline until ~18 ky b2k. Sea level continued its long decline, in concert with $CO_2$, reaching a minimum at least 120 m below today's sea level (Peltier and Fairbanks, 2006; Lambeck et al., 2014).

Progress achieved by the paleoclimate and oceanographic research communities allows interpretation of the role of the Southern Ocean in the tight relationship between $CO_2$ and temperature, as well as discussion of the role of subsurface ocean warming in sea level rise. Both topics are needed to interpret end-Eemian climate change and ongoing climate change.

[12] Other parts of Fig. 24 are discussed later, but they are most informative if aligned together. In interpreting Fig. 24, note that long-lived greenhouse gas amounts in ice cores have global relevance, but ice core temperatures are local to Greenland and Antarctica. Also, because our analysis does not depend on absolute temperature, we do not need to convert the temperature proxy, $\delta^{18}O$, into an estimated absolute temperature. We include $CH_4$ and $N_2O$ in the total GHG climate forcing, but we do not discuss the reasons for $CH_4$ and $N_2O$ variability (see Schilt et al., 2010), because $CO_2$ provides ~80% of the GHG forcing.

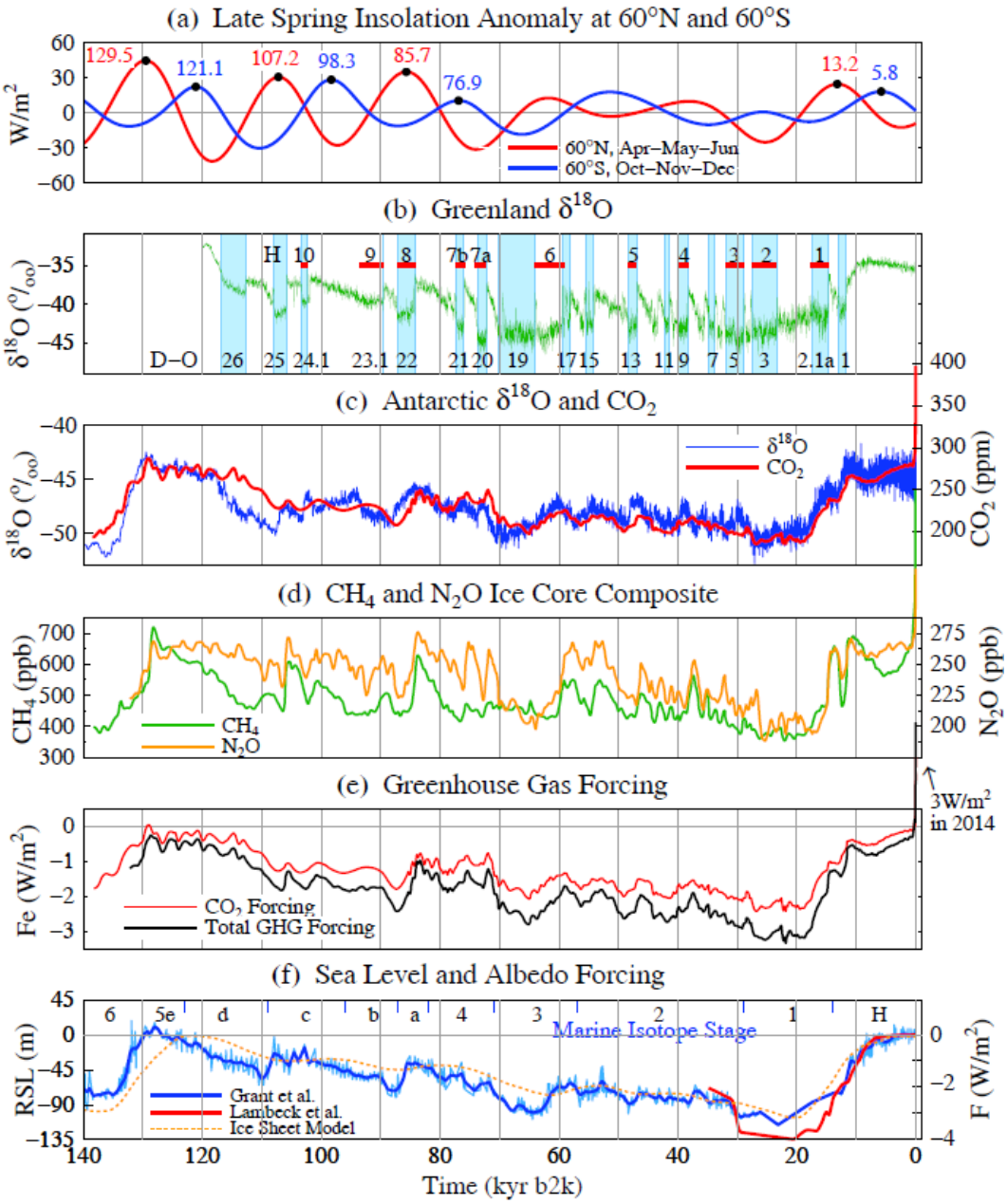


**Fig. 24.** (a) Late spring insolation anomalies relative to the mean for the past million years, (b) $\delta^{18}O_{ice}$ of composite Greenland ice cores (Rassmussen et al., 2014) with Heinrich events of Guillevic et al. (2014), (c, d) $\delta^{18}O_{ice}$ of EDML Antarctic ice core (Ruth et al., 2007), multi-ice core $CO_2$, $CH_4$, and $N_2O$ based on spline fit with 1000-year cut-off (Schilt et al., 2010), scales are such that $CO_2$ and $\delta^{18}O$ means coincide and standard deviations have the same magnitude, (e) GHG forcings from equations in Table 1 of Hansen et al. (2000), but with the $CO_2$, $CH_4$, and $N_2O$ forcings multiplied by factors 1.024, 1.60, and 1.074, respectively, to account for each forcing's "efficacy" (Hansen et al., 2005), with $CH_4$ including factor 1.4 to account for indirect effect on ozone and stratospheric water vapor, (f) sea level data from Grant et al. (2012) and Lambeck et al. (2014) and ice sheet model results from de Boer et al. (2010). Marine isotope stage boundaries from Lisiecki and Raymo (2005). (b-e) are on AICC2012 time scale (Bazin et al., 2013),

## 5.2 Southern Ocean and atmospheric $CO_2$

Reduced atmospheric $CO_2$ in glacial times, at least in substantial part, results from increased stratification of the Southern Ocean that reduces ventilation of the deep ocean (Toggweiler, 1999; Anderson et al., 2009; Skinner et al., 2010; Tschumi et al., 2011; Burke and Robinson, 2012; Schmitt et al., 2012; Marcott et al., 2014). Today the average "age" of deep water, i.e., the time since it left the ocean surface, is ~1000 years (DeVries and Primeau, 2011), but it was more than twice that old during the last glacial maximum (Skinner et al., 2010). The Southern Ocean dominates exchange between the deep ocean and atmosphere because ~80% of deep water resurfaces in the Southern Ocean (Lumpkin and Speer, 2007), as westerly circumpolar winds and surface flow draw up deep water (Talley, 2013).

Mechanisms causing more rapid deep ocean ventilation during interglacials include warmer Antarctic climate that increases heat flux into the ocean and buoyancy mixing that supports upwelling (Watson and Garabato, 2006), poleward shift of the westerlies (Toggweiler et al., 2006), and reduced sea ice (Keeling and Stephens, 2001). Fischer et al. (2010) question whether the latitudinal shift of westerlies is an important contributor; however, the basic point is the empirical fact that a warmer interglacial Southern Ocean produces faster ventilation of the deep ocean via a combination of mechanisms.

Poor ocean ventilation in glacial periods allows carbon to be sequestered via the "biological pump", the rain of organic matter from the surface ocean that affects burial of calcium carbonate in sediments (Sigman and Boyle, 2000). Dust-borne iron fertilization of the biological pump (Martin and Fitzwater, 1988) contributes to millennial and full glacial $CO_2$ drawdown (Martinez-Garcia et al., 2014). In concert, global cooling drives the simple "solubility pump", as the temperature dependence of $CO_2$ solubility increases dissolved inorganic carbon (Raven and Falkowski, 1999). The increased acidity of deep water makes it more corrosive to carbonate sediments, thus increasing ocean alkalinity and further lowering atmospheric $CO_2$ (Boyle, 1988).

Much remains to be learned about glacial-interglacial carbon cycle mechanisms. Carbon isotopes indicate that increased deep ocean ventilation during deglaciation from the last ice age caused a 30-35 ppm $CO_2$ increase within 2000 years (Schmitt et al., 2012; Tschumi et al., 2011). However, AMOC changes are associated with at least two rapid $CO_2$ increases of about 10 ppm, as revealed by a high resolution West Antarctic ice core (Marcott et al., 2014). Another indication of possible Atlantic involvement in the carbon cycle is the change of the North Atlantic's Western Boundary Undercurrent during the transition to full glacial conditions at ~70 ky b2k when $CO_2$ dropped below 200 ppm (Fig. 24); the flow became stronger in the upper 2 km while the deeper circulation weakened (Thornalley et al., 2013). No doubt the terrestrial biosphere also contributes to atmospheric $CO_2$ change (Archer et al., 2000; Sigman and Boyle, 2000; Kohler et al., 2005; Menviel et al., 2012; Fischer et al., 2015). Nevertheless, it is reasonably clear that sequestration of $CO_2$ in the glacial ocean is the largest cause of glacial-interglacial $CO_2$ change, and ocean ventilation occurs mainly via the Southern Ocean.

Southern Ocean ventilation, as the dominant cause of atmospheric $CO_2$ change, helps explain temperature-$CO_2$ leads and lags. Temperature and $CO_2$ rises are almost congruent at ice age terminations (Masson-Delmotte, 2010; Pedro et al., 2012; Parrenin et al., 2013). Southern Ocean temperature is expected to lead, spurring deep ocean ventilation and atmospheric $CO_2$ increase, with global temperature following. Termination I is dated best and Shakun et al. (2012) have reconstructed global temperature then, finding evidence for this expected order of events.

Correlation of $\delta^{18}O$ and $CO_2$ over the past 140 ky (Fig. 24c) is 84.4% with $CO_2$ lagging by 760 years. For the period 100-20 ky b2k, which excludes the two terminations, the correlation is 77.5% with $CO_2$ lagging by 1040 years. Briefer lag for the longer period and longer lag during glacial inception are consistent with the rapid deep ocean ventilation that occurs at terminations.

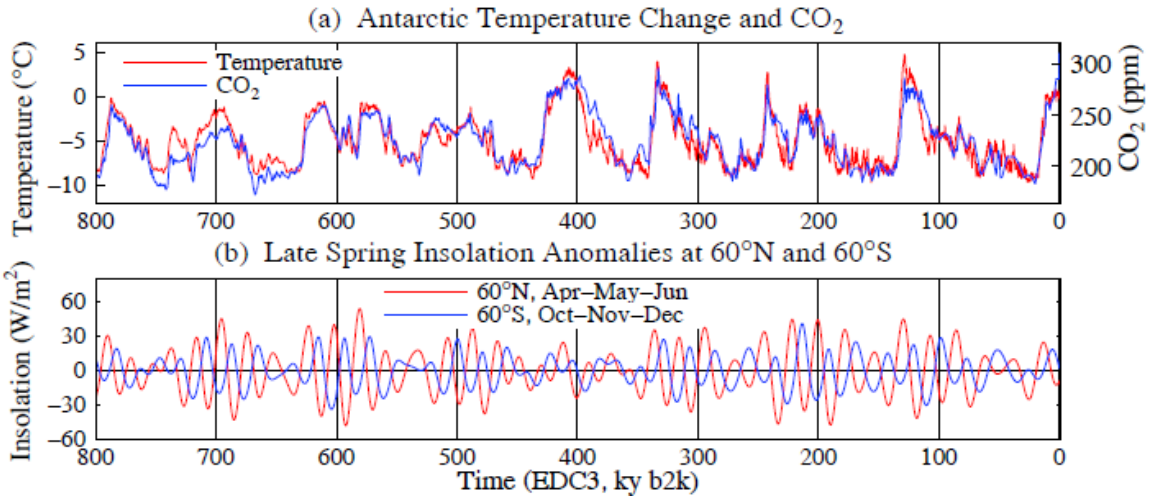


**Fig. 25.** (a) Antarctic (Dome C) temperature relative to last 10 ky (Jouzel et al., 2007) on AICC2012 time scale and $CO_2$ amount (Luthi et al., 2008). Temperature scale is such that standard deviation of T and $CO_2$ are equal, yielding $\Delta T$ (°C) = 0.114 $\Delta CO_2$ (ppm), (b) Late Spring insolation anomalies at 60°N and 60°S.

### 5.3 $CO_2$ as climate control knob

$CO_2$ is the principal determinant of Earth's climate state, the "control knob" that sets global mean temperature (Lacis et al., 2010, 2013). The degree of control is shown by comparison of $CO_2$ amount with Antarctic temperature for the past 800,000 years (Fig. 25a). Control should be even tighter for global temperature than for Antarctic temperature, because of regional anomalies such as Antarctic temperature overshoot at terminations (Masson-Delmotte, 2006, 2010), but global data are not available.[13]

The $CO_2$ dial must be turned to ~260 ppm to achieve a Holocene-level interglacial. $CO_2$ ~ 250 ppm was sufficient for quasi-interglacials in the period 800-450 ky b2k, with sea level 10-25 m lower than in the Holocene (Fig. S18 of Hansen et al., 2008). Interglacials with $CO_2$ ~ 280 ppm, i.e., the Eemian and Holsteinian (~400 ky b2k), were warmer than the Holocene and had sea level at least several meters higher than today.

$CO_2$ and albedo change are closely congruent over the last 800,000 years (Fig. S18 of Hansen et al., 2008). GHG and albedo forcings, which are both amplifying feedbacks that boost each other, are each of amplitude ~3 W/m$^2$. So why do we say that $CO_2$ is the control knob?

First, $CO_2$, in addition to being a slow climate feedback, changes independently of climate. Natural $CO_2$ change includes increase to ~1000 ppm about 50 million years ago (Zachos et al., 2001) as a result of plate tectonics, specifically volcanic emissions associated with movement of the Indian plate across the Tethys Ocean and collision with Asia (Kent and Muttoni, 2008). Humankind, mainly by burning fossil fuels, also moves the $CO_2$ control knob.

Second, $CO_2$ is more recalcitrant than snow and ice, i.e., its response time is longer. $CO_2$ inserted into the climate system, by humans or plate tectonics, remains in the climate system of order 100,000 years before full removal by weathering (Archer, 2005). Even $CO_2$ exchange between the atmosphere (where it affects climate) and ocean has a lag of the order a millennium

[13] The tight fit of $CO_2$ and Antarctic temperature (Fig. 25a) implies an equilibrium Antarctic sensitivity 20°C for 2×$CO_2$ (4 W/m$^2$) forcing (200 → 300 ppm forcing is ~2.3 W/m$^2$, Table 1 of Hansen et al., 2000), thus 10°C global climate sensitivity (Antarctic temperature change is ~ twice global change) with $CO_2$ taken as the ultimate control knob, i.e., if snow/ice area and other GHGs are taken to be slaves to $CO_2$-driven climate change. This implies a conventional climate sensitivity of 4°C for 2×$CO_2$, as GHG and albedo forcings are similar for glacial-to-interglacial climate change and non-$CO_2$ GHGs account for ~20% of the GHG forcing. The inferred sensitivity is reduced to 2.5-3°C for 2×$CO_2$ if, as some studies suggest, global mean glacial-interglacial temperature change is only about one-third of the Antarctic temperature change (Palaeosens, 2012; Hansen et al., 2013b).

(Fig. 24). In contrast, correlations of paleo temperatures and sea level show that lag of sea level change behind temperature is of order a century, not a millennium (Grant et al., 2012).

We suggest that limitations on the speed of ice volume (thus sea level) changes in the paleo record are more a consequence of the pace of orbital changes and $CO_2$ changes, as opposed to being a result of lethargic ice physics. "Fast" changes of $CO_2$ have been identified, e.g., an increase of ~10 ppm in about a century at ~39.6 ky b2k (Ahn et al., 2012) and three increases of 10-15 ppm each within 1-2 centuries during the deglaciation following the last ice age (Marcott et al., 2014), but the magnitude of these $CO_2$ increases is not sufficient to provide a good empirical test of ice sheet sensitivity to the $CO_2$ forcing.

Supremacy of SMOC, the Southern Ocean meridional overturning circulation, in affecting the $CO_2$ control knob and thus glacial-interglacial change is contrary to the idea that AMOC is a prime driver that flips global climate between quasi-stable glacial and interglacial states, yet AMOC retains a significant role. AMOC can affect $CO_2$ via the volume and residence time of NADW, but its largest effect is probably via its impact on the Southern Ocean. When AMOC is not shut down it cools the Southern Hemisphere, transferring heat from the Southern to the Northern Hemisphere at a rate ~1 petawatt, which is ~4 W/m$^2$ averaged over a hemisphere (Crowley, 1992). However, the Southern Ocean slowly warms when AMOC shuts (or slows) down; the response time is of the order of 1000 years because of the Southern Ocean's large thermal inertia (Stocker and Johnson, 2003). These mechanisms largely account for the nature of the "bipolar seesaw" (Broecker, 1998; Stocker, 1998; Stenni et al., 2011; Landais et al., 2015), including the lag between AMOC slowdown and Antarctic warming.

### 5.4 Dansgaard-Oeschger events and subsurface ocean warming

The magnitude and rapidity of Greenland climate change during Dansgaard-Oeschger events would deter prediction of human-made climate effects, if D-O events remained a mystery. Instead, however, enough is now understood about D-O events that they provide insight related to the vulnerability of ice shelves and ice sheets, including the role of subsurface ocean warming.

Broecker (2000) inferred from the rapidity of D-O warmings that a reduction of sea ice cover was probably involved. Li et al. (2005, 2010) modeling showed that removal of Nordic Seas ice cover is needed to yield the magnitude of observed Greenland warming. The spatial gradient of D-O warming, with smaller warming in northwest Greenland, agrees with that picture (Guillevic et al., 2013; Buizert et al., 2014). Such sea ice change is consistent with changes in deuterium excess in Greenland ice cores at D-O transitions, which indicate shifts of Greenland moisture source regions (Masson-Delmotte et al., 2005; Jouzel et al., 2007).

Fluckiger et al. (2006), Alvarez-Solas et al. (2010, 2011, 2013) and Marcott et al. (2011) noted modern and paleo data that point to ocean-ice shelf interaction as key to the ice discharge of accompanying Heinrich events, and they used a range of models to support this interpretation and overturn earlier suggestions of a central role for ice sheets via binge-purge oscillations (MacAyeal, 1993) or outburst flooding from subglacial reservoirs (Alley et al., 2006). Shaffer et al. (2004) and Petersen et al. (2013) conclude that subsurface ocean warming in the North Atlantic takes place during the stadial (cold) phase of all D-O events, and eventually this subsurface warming leads to ice shelf collapse or retreat, ice rafting, sea level rise, and sea ice changes. Rasmussen et al. (2003) examined ocean cores from the southeast Labrador Sea and found that for all 11 Heinrich events "…the icy surface water was overlying a relatively warm, poorly ventilated and nutrient rich intermediate water mass to a water depth of at least 1251 m." Collapse of a Greenland ice shelf fronting the Jakoshavn ice stream during the Younger Dryas cold event has been documented (Rinterknecht et al., 2014), apparently due to subsurface warming beneath the ice shelf leading to rapid discharge of icebergs.

Some D-O details are uncertain, e.g., the relation between changing sea ice cover and changing location of deep water formation (Rahmstorf, 1994) and whether an ice shelf between Greenland and Iceland contributed to the sea ice variability (Petersen et al., 2013). However, ocean-ice interactions emerge as key mechanisms, spurred by subsurface ocean warming, as ocean stratification slows but does not stop northward heat transport by AMOC.

We consider a specific D-O event for the sake of discussing mechanisms. D-O 22 cold phase, labeled C22 in ocean cores and coinciding with Heinrich H8 (Fig. 24), occurred as Northern Hemisphere insolation was rising (Fig. 24a). The North Atlantic surface was cooled by rapid ice discharge; sea level rose more than 40 m, a rate exceeding 1.6 m per century (Cutler et al., 2003). Ice discharge kept the North Atlantic highly stratified, slowing AMOC. Antarctic warming from a slowed AMOC increases almost linearly with the length of the D-O cold phase (Fig. 3, EPICA Community Members, 2006; Fig. 6, Capron et al., 2010) because of the Southern Ocean's large heat capacity (Stocker and Johnson, 2003). Antarctic warming, aided by the 2500-year D-O 22 event, spurred SMOC enough to raise atmospheric $CO_2$ 40 ppm (Fig. 24c).

As the Antarctic warmed, ocean heat transport to the North Atlantic would have increased, with most heat carried at depths below the surface layer. When the North Atlantic became warm enough at depth, stratification of cold fresh surface water eventually could not be maintained. The warming breakthrough may have included change of NADW formation location (Rahmstorf, 1994) or just large movement of the polar front. Surface warming east of Greenland removed most sea ice and Greenland warmed ~10°C (Capron et al., 2010). As the warm phase of D-O 21 began, AMOC was pumping heat from the Antarctic into the Nordic seas and Earth must have been slightly out of energy balance, cooling to space, so both Antarctica and Greenland slowly cooled. Once the North Atlantic had cooled enough, sea formed east of Greenland again, ice sheets and ice shelves grew, sea level fell, and the polar front moved southward.

Sea level rise associated with D-O events covers a wide range. Sea level increases as large as ~40 m were associated with large insolation forcings at 107 and 86 ky b2k (Fig. 24). However, rapid sea level change occurred even when forcing was weak. Roche et al. (2004) conclude from analyses of $\delta^{18}O$ that H4, at a time of little insolation forcing (~ 40 ky b2k, Fig. 24), produced 1.9 ±1.1 m sea level rise over 250 ±150 years. Sea level rise as great as 10-15 m occurred in conjunction with some other D-O events during 65-30 ky b2k (Lambeck and Chappell, 2001; Yokoyama et al., 2001; Chappell, 2002).

Questions about possible D-O periodicity and external forcing were raised by a seeming 1470-year periodicity (Schulz, 2002). However, improved dating indicates that such periodicity is an artifact of ice core chronologies and not statistically significant (Ditlevsen et al., 2007) and inspection of Fig. 24b reveals a broad range of time scales. Instead, the data imply a climate system that responds sensitively to even weak forcings and stochastic variability, both of which can spur amplifying feedbacks with a range of characteristic response times.

Two conclusions are especially germane. First, subsurface ocean warming is an effective mechanism for destabilizing ice shelves and thus the ice sheets buttressed by the ice shelves. Second, large rapid sea level rise can occur as a result of melting ice shelves.

However, ice shelves probably were more extensive during glacial times. So are today's ice sheets much more stable? The need to understand ice sheet vulnerability focuses attention on end-Eemian events, when ice sheets were comparable in size to today's ice sheets.

### 5.5 End-Eemian climate and sea level change

Termination II, ushering in the Eemian, was spurred by a late spring 60°N insolation anomaly peaking at +45 W/m$^2$ at 129.5 ky b2k (Fig. 24a), the largest anomaly in at least the past 425 ky (Fig. 3, Hansen et al., 2007b). $CO_2$ and albedo forcings were mutually reinforcing. $CO_2$ began to rise before Antarctic $\delta^{18}O$, as deglaciation and warming began in the Northern Hemisphere.

Most of the total $CO_2$ rise was presumably from deep ocean ventilation in the Southern Ocean, aided by meltwater that slowed the AMOC and thus helped to warm the Southern Ocean.

The northern insolation anomaly fell rapidly, becoming negative at 123.8 ky b2k (Fig. 24a). Northern Hemisphere ice sheets must have increased intermittently while Southern Hemisphere ice was still declining, consistent with minor, growing ice rafting events C27, C27a, C27b and C26 and a sea level minimum during 125-121 ky b2k (Sec 2.1). High Eemian climate variability in the Antarctic (Pol et al., 2014) was likely a result of the see-saw relation with North Atlantic events.

$CO_2$ (Fig. 24c) remained at ~270 ppm for almost 15 ky as the positive insolation anomaly on the Southern Ocean (Fig. 24a) kept the deep ocean ventilated. Sea level in the Red Sea analysis (Grant et al., 2012) shown in Fig. 24f seems to be in decline through the Eemian, but that must be a combination of dating and sea level error, as numerous sea level analyses cited in section 2.1 and others (e.g., Chen at al., 1991; Stirling et al., 1998; Cutler et al., 2003), indicate high sea level throughout the Eemian and allow a possible late-Eemian maximum. Chen et al. (1991), using a U-series dating with $2\sigma$ uncertainty ±1.5 ky, found that the Eemian sea level high stand began between 132 and 129 ky b2k, lasted for 12 ky, and was followed by rapid sea level fall.

We assume that C26, the sharp cooling at 116.72 ky b2k in the NGRIP ice on the AICC2012 time scale, marks the end of fully interglacial Eemian conditions, described as 5e *sensu stricto* by Bauch and Erlenkeuser (2008). $\delta^{18}O$ in Antarctica was approaching a relative minimum (−46.7 per mil at EDML, see Fig. S19 for detail) and $CO_2$ was slowly declining at 263 ppm. In the next 300 years $\delta^{18}O$ increased to −45.2 and $CO_2$ increased by 13 ppm with lag ~1500 years, which we interpret as see-saw warming of the Southern Ocean in response to the C26-induced AMOC slowdown and resulting increased SMOC ventilation of $CO_2$.

Freshwater causing the C26 AMOC shutdown could not have been Greenland surface melt. Greenland was already 2000 years into a long cooling trend and the northern insolation anomaly was in the deepest minimum of the last 150 ky (Fig. 24a). Instead C26 was one event in a series, preceded by C27b and followed by C25, each a result of subsurface North Atlantic warming that melted ice shelves, causing ice sheets to discharge ice. Chapman and Shackleton (1999) did not find IRD from C26 in the mid-Atlantic, but Carlson et al. (2008) found a sharp increase in sediments near the southern tip of Greenland that they identified with C26.

We suggest that the Southern Hemisphere was the source for brief late-Eemian sea level rise. The positive warm-season insolation anomaly on the Southern Ocean and AMOC slowdown due to C26 added to Southern Ocean heat, causing ice shelf melt, ice sheet discharge, and sea level rise. Rapid Antarctica ice loss would cool the Southern Ocean and increase sea ice cover, which may have left telltale evidence in ice cores. Indeed, Masson-Delmotte et al. (2011) suggest that abrupt changes of $\delta^{18}O$ in the EDML and TALDICE ice cores (those most proximal to the coast) indicate a change in moisture origin, likely due to increased sea ice. Further analysis of Antarctic data for the late Eemian might help pinpoint the melting and help assess vulnerability of Antarctic ice sheets to ocean warming, but this likely will require higher resolution models with more realistic sea ice distribution and seasonal change than our present model produces.

Terrestrial records in Northern Europe reveal rapid end-Eemian cooling. Sirocko et al. (2005) find cooling of 3°C in summer and 5-10°C in winter in southern Germany, annual layering in a dry Eifel maar lake revealing a 468 year period of aridity, dust storms, bushfires, and a decline of thermophilous trees. Similar cooling is found at other German sites and La Grande Pile in France (Kuhl and Litt, 2003). Authors in both cases interpret the changes as due to a southward shift of the polar front in the North Atlantic corresponding to C26. Cooling of this magnitude in northern Europe and increased aridity are found by Brayshaw et al. (2009) and Jackson et al. (2015) in simulations with high resolution climate models forced by AMOC shutdown.

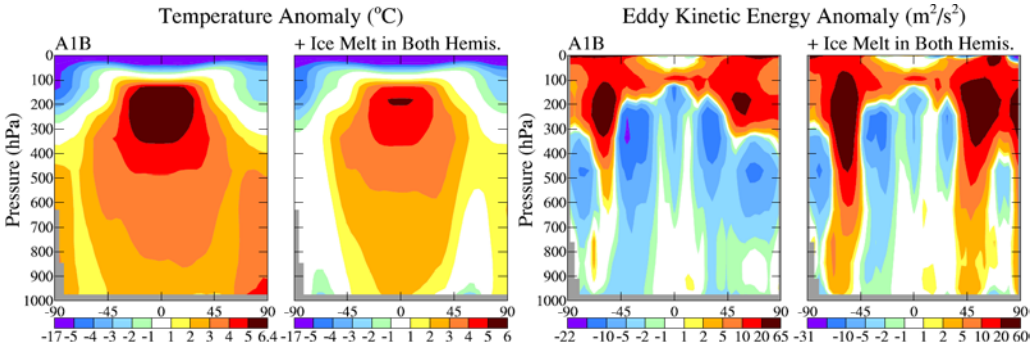


**Fig. 26.** Simulated zonal mean temperature and eddy kinetic energy in 2078-2082 relative to 1880-1920 base period for A1B scenario and A1B plus 2.5 m ice melt in each hemisphere (simulations of Section 3).

While reiterating dating uncertainties, we note that the cool period with reduced NADW formation identified in recent high resolution ocean core studies for Eirik Drift site MD03-2664 (Fig. 3) near Greenland (Irvali et al., 2012; Galaasen et al., 2014) at ~117 ky b2k has length similar to the 468-year cold stormy period found in a German lake core (Sirocko et al., 2005). The Eirik core data show a brief return to near-Eemian conditions and then a slow decline, similar to the oscillation in the NGRIP ice core at 116.72 ky b2k on the AICC2012 time scale.

The principal site of NADW formation may have moved from the GIN Seas to just south of Greenland at end of the Eemian. Southward shift of NADW formation and the polar front is consistent with the sudden, large end-Eemian cooling in the North Atlantic and northern Europe, while cooling in Southern European was delayed by a few millennia (Brauer et al., 2007). Thus end-Eemian mid-latitude climate was characterized by an increased zonal temperature gradient, an important ingredient for strengthening storms.

## 6 Impact of ice melt on storms

We can draw some conclusions about the effect of ice melt on winds and severe weather, despite limitations of our current climate model. Principal model limitations are its coarse resolution and unrealistic location of Northern Hemisphere deep water formation, this latter problem being likely related to the model's excessive Northern Hemisphere sea ice cover.

Despite these caveats, we have shown that the model realistically simulates zonal changes of sea level pressure in response to climate forcings. Specifically, the model yields a realistic trend to the positive phase of the Southern Annular Mode (SAM) in response to decrease of stratospheric ozone and increase of other GHGs (Fig. S17).

The modeled response of atmospheric pressure to the cooling effect of ice melt is large scale, tending to be of a zonal nature that should be handled by our model resolution. Freshwater injection onto the North Atlantic and Southern Oceans causes increase of sea level pressure at middle latitudes and decrease at polar latitudes (Figs. 13, S11). These pressure changes have implications for the strength of prevailing winds and for severe weather.

The robust increase of high pressure in the North Atlantic strengthens prevailing northeasterly winds blowing onto the Bahamas (Fig. 13). The Eemian-age chevron beach structures with consistent southwesterly direction throughout windward shores in the Bahamas (Sec. 2.2), with wave runup deposits at elevations as much as 20-40 m above today's sea level and reaching as far as a few kilometers inland, must have been formed by massive storms in the direction of the prevailing winds. Consistent increase of wind speed in the appropriate direction would contribute to creation of long wavelength, deep ocean waves that can scour the ocean floor as they reach the shallow near-shore region. The most extreme events probably required the combined effect of these increased prevailing winds and tropical storms, the latter nurtured by

the unusually warm tropical sea surface temperatures in the late Eemian and guided by the strong prevailing winds. On theoretical grounds, it is known that the higher low latitude sea surface temperatures of the late Eemian (Cortijo et al., 1999) would favor more powerful tropical storms (Emanuel, 1987). The zonal temperature gradient, warmer tropics and cooler high latitudes, was enhanced by low obliquity of Earth's spin axis in the late Eemian. Empirical evidence for intense Eemian storms includes standing forests of 8-10 m trees that were rapidly buried in shelf sand and preserved on Bermuda at elevations several meters above sea level (Hearty and Olson, 2011), as well as other evidence discussed in Sec. 2.2. The late Eemian is typically associated with a massive flux of oolitic shelf sediments mobilized in the offshore shelf environment and further transported by intense winds into enormous land-based dunes that dominate a majority of modern landscapes of the Bahamas archipelago (Hearty and Neumann, 2001).

Shutdown or substantial slowdown of the AMOC, besides possibly contributing to extreme end-Eemian events, will cause a more general increase of severe weather. This is shown by the change of zonal mean temperature and eddy kinetic energy in our simulations with and without ice melt (Fig. 26). Without ice melt, surface warming is largest in the Arctic (Fig. 26, left), resulting in a decrease of lower tropospheric eddy energy. However, the surface cooling from ice melt increases surface and lower tropospheric temperature gradients, and in stark contrast to the case without ice melt, there is a large increase of mid-latitude eddy energy throughout the midlatitude troposphere. The increase of zonal-mean midlatitude baroclinicity that we find (Fig. 26) is in agreement with the localized, N. Atlantic-centered increases in baroclinicity found in the higher resolution simulations of Jackson et al. (2015) and Brayshaw et al. (2009).

Increased baroclinicity produced by a stronger temperature gradient provides energy for more severe weather events. Many of the most memorable and devastating storms in eastern North America and western Europe, popularly known as superstorms, have been winter cyclonic storms, though sometimes occurring in late fall or early spring, that generate near-hurricane force winds and often large amounts of snowfall (Chapter 11, Hansen, 2009). Continued warming of low latitude oceans in coming decades will provide more water vapor to strengthen such storms. If this tropical warming is combined with a cooler North Atlantic Ocean from AMOC slowdown and an increase in midlatitude eddy energy (Fig. 26), we can anticipate more severe baroclinic storms. Increased high pressure due to cooler high latitude ocean (Fig. 13) can make blocking situations more extreme, with a steeper pressure gradient between the storm's low pressure center and the blocking high, thus driving stronger North Atlantic storms.

Large freshwater injection on the North Atlantic Ocean has a different impact on winds than freshwater injection on the Southern Ocean (Fig. 13). In the Southern Ocean the increased meridional temperature gradient increases the strength of the westerlies in all seasons at all longitudes. In the North Atlantic Ocean the increase of sea level pressure in the winter slows the westerlies (Fig. 13). Thus instead of a strong zonal wind that keeps cold polar air locked in the Arctic, there is a tendency for more cold air outbreaks to middle latitudes.

## 7 Modern data

### 7.1 Southern Ocean

The Southern Ocean, as the gateway to the global deep ocean, has exerted a powerful control over glacial/interglacial climate. However, the Southern Ocean's control over the Antarctic ice sheet, and thus global sea level, will be of greater concern to humanity.

Our model, due to moderately excessive mixing, may be less sensitive to freshwater forcing than the real world. Yet the model (Fig. 27a) indicates that a slowing of Antarctic Bottom Water Formation should already be underway, a conclusion consistent with transient tracer observations

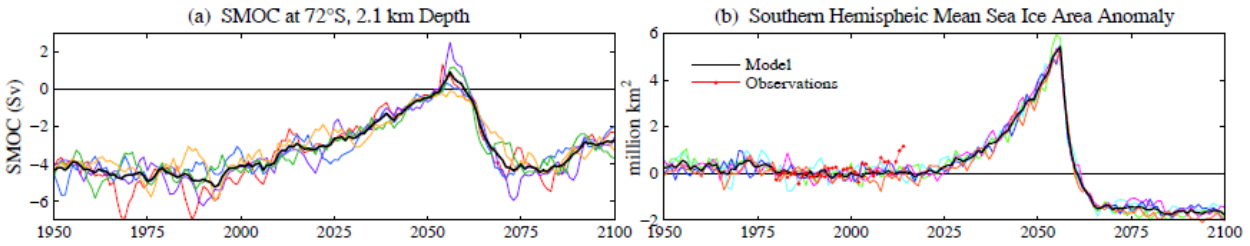


**Fig. 27.** (a) SMOC, the global meridional overturning circulation at 72°S, in climate model runs including freshwater injection around Antarctica at a rate 720 Gt/year in 2011, increasing with a 10-year doubling time, and half that amount around Greenland. SMOC diagnostic includes only the mean (Eulerian) term. (b) Annual-mean Southern Hemisphere sea ice area anomaly (relative to 1979-2000) in the five runs.

in the Weddell Sea by Huhn et al. (2013), which reveal a 15-21% reduction in the ventilation of Weddell Sea Bottom Water and Weddell Sea Deep Water over the period 1984-2008.

The Southern Ocean has significant control on release of ocean heat to space. In an extreme case, polynyas form in the dead of Antarctic winter, as upwelling warm water melts the sea ice and raises the air temperature by tens of degrees, increasing thermal radiation to space, thus serving as a valve that releases ocean heat. Today, as surface meltwater stabilizes the vertical water column, that valve is being partially closed. de Lavergne et al. (2014) relate the absence of large open ocean polynyas in recent decades to surface freshening.

Release of heat to the atmosphere and space, which occurs without the need for large open ocean polynyas, is slowed by increasing sea ice cover in response to increasing ice shelf melt (Bintanja et al., 2013). Schmidtko et al. (2014) and Roemmich et al. (2015) document changes in the Southern Ocean in recent decades, especially warming of Circumpolar Deep Water (CDW), which they and others (Jacobs et al., 2011; Rignot et al., 2013) note is the likely cause of increased ice shelf melt. Observations of ocean surface freshening and freshening of the water column (Rintoul, 2007; Jacobs and Giulivi, 2010) and deep ocean warming (Johnson et al., 2007; Purkey and Johnson, 2013) leave little doubt that these processes are occurring.

Loss of ice shelves that buttress the ice sheets potentially can lead to large sea level rise (Mercer, 1978). The ocean depths with largest warming in response to surface freshening (Fig. 16) encompass ice shelf grounding lines that exert the strongest restraining force (Jenkins and Doake, 1991). The impact of warming CDW varies among ice shelves because of unique geometries and proximity to the CDW current, but eventually a warming ocean will likely affect them all. As ice shelves weaken and ice sheet discharge increases the process is self-amplifying via the increasing freshwater discharge.

Weber et al. (2014) used ocean cores near Antarctica to study the deglacial evolution of the Antarctic ice sheet following the last glacial maximum. They identified eight episodes of large iceberg flux, with the largest flux occurring ~14,600 years ago, providing evidence of an Antarctic contribution to Meltwater Pulse 1A, when sea level rose an average of 3-5 m/century for a few centuries (Fairbanks, 1989). Ice sheets today may not have as much vulnerable ice as they had during the ice age. On the other hand, $CO_2$ and the global climate forcing are increasing much more rapidly today, and heat is being pumped into the ocean at a high rate via the resulting positive (incoming) planetary energy imbalance (Hansen et al., 2011; Roemmich et al., 2015) providing ample energy to spur increasing ice melt.

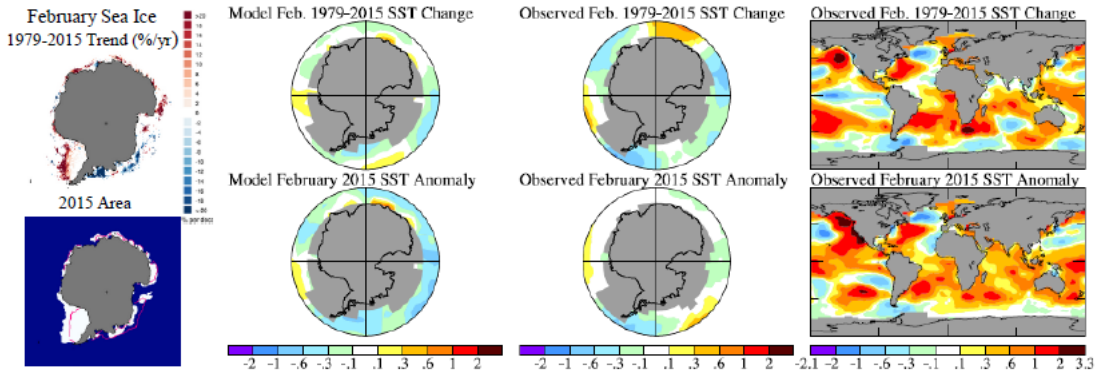


**Fig. 28.** Observed February sea ice extent (left); modeled and observed SST near Antarctica and global. Upper: 1979-2015 change based on local linear trend. Lower: 2015 anomaly relative to 1951-1980. Sea ice data is update of Fetterer et al. (2002), temperature data is update of Hansen et al. (2010).

### 7.2 Surface change today

Ocean surface cooling near Antarctica is emerging now (Fig. 28) and is large by midcentury (Fig. 20) in our simulations. The modeled sea ice increase is delayed relative to observations (Fig. 27b) for reasons noted below. However, freshwater effects already dominate over direct effects of $O_3$ and other GHGs. D. Thompson et al. (2011) suggested that $O_3$ depletion may account for Antarctic sea ice growth, but Sigmond and Fyfe (2014) found that all CMIP5 models yield decreasing sea ice in response to observed changes of $O_3$ and other GHGs. Ferreira et al. (2015) show that $O_3$ depletion yields a short time scale sea ice increase that is soon overtaken by warming and sea ice decrease with realistic GHG forcing. We conclude that these models are missing the dominant driver of change on the Southern Ocean: freshwater input.

Delay of our modeled sea ice increase relative to observations is probably related to difficulty in maintaining vertical stratification (Fig. S18), which in turn is a result of excess small scale mixing from a large background diapycnal diffusivity (0.3 $cm^2/s$) used to damp numerical noise, and the noise itself. Also sea ice increase occurred earlier in our experiments with freshwater spread over a broad area rather than being placed only in coastal gridboxes. In the real world half of the freshwater is calving (icebergs) that float some distance before melting, which may increase the effectiveness of the freshwater flux.

Depoorter et al. (2012) show that the proportion of calving varies strongly with location (see their Fig. 1). The Weddell and Ross Sea regions have large freshwater flux that is mainly icebergs. In contrast, the large Amundsen- Bellingshausen freshwater flux is mainly basal melt. This distinctive spatial variation may help account for observed sea ice increasing in the Weddell and Ross Seas, while decreasing in the Amundsen and Bellingshausen Seas. Note also that the Weddell Sea and Ross Sea sectors are respectively the regions where the EDML and TALDICE Antarctic ice cores are suggestive of expanding sea ice (Masson-Delmotte et al., 2011) at end-Eemian time.

Observations and our model concur in showing a “global warming hole” near the southern tip of Greenland. Drijfhout et al. (2012) find this feature in most models and conclude that it is a precursor of a weakening AMOC. Freshwater injection in our model makes this feature stronger. We note that this feature creates a blocking situation (Fig. 13) that may have consequences such as directing winter cold air outbreaks southward in Eastern North America. This and possible influence on weather patterns in late spring that initiate melt season conditions should be investigated with models that include the most realistic distribution of Greenland freshwater input (e.g., Fig. 1 of Velicogna et al., 2014) as well as melt from ice shelves and small ice caps.

### 7.3 Ice sheet mass loss and sea level rise

The fundamental question we raise is whether ice sheet melt in response to rapid global warming will be nonlinear and better characterized by a doubling time for its rate of change or whether more linear processes dominate. Hansen (2005, 2007) argued on heuristic grounds that ice sheet disintegration is likely to be nonlinear if climate forcings continue to grow, and that sea level rise of several meters is possible on a time scale of the order of a century. Given current ice sheet melt rates, a 20-year doubling rate produces multi-meter sea level rise in a century, while 10-year and 40-year doubling times require 50 years and 200 years, respectively.

The IPCC (2013) report increased estimates of sea level rise compared to prior IPCC reports, but scenarios they discuss are close to linear responses to the assumed rising climate forcing. The most extreme climate forcing (RCP8.5, 936 ppm $CO_2$ in 2100 and GHG forcing 8.5 W/m$^2$) is estimated to produce 0.74 m sea level rise in 2100 relative to the 1986-2005 mean sea level, with the "likely" range of uncertainty 0.52-0.98 m. IPCC (2013) also discusses semi-empirical estimates of sea level rise, which yield ~0.7-1.5 m for the RCP8.5 scenario, but preference is given to the model-based estimate of 0.52-0.98 m.

Empirical analyses are needed if we doubt the realism of ice sheet models, but semi-empirical analyses lumping multiple processes together may yield a result that is too linear. Sea level rises as a warming ocean expands, as water storage on continents changes (e.g., in aquifers and behind dams), and as glaciers, small ice caps, and the Greenland and Antarctic ice sheets melt. We must isolate the ice sheet contribution, because only the ice sheets threaten multi-meter sea level rise.

Hay et al. (2015) reanalyzed tide-gauge data for 1901-1990 in a probabilistic framework, including isostatic adjustment at each station, finding global sea level rise 1.2 ± 0.2 mm/year. Prior tide gauge analyses of 1.6-1.9 mm/year were inconsistent with estimates for each process, which did not add up to such a large value (IPCC, 2013). The reduced 20$^{th}$ century sea level rise alters perceptions of near-linear sea level rise (Fig. 13.3, IPCC, 2013). For example, Fig. 29 compares satellite altimetry data for 1993-2015 with 20$^{th}$ century sea level change, the latter obtained by multiplying a tide gauge analysis (Church and White, 2011) by the factor (0.78) required to yield sea level rise 1.2 mm/year for 1901-1990. Different tide gauge analyses could alter the shape of this curve, but the trend toward earlier times must be toward zero due to near-constancy of millennial sea level (IPCC, 2013).

Fig. 29 reveals an accelerating sea level rise, but it includes the effect of all processes affecting sea level and thus may understate the growth rate for ice sheet melt. Recent analysis of satellite gravity measurements (Velicogna et al., 2014) finds Greenland's mass loss in 2003-2013 to be 280 ± 58 Gt/yr[14], with mass loss accelerating by 25.4 ± 1.2 Gt/yr$^2$, and Antarctic mass loss 67 ± 44 Gt/year accelerating by 11 ± 4 Gt/year/year (Fig. S20). Their analysis, which is the source of the quantitative mass changes in the remainder of this section, is especially useful because it breaks down the mass changes on Greenland and Antarctica into several regions.

Reliability of the inferred mass loss in 2003-2013 is supported by comparison to surface mass balance studies in regions with little contribution from ice dynamics (Velicogna et al., 2014). Mass loss accelerations over 1992-2011 obtained via the mass budget method (Rignot et al., 2011) for Greenland (21.9 ± 1 Gt/year/year) and Antarctica (14.5 ± 2 Gt/year/year) are similar to results from gravity analysis for 2003-2013. A third approach, based on satellite radar altimetry, is consistent with the other two for mass loss from Greenland and West Antarctica (Shepherd et

[14] For comparison, our assumed freshwater injection of 360 Gt/year in 2011 with 10 year doubling yields an average mass loss 292 Gt/year for 2003-2013. Further, Velicogna et al. (2014) find an ice mass loss of 74 ±7 Gt/yr from nearby Canadian glaciers and ice caps with acceleration 10 ± 2 Gt/yr$^2$, and there is an unknown freshwater input from melting ice shelves. Thus our assumed Northern Hemisphere meltwater was conservative.

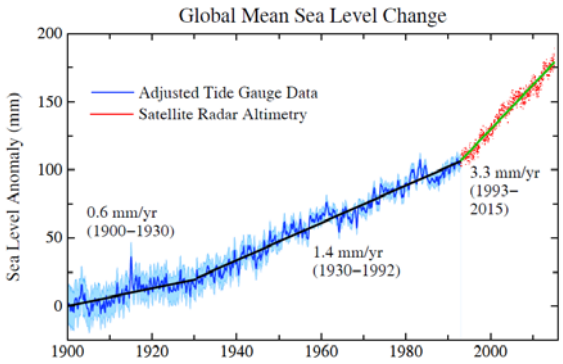


**Fig. 29.** Sea level change based on satellite altimetry data (Nerem et al., 2010, updated at http://sealevel.colorado.edu) and tide gauge data (Church and White, 2011) with the latter change rate multiplied by 0.78, as required to yield a mean 1901-1990 change rate 1.2 mm/year (Hay et al., 2015).

al., 2012), including the Amundsen Sea sector, which is the dominant contributor to Antarctic ice mass loss (Sutterley et al., 2014). Differences among techniques exist in East Antarctica, but mass changes there are small (Shepherd et al., 2012).

Mass loss acceleration for Greenland implies a doubling time of order 10 years, but this high rate may not continue. Greenland mass loss in 2003-2013 was affected by a tendency in 2007-2012 for summer high pressure over Greenland that contributed to melt acceleration (Fettweis, 2013; Bellflamme et al., 2015), especially in 2012 (Hanna et al., 2013). Extreme 2012 melt was associated an "atmospheric river" of warm moist air (Neff et al., 2014), a rare meteorological situation not representative of near-term expectations. Yet extreme events are a combination of slow climate change and infrequent weather patterns, and additional and more summer extreme events can be anticipated if global warming continues (Hansen et al., 2012).

The Antarctic situation, in contrast, is more threatening than suggested by continental mass loss. Net mass loss combines mass loss via ice streams and regions of net snow accumulation. Queen Maud Land is gaining 63 ± 6 Gt/year, accelerating 15 ± 1 Gt/year/year, but this mass gain may be temporary. Our simulations with increasing freshwater input indicate that circum-Antarctic cooling and sea ice increase eventually will limit precipitation reaching the continent.

Amundsen Sea glaciers are a gateway to West Antarctic ice with potential for several meters of sea level. Mass loss of the Amundsen Sea sector was 116 ± 6 Gt/year in 2003-2013, growing 13 ± 2 Gt/year/year (Velicogna et al., 2014; Rignot et al., 2014; Sutterley et al., 2014).

Totten glacier in East Antarctica fronts the Aurora Subglacial Basin, which has the potential for ~6.7 m of sea level (Greenbaum et al., 2015). Williams et al. (2011) find that warm modified Circumpolar Deep Water is penetrating the continental shelf near Totten beneath colder surface layers. Details of how warmer water reaches the ice shelf are uncertain (Khazendar et al., 2013), but, as in West Antarctica, the inland sloping trough connecting the ocean with the main ice shelf cavity (Greenbaum et al., 2015) makes Totten glacier susceptible to unstable retreat (Goldberg et al., 2009). Cook glacier, further east in East Antarctica, also rests on a submarine inland-sloping bed and fronts ice equivalent to 3-4 meters of sea level. The Velicogna et al. (2014) analysis of gravity data for 2003-2013 finds the Totten sector of East Antarctica losing 17 ± 4 Gt/year, with the loss accelerating by 4 ± 1 Gt/year/year, and the Victoria/Wilkes sector including Cook glacier losing 16 ± 5 Gt/year, with a small deceleration (2 ± 1 Gt/year/year).

Ice mass losses from Greenland, West Antarctica and Totten/Aurora basin in East Antarctica are growing nonlinearly with doubling times of order 10 years. Continued exponential growth at that rate seems unlikely for Greenland, and reduced mass loss in the past two years (Fig. S20) is consistent with a slower growth of the mass loss rate for Greenland. However, if GHGs continue to grow, the amplifying feedbacks in the Southern Ocean, including expanded sea ice and SMOC slowdown likely will continue to grow and facilitate increasing Antarctic mass loss.

### 7.4 The Anthropocene

The Anthropocene (Crutzen and Stoermer, 2000), the era in which humans have contributed to global climate change, is usually assumed to have begun in the past few centuries. Ruddiman (2003) suggested that it began earlier, with deforestation affecting $CO_2$ about 8000 years ago. Southern Ocean feedbacks considered in our present paper are relevant to that discussion.

Ruddiman (2003) assumed that 40 ppm of human-made $CO_2$ was needed to explain a 20 ppm $CO_2$ increase in the Holocene (Fig. 24c), because $CO_2$ decreased ~20 ppm, on average, during several prior interglacials. Such a large human source should have left an imprint on $\delta^{13}CO_2$ that is not observed in ice core $CO_2$ (Elsig, et al., 2009). Ruddiman (2013) suggests that $^{13}C$ was taken up in peat formation, but the required peat formation would be large and no persuasive evidence has been presented to support such a dominant role for peat in the glacial carbon cycle.

We suggest that Ruddiman overestimated the anthropogenic $CO_2$ needed to prevent decline of Antarctic temperature. The $CO_2$ decline in interglacial periods is a climate feedback: declining Southern Ocean temperature slows the ventilation of the deep ocean, thus sequestering $CO_2$. Avoidance of the cooling and $CO_2$ decline requires only human-made $CO_2$ forcing large enough to counteract the weak natural forcing trend, not the larger feedback-driven $CO_2$ changes in prior interglacials, because, if the natural forcings are counteracted, the feedback does not occur. The required human-made contribution to atmospheric $CO_2$ would seem to be at most ~20 ppm, but less if human-made $CO_2$ increased deep ocean ventilation. The smaller requirement on the human source and the low $\delta^{13}C$ content of deep-ocean $CO_2$ make the Ruddiman hypothesis more plausible, but recent carbon cycle models (Kleinen et al., 2015) have been able to capture $CO_2$ changes in the Holocene and earlier interglacials without an anthropogenic source.

Even if the Anthropocene began millennia ago, a fundamentally different phase, a Hyper-Anthropocene, was initiated by explosive 20$^{th}$ century growth of fossil fuel use. Human-made climate forcings now overwhelm natural forcings. $CO_2$, at 400 ppm in 2015, is off the scale in Fig. 24c. $CO_2$ climate forcing is a reasonable approximation of the net human forcing, because forcing by other GHGs tends to offset negative human forcings, mainly aerosols (IPCC, 2013). Most of the forcing growth occurred in the past several decades, and two-thirds of the 0.9°C global warming (since 1850) has occurred since 1975 (update of Hansen et al., 2010, available at http://www.columbia.edu/~mhs119/Temperature/).

Our analysis paints a different picture than IPCC (2013) for how this Hyper-Anthropocene phase is likely to proceed if GHG emissions grow at a rate that continues to pump energy at a high rate into the ocean. We conclude that multi-meter sea level rise would become practically unavoidable. Social disruption and economic consequences of such large sea level rise could be devastating. It is not difficult to imagine that conflicts arising from forced migrations and economic collapse might make the planet ungovernable, threatening the fabric of civilization.

This image of our planet with accelerating meltwater includes growing climate chaos and storminess, as meltwater causes cooling around Antarctica and in the North Atlantic while the tropics and subtropics continue to warm. Rising seas and more powerful storms together are especially threatening, providing strong incentive to phase down $CO_2$ emissions rapidly.

## 8 Summary Implications

Humanity faces near certainty of eventual sea level rise of at least Eemian proportions, 5-9 m, if fossil fuel emissions continue on a business-as-usual course, e.g., IPCC scenario A1B that has $CO_2$ ~700 ppm in 2100 (Fig. S21). It is unlikely that coastal cities or low-lying areas such as Bangladesh, European lowlands, and large portions of the United States eastern coast and northeast China plains (Fig. S22) could be protected against such large sea level rise.

Rapid large sea level rise may begin sooner than generally assumed. Amplifying feedbacks, including slowdown of SMOC and cooling of the near-Antarctic ocean surface with increasing sea ice, may spur nonlinear growth of Antarctic ice sheet mass loss. Deep submarine valleys in West Antarctica and the Wilkes Basin of East Antarctica, each with access to ice amounting to several meters of sea level, provide gateways to the ocean. If the Southern Ocean forcing (subsurface warming) of the Antarctic ice sheets continues to grow, it likely will become impossible to avoid sea level rise of several meters, with the largest uncertainty being how rapidly it will occur.

The Greenland ice sheet does not have as much ice subject to rapid nonlinear disintegration, so the speed at which it adds to 21st century sea level rise may be limited. However, even a slower Greenland ice sheet response is expected to be faster than carbon cycle or ocean thermal recovery times. Therefore, if climate forcing continues to grow rapidly, amplifying feedbacks will assure large eventual mass loss. Also with present growth of freshwater injection from Greenland, in combination with increasing North Atlantic precipitation, we already may be on the verge of substantial North Atlantic climate disruption.

Storms conjoin with sea level rise to cause the most devastating coastal damage. End-Eemian and projected 21st century conditions are similar in having warm tropics and increased freshwater injection. Our simulations imply increasing storm strengths for such situations, as a stronger temperature gradient caused by ice melt increases baroclinicity and provides energy for more severe weather events. A strengthened Bermuda High in the warm season increases prevailing northeasterlies that can help account for stronger end-Eemian storms. Weakened cold season sea level pressure south of Greenland favors occurrence of atmospheric blocking that can increase wintertime Arctic cold air intrusions into northern midlatitudes.

Effects of freshwater injection and resulting ocean stratification are occurring sooner in the real world than in our model. We suggest that this is an effect of excessive small scale mixing in our model that limits stratification, a problem that may exist in other models (Hansen et al., 2011). We encourage similar simulations with other models, with special attention to the model's ability to maintain realistic stratification and perturbations. This issue may be addressed in our model with increased vertical resolution, more accurate finite differencing method in ocean dynamics that reduces noise, and use of a smaller background diffusivity.

There are many other practical impacts of continued high fossil fuel emissions via climate change and ocean acidification, including irreplaceable loss of many species, as reviewed elsewhere (IPCC, 2013, 2014; Hansen et al., 2013a). However, sea level rise sets the lowest limit on allowable human-made climate forcing and $CO_2$, because of the extreme sensitivity of sea level to ocean warming and the devastating economic and humanitarian impacts of a multi-meter sea level rise. Ice sheet response time is shorter than the time for natural geologic processes to remove $CO_2$ from the climate system, so there is no morally defensible excuse to delay phase.out of fossil fuel emissions as rapidly as possible.

We conclude that the 2°C global warming "guardrail", affirmed in the Copenhagen Accord (2009), does not provide safety, as such warming would likely yield sea level rise of several meters along with numerous other severely disruptive consequences for human society and ecosystems. The Eemian, less than 2°C warmer than pre-industrial Earth, itself provides a clear indication of the danger, even though the orbital drive for Eemian warming differed from today's human-made climate forcing. Ongoing changes in the Southern Ocean, while global warming is less than 1°C, provide a strong warning, as observed changes tend to confirm the mechanisms amplifying change. Predicted effects, such as cooling of the surface ocean around Antarctica, are occurring even faster than modeled.

Our finding of global cooling from ice melt calls into question whether global temperature is the most fundamental metric for global climate in the 21st century. The first order requirement to

stabilize climate is to remove Earth's energy imbalance, which is now about +0.6 W/m$^2$, more energy coming in than going out. If other forcings are unchanged, removing this imbalance requires reducing atmospheric $CO_2$ from ~400 ppm to ~350 ppm (Hansen et al., 2008, 2013a).

The message that the climate science delivers to policymakers, instead of defining a safe "guardrail", is that fossil fuel $CO_2$ emissions must be reduced as rapidly as practical. Hansen et al. (2013a) conclude that this implies a need for a rising carbon fee or tax, an approach that has the potential to be near-global, as opposed to national caps or goals for emission reductions. Although a carbon fee is the sine qua non for phasing out emissions, the urgency of slowing emissions also implies other needs including widespread technical cooperation in clean energy technologies (Hansen et al., 2013a).

The task of achieving a reduction of atmospheric $CO_2$ is formidable, but not impossible. Rapid transition to abundant affordable carbon-free electricity is the core requirement, as that would also permit production of net-zero-carbon liquid fuels from electricity. The rate at which $CO_2$ emissions must be reduced is about 6%/year to reach 350 ppm atmospheric $CO_2$ by about 2100, under the assumption that improved agricultural and forestry practices could sequester 100 GtC (Hansen et al., 2013a). The amount of $CO_2$ fossil fuel emissions taken up by the ocean, soil and biosphere has continued to increase (Fig. S23), thus providing hope that it may be possible to sequester more than 100 GtC. Improved understanding of the carbon cycle and non-$CO_2$ forcings are needed, but it is clear that the essential requirement is to begin to phase down fossil fuel $CO_2$ emissions rapidly. It is also clear that continued high emissions are likely to lock-in continued global energy imbalance, ocean warming, ice sheet disintegration, and large sea level rise, which young people and future generations would not be able to avoid. Given the inertia of the climate and energy systems, and the grave threat posed by continued high emissions, the matter is urgent and calls for emergency cooperation among nations.

**Acknowledgments.** Completion of this study was made possible by a generous gift from The Durst Family to the Climate Science, Awareness and Solutions program at the Columbia University Earth Institute. That program was initiated in 2013 primarily via support from the Grantham Foundation for Protection of the Environment, Jim and Krisann Miller, and Gerry Lenfest and sustained via their continuing support. Other substantial support has been provided by the Flora Family Foundation, Dennis Pence, the Skoll Global Threats Fund, Alexander Totic and Hugh Perrine. We thank Anders Carlson, Elsa Cortijo, Nil Irvali, Kurt Lambeck, Scott Lehman, and Ulysses Ninnemann for their kind provision of data and related information. Support for climate simulations was provided by the NASA High-End Computing (HEC) Program through the NASA Center for Climate Simulation (NCCS) at Goddard Space Flight Center.

**References**

Abdalati, W., Krabill, W., Frederick, E., Manizade, S., Martin, C., Sonntag, J., Swift, R., Thomas, R., Yungel, J., and Koerner, R.: Elevation changes of ice caps in the Canadian Arctic Archipelago, J. Geophy. Res., 109, F04007, doi:10.1029/2003JF000045, 2004.

Adkins, J.F., Boyle, E.A., Keigwin, L., and Cortijo, E.: Variability of the North Atlantic thermohaline circulation during the last interglacial period, Nature, 390, 154-156, 1997.

Ahn, J., Brrok, E.J., Schmittner, A., and Kreutz, K.: Abrupt change in atmospheric $CO_2$ during the last ice age, Geophys. Res. Lett., 39, L18711, doi:10.1029/20`12GL053018, 2012.

Alley, R.B., Dupont, T.K., Parizek, B.R., Anandakrishnan, S., Lawson, D.E., Larson, G.J., and Evenson, E.B.: Outburst flooding and the initiation of ice-strem surges in response to climatic cooling: a hypothesis, Geomorphology, 75, 76-89, 2006.

Alvarez-Solas, J., Charbit, S., Ritz, C., Paillard, D., Ramstein, G., and Dumas, C.: Links between ocean temperature and iceberg discharge during Heinrich events, Nature Geosci., 3, 122-126, 2010.

Alvarez-Solas, J., Montoya, M., Ritz, C., Ramstein, G., Charbit, S., Dumas, C., Nisancioglu, K., Dokken, T., and Ganopolski, A.: Heinrich event 1: an example of dynamical ice-sheet reaction to oceanic changes, Clim.Past, 7, 1297-1306, 2011.

Alvarez-Solas, J., Robinson, A., Montoya, M., and Ritz, C.: Iceberg discharges of the last glacial period driven by oceanic circulation changes, Proc. Natl. Acad. Sci. USA, 110, 16350-16354, 2013.

Anderson, R.F., Ali, S., Bradtmiller, L.I., Nielsen, S.H.H., Fleisher, M., Andersen, B., and Burckle, L.: Wind-driven upwelling in the Southern Ocean and the deglacial rise in atmospheric $CO_2$, Science, 323, 1443-1448, 2009.
Antonov, J.I., Seidov, D., Boyer, T.P., Locarnini, R.A., Mishonov, A.V., Garcia, H.E., Baranova, O.K., Zweng, M.M., and Johnson, D.R..: World Ocean Atlas 2009, Vol. 2: Salinity. NOAA Atlas NESDIS 68. S. Levitus, Ed. U.S. Government Printing Office, Washington, D.C., 184 pp., 2010.
Archer, D.: Fate of fossil fuel $CO_2$ in geologic time, J. Geophys. Res., 110, C09505, doi:10.1029/2004JC002625, 2005.
Archer, D., Winguth, A., Lea, D., and Mahowald, N.: What caused the glacial/interglacial atmospheric $CO_2$ cycles?, 38(2), 159-189, 2000.
Bahr, D.B., Dyurgerov, M., and Meier, M.F.: Sea-level rise from glaciers and ice caps: a lower bound, Geophys. Res. Lett., 36, L03501, doi:10.1029/2008GL036309, 2009.
Bain, R.J., and Kindler, P.: Irregular fenestrae in Bahamian eolianites: a rainstorm-induced origin, J. Sedimen. Petrology, A64(1), 140-146, 1994.
Bard, E., Fairbanks, R.G., and Hamelin, B.: How accurate are the U-Th ages obtained by mass spectrometry on coral terraces?, in Kukla, G., and Went, E. (Eds.), Start of a Glacial, Springer-Verlag, Berlin, pp. 15-21, 1992.
Baringer, M.O., Johns, W.E., McCarthy, G., Willis, J., Garzoli, S., Lankhortst, M., Meinen, C.S., Send, U., Hobbs, W.R., Cunningham, S.A., Rayner, D., Smeed, D.A., Kanzow, T.O., Heimbach, P., Frajka-Williams, E., Macdonald, A., Dong, S., and Marotzke, J.:Meridional overturning circulation and heat transport observations in the Atlantic Ocean, in Stae of the Climate in 2012, Bull. Amer. Meteorol. Soc., 94(8), S65-S68, 2013.
Barletta, V.R., Sorensen, L.S., and Forsberg, R.: Scatter of mass changes estimates at basin scale for Greenland and Antarctica, Cryosphere, 7, 1411-1432, 2013.
Barreiro, M., Fedorov, A., Pacanowski, R., and Philander, S.G.: Abrupt climate changes: how freshening of the northern Atlantic affects the thermohaline and wind-driven oceanic circulations, Ann. Rev. Earth Planet. Sci., 36, 33-58, 2008.
Bauch, D., Holemann, J.A. Dmitrenko, I.A., Janout, M.A., Nikulina, A., Kirillov, S.A., Krumpen, T., Kassens, H., and Timokhov, L.: Impact of Siberian coastal polynyas on shelf-derived Arctic Ocean halocline waters, J. Geophys. Res., 117, C00G12, doi:10.1029/2011JC007282, 2012.
Bauch, H.A., and Erlenkeuser, H.: A “critical” climatic evaluation of the last interglacial (MIS 5e) records from the Norwegian Sea, Polar Res., 27, 135-151, 2008.
Bauch, H.A., and Kandiano, E.S.: Evidence for early warming and cooling in North Atlantic surface waters during the last interglacial, Paleoceanography, 22, PA1201, doi:10.1029/2005PA001252, 2007.
Bauch, H.A., Kandiano, E.S., and Helmke, J.P.: Contrasting ocean changes between the subpolar and polar North Atlantic during the past 135 ka, Geophys. Res. Lett., 39, L11604, doi:10.1029/2012GL051800, 2012.
Bazin, L., Landais, A., Lemieux-Dudon, B., Toye Mahamadou Kele, H., Veres, D., Parrenin, F., Martinerie, P., Ritz, C., Capron, E., Lipenkov, V., Loutre, M.F., Raynaud, D., Vinther, B., Svensson, A., Rasmussen, S.O., Severi, M., Blunier, T., Leuenberger, M., Fischer, H., Masson-Delmotte, V., Chappellaz, J., and Wolff, E.: An optimized multi-proxy, multi-site Antarctic ice and gas orbital chronology (AICC2012): 120-800 ka, Clim. Past, 9, 1715-1731, 2013.
Bellflamme, A., Fettweis, X., and Erpicum, M.: Recent summer Arctic atmospheric circulation anomalies in a historical perspective, The Cryosphere, 9, 53-64, 2015.
Berger, A.L.: Long-term variations of caloric insolation resulting from the Earth’s orbital elements, Quatern. Res., 9, 139-167, 1978.
Bintanja, R., van Oldenborgh, G.J., Drijfhout, S.S., Wouters, B., and Katsman, C.A.: Important role for ocean warming and increased ice-shelf melt in Antarctic sea-ice expansion, Nature Geosci., 6, 376-379, 2013.
Blanchon, P., Eisenhauer, A., Fietzke, J., and Liebetrau, V.: Rapid sea-level rise and reef back-stepping at the close of the last interglacial highstand, Nature, 458, 881-885, 2009.
Box, J.E., Fettweis, X., Stroeve, J.C., Tedesco, M., Hall, D.K., and Steffen, K.: Greenland ice sheet albedo feedback: thermodynamics and atmospheric drivers, Cryosphere, 6, 821-839. doi:10.5194/tc-6-821-2012, 2012.
Boyle, E.A.: Vertical oceanic nutrient fractionation and glacial/interglacial $CO_2$ cycles, Nature, 331, 55-56, 1988.
Brauer, A., Allen, J.R.M., Minigram, J., Dulski, P., Wulf, S., and Huntley, B.: Evidence for last interglacial chronology and environmental change from Southern Europe, Proc. Nat. Acad. Sci. USA, 104, 450-455, 2007.
Brayshaw, D.J., Woollings, T., and Vellinga, M.: Tropical and extratropical responses of the North Atlantic atmospheric circulation to a sustained weakening of the MOC, J. Clim., 22, 3146-3155, 2009.
Broecker, W.S.: Terminations, in Milankovitch and Climate, Part 2, eds. A. Berger et al., pp. 687-698, D. Reidel, Norwell, MA, 1984.
Broecker, W.S.: Salinity history of the northern Atlantic during the last deglaciation, Paleocean., 5, 459-467, 1990.
Broecker, W.S.: Abrupt climate change: causal constraints provided by the paleoclimate record, Earth Sci. Rev., 51, 137-154, 2000.

Broecker, W.S.: Massive iceberg discharges as triggers for global climate change, Nature, 372, 421-424, 2002.
Broecker, W.S.: Paleocean circulation during the last deglaciation: A bipolar seesaw?, Paleoceanography, 13, 119-121, 1998.
Broecker, W.S., Bond, G., Klas, M., Bonani, G., and Wolfli, W.: A salt oscillator in the glacial Atlantic? 1. The concept, Paleocean., 5, 469-477, 1990.
Buizert, C., Gkinis, V., Severinghaus, J.P., He, F., Lecavalier, B.S., Kindler, P., Leuenberger, M., Carlson, A.E., Vinther, B., Masson-Delmotte, V., White, J.W.C., Liu, Z., Otto-Bliesner, B., and Brook, E.J.: Greenland temperature response to climate forcing during the last deglaciation, Science, 345, 1177-1180, 2014.
Burke, A., and Robinson, L.F.: The Southern Ocean's role in carbon exchange during the last deglaciation, Science, 335, 557-561, 2012.
Capron, E., Landais, A., Lemieux-Dudon, B., Schilt, A., Masson-Delmotte, V., Buiron, D., Chappellaz, J., Dahl-Jensen, D., Johnsen, S., Leuenberger, M., Loulergue, L., and Oerter, H.: Synchronizing EDML and NorthGRIP ice cores using $\delta^{18}O$ of atmospheric oxygen ($\delta^{18}O_{atm}$) and $CH_4$ measurements over MIS5 (80-123 kyr), Quatern. Sci. Rev., 29, 222-234, 2010.
Carlson, A.E., Stoner, J.S., Donnelly, J.P., and Hillaire-Marcel, C.: Response of the southern Greenland ice sheet during the last two deglaciations, Geology, 36, 359-362, 2008.
Carton, J.A., and Hakkinen, S.: Introduction to: Atlantic Meridional Overturning Circulation (AMOC), Deep-Sea Res. II, 58, 1741-1743, 2011.
Chapman, M.R., and Shackleton, N.J.: Global ice-volume fluctuations, North Atlantic ice-rafting events, and deep-ocean circulation changes between 130 and 70 ka, Geology, 27, 795-798, 1999.
Chappell, J.: Sea level changes forced ice breakouts in the Last Glacial cycle: new results from coral terraces, Quatern. Sci. Rev., 21, 1229-1240, 2002.
Chen, J.H., Curran, H.A. White, B., and Wasserburg, G.J.: Precise chronology of the last interglacial period: $^{234}U$-$^{230}Th$ data from fossil coral reefs in the Bahamas, Geol. Soc. Amer. Bull, 103, 82-97, 1991.
Cheng, W., Chiang, J.C.H., and Zhang, D.: Atlantic Meridional Overturning Circulation (AMOC) in CMIP5 models: RCP and historical simulations, J. Clim., 26, 7187-7198, 2013.
Church, J.A. and White, N.J.: Sea level rise from the late 19$^{th}$ to the early 21$^{st}$ century, Surv. Geophys., 32, 585-602, 2011.
Clarke, G.K.C., Leverington, D.W., Teller, J.T., and Dyke, A.S.: Paleohydraulics of the last outburst flood from glacial Lake Agassiz and the 8200 B.P. cold event, Quat. Sci. Rev., 23(3-4), 389-407, 2004.
Copenhagen Accord: United Nations Framework Convention on Climate Change, Draft decision -- /CP.15 FCCC/CP/2009/L.7 18 December, 2009.
Cortijo, E., Lehman, S., Keigwin, L., Chapman, M., Paillard, D., and Labeyrie, L.: Changes in meridional temperature and salinity gradients in the North Atlantic Ocean (30°-72°N) during the last interglacial period, Paleoceanography, 14, 23-33, 1999.
Crowley, T.J.: North Atlantic deep water cools the Southern Hemisphere, Paleoceanography, 7, 489-497, 1992.
Crutzen, P.J. and Stoermer, F.F.: The "Anthropocene", IGBP Newsl., 41, 12-14, 2000.
Curran, H.A., Wilson, M.A., and Mylroie, J.E.: Fossil palm frond and tree trunk molds: occurrence and implications for interpretation of Bahamian Quaternary carbonate eolianites, in Park, L.E. and Freile, D. eds., Proc. 13$^{th}$ Symposium on the Geology of the Bahamas and Other Carbonate Regions: Gerace Reserch Center, San Salvador, Bahamas, pp. 183-195, 2008.
Cutler, K.B., Edwards, R.L., Taylor, F.W., Cheng, H., Adkins, J., Gallup, C.D., Cutler, P.M., Burr, G.S., Bloom, A.L.: Rapid sea-level fall and deep-ocean temperature change since the last interglacial period, Earth Planet. Sci. Lett., 206, 253-271, 2003.
Dansgaard, W., Johnsen, S.J., Clausen, H.B., Dahl-Jensen, D., Gudestrup, N.S., Hammer, C.U., Hvidberg, C.S., Steffensen, J.P., Sveinbjornsdottir, A.E., Jouzel, J., and Bond, G., Evidence for general instability of past climate from a 250-kyr ice-core record, Nature, 364, 218-220, 1993.
de Boer, B., Van de Wal, R.S.W., Bintanja, R., Lourens, L.J., and Tuenter, E.: Cenozoic global ice-volume and temperature simulations with 1-D ice-sheet models forced by benthic $\delta^{18}O$ records, Ann. Glaciol., 51, 23-33, 2010.
De Boyer Montegut, C., Madec, G., Fisher, A.S., Lazar, A., and Iudicone, D.: Mixed layer depth over the global ocean: an examination of profile data and a profile-based climatology, J. Geophys. Resl, 109, C12003, 2004.
De Lavergne, C.,Palter, J.B., Galbraith, E.D., Bernardello, R., and Marinov, I.: Cessation of deep convection in the open Southern Ocean under anthropogenic climate change, Nature Clim. Change, publ. online: 2 March, doi:10.1038/nclimate2132, 2014
Deporter, M.A., Bamber, J.L., Griggs, J.A., Lenaerts, J.T.M., Ligtenberg, S.R.M., van den Broeke, M.R., and Moholdt, G.: Calving fluxes and basal melt rates of Antarctic ice shelves, Nature, 502, 89-92, 2013.

Deschamps, P., Durand, N., Bard, E., Hamelin, B., Camoin, G., Thomas, A.L., Henderson, G.M., Okuno, J., and Yokoyama, Y.: Ice-sheet collapse and sea-level rise at the Bolling warming 14,600 years ago, Nature, 559-564, 2012.
DeVries, T. and Primeau, F.: Dynamically and observationally constrained estimates of water-mass distributions and ages in the global ocean, J. Phys. Oceanogr., 41, 2381-2401, 2011.
Ditlevsen, P.D., Anderson, KK., and Svensson, A.: The DO-climate events are probably noise induced: statistical investigation of the claimed 1470 years cycle, Clim. Past, 3, 129-134, 2007.
Drijfhout, S., Oldenborgh, G.J. and Cimatoribus, A.: Is a decline of AMOC causing the warming hole above the North Atlantic in observed and modeled warming patterns?, J. Climate, 25, 8373-8379, 2012.
Duplessy, J.C., Shackleton, N.J., Fairbanks, R.G., Labeyrie, L., Oppo, P., and Kallel, N.: Deep water source variations during the last climatic cycle and their impact on the global deep water circulation, Paleoceanography, 3, 343-360, 1988.
Durack, P.J., and Wijffels, S.E.: Fifty-year trends in global ocean salinities and their relationship to broad-scale warming, J. Clim., 23, 4342-4362, 2010.
Durack, P.J., Wijffels, S.E., Matear, R.J.: Ocean salinities reveal strong global water cycle intensification during 1950 to 2000, Science, 336, 455-458, 2012.
Dutton, A., and Lambeck, K.: Ice volume and sea level during the last interglacial, Science, 337, 216-219, 2012.
Edwards, R.L., Gallup, C.D., and Cheng, H.: Uranium-series dating of marine and lacustrine carbonates, in: Bourdon, B., Henderson, G.M., Lundstrom, C.C., and Turner, S.P., Eds., Uranium-series Geochemistry, Mineralogical Society of America, Washington, DC, 656 pp., 2003.
Elsig, J., Schmitt, J., Leuenberger, D., Schneider, R., Eyer, M., Leuenberger, M., Joos, F., Fischer, H., and Stocker, T.F.: Stable isotope constraints on Holocene carbon cycle changes from an Antarctic ice core, Nature, 461, 507-510, 2009.
Emanuel, K.A.: The dependence of hurricane intensity on climate, Nature, 326, 483-485, 1987.
Emanuel, K.: Increasing destructiveness of tropical cyclones over the past 30 years, Nature, 436, 686-688, 2005.
Engelbrecht, A.C., and Sachs, J.P.: Determination of sediment provenance at drift sites using hydrogen isotopes and unsaturation ratios in alkenones, Geochim. Cosmochim. Acta, 69, 4253-4265, 2005.
EPICA Community Members: One-to-one coupling of glacial climate variability in Greenland and Antarctica, Nature, 444, 195-198, 2006.
Fairbanks, R.G.: A 17,000-year glacio-eustatic sea-level record-influence of glacial melting rates on the younger rates on the Younger Dryas event and deep-ocean circulation. *Nature*, 342, 637-642, 1989.
Ferreira, D., Marshall, J., Bitz, C.M., Solomon, S., and Plumb, A.: Antarctic Ocean and sea ice response to ozone depletion: a two-time-scale problem, J. Clim., 28, 1206-1226, 2015.
Fetterer, F., Knowles, K., Meier, W., and Savoie, M.: Sea Ice index updated daily, National Snow and Ice Data Center, http://dx.doi.org/10.7265/N5QJ7F7W, Boulder, CO, USA, 2002.
Fettweis, X., Hanna, E., Lang, C., Belleflamme, A., Erpicum, M., and Gallee, H.: Important role of mid-tropospheric circulation in the recent surface melt increase over the Greenland ice sheet, Cryosphere, 7, 241-248, 2013.
Fichefet, T., Poncin, C., Goosse, H., Huybrechts, P., Janssens, I., and Le Treut, H.: Implications of changes in freshwater flux from the Greenland ice sheet for the climate of the 21st century, Geophys. Res. Lett., 30, 1911, doi:10.1029/2003GL017826, 2003.
Fischer, H., Schmitt, J., Luthi, D., Stocker, T.F., Tschumi, T., Parekh, P., Joos, F., Kohler, P., Volker, C., Gersonde, R., Barbante, C., Le Floch, M., Raynaud, D., and Wolff, E.: The role of Southern Ocean processes in orbital and millennial $CO_2$ variations – a synthesis, Quatern. Sci. Rev., 29, 193-205, 2010.
Fischer, H., Schmitt, J., Eggleston, S., Schneider, R., Elsig, J., Joos, F., Leuenberger, Stocker, T.F., Kohler, P., Brovkin, V., and Chappellaz, J.: Ice core-based isotopic constraints on past carbon cycle changes, PAGES, 23(1), 12-13, 2015.
Fluckiger, J., Knutti, R.,.and White, J.W.C.: Oceanic processes as potential trigger and amplifying mechanisms for Heinrich events, Paleoceanography, 21, PA2014, doi:10.1029/2005PA001204, 2006.
Fretwell, P., Pritchard, H.D., Vaughan, D.G., Bamber, J.L., Barrand, N.E., Bell, R., Bianchi, C., bingham, R.G., Blankenship, D.D., Casassa, G., Catania, G., Callens, D., Conway, H., Cook, A.J., Corr, H.F.J.Damaske, D., Damm, V., Ferraccioli, F., Forsberg, R., Fujita, S., Gim, Y., Gogineni, P., Griggs, J.A., Hindmarsh, R.C.A., Holmlund, P., Holt, J.W., Jacobel, R.W., Jenkins, A., Jokat, W., Jordan, T., King, E.C., et al.: Bedmap2: improved ice bed, surface and thickness datases for Antarctica, The Cryosphere, 7, 375-393, 2013.
Frieler, K., Clark, P.U., He, F., Buizert, C., Reese, R., Ligtenberg, S.R.M., van den Broeke, M.R., Winkelmann, R., and Levermann, A.: Consistent evidence of increasing Antarctic accumulation with warming, Nature Clim. Chan., 5, 348-352, 2015.
Fronval, T., and Jansen, E.: Rapid changes in ocean circulation and heat flux in the Nordic seas during the last interglacial period, Nature, 383, 806-810, 1996.

Galaasen, E.V., Ninnemann, U.S., Irvali, N., Kleiven, H.F., Rosenthal, Y., Kissel, C., Hodell, D., Rapid reductions in North Atlantic deep water during the peak of the last interglacial period, Science, 343, 1129-1132, 2014.
Gent, P.R., and McWilliams, J.C.: Isopycnal mixing in ocean circulation models, J. Geophys. Res., 20, 150-155, 1990.
Goldberg, D., Holland, D.M., and Schoof, C.: Grounding line movement and ice shelf buttressing in marine ice sheets, J.GEophys. Res., 114, F04026, 2009.
Govin, A., Michel, E., Labeyrie, Laurent, Waelbroeck, C., Dewilde, F., and Jansen, E.: Evidence for northward expansion of Antarctic Bottom Water mass in the Southern Ocean during the last glacial inception, Paleocenography, 24, PA1202, doi:10.1029/2008PA001603, 2009.
Grant, K.M., Rohling, E.J., Bar-Matthews, M., Ayalon, A., Medina-Elizade, M., Ramsey, C.B., Satow, C., and Roberts, A.P.: Rapid couplings between ice volume and polar temperature over the past 150,000 years, Nature, 491, 744-747, 2012.
Greenbaum, J.S., Blankenship, D.D., Young, D.A., Richter, T.G., Roberts, J.L., Aitken, A.R.A., Legresy, B., Schroeder, D.M., Warner, R.C., van Ommen, T.D., and Siegert, M.J.: Ocean access to a cavity beneath Totten Glacier in East Antarctica, Nature Geosci., publ. online 16 March doi:10.1038/NGEO2388, 2015.
Gregory, J.M., Dixon, K.W., Stouffer, R.J., Weaver, A.J., Driesschaert, E., Eby, M., Fichefet, T., Hasumi, H., Hu, A., Jungclaus, J.H., Kamenkovich, I.V., Levermann, A., Montoya, M., Murakami, S., Nawrath, S., Oka, A., Sokolov, A.P., and Thorpe, R.B.: A model intercomparison of changes in the Atlantic thermohaline circulation in response to increasing atmospheric $CO_2$ concentration, Geophys. Res. Lett., 32, L12703, doi:10.1029/2005GL023209, 2005.
Guillevic, M., Bazin, L., Landais, A., Kindler, P., Orsi, A., Masson-Delmotte, V., Blunier, T., Buchardt, S., Capron, E., Leuenberger, M., Martinerie, P., Prie, F., and Vinther, B.M.: Spatial gradients of temperature, accumulation and δ18O-ice in Greenland over a series of Dansgaard-Oeschger events, Clim. Past, 9, 1029-1051, 2013.
Guillevic, M., Bazin, L., Landais, A., Stowasser, C., Masson-Delmotte, V., Blunier, T., Eynaud, F., Falourd, S., Michel, E., Minster, B., Popp, T., Prie, F., and Vinther, B.: Evidence for a three-phase sequence during Heinrich Stadial 4 using a multiproxy approach based on Greenland ice core records, Clim. Past, 10, 2115-2133, 2014.
Hanna, E., Jones, J.M., Cappelen, J., Mernild, S.H., Wood, L., Steffen, K., and Huybrechts, P.: The influence of North Atlantic atmospheric and oceanic forcing effects on 1900-2010 Greenland summer climate and ice melt/runoff, Inter. J. Climatol., 33, 862-880, 2013.
Hansen, J., Sato, M., Ruedy, R., Lacis, A., and Oinas, V.: Global warming in the twenty-first century: an alternative scenario, Proc. Natl. Acad. Sci. USA, 97, 9875-9880, 2000.
Hansen, J.: A slippery slope: How much global warming constitutes "dangerous anthropogenic interference"? *Climatic Change*, 68, 269-279, 2005.
Hansen, J., Sato, M., Ruedy, R., Nazarenko, L., Lacis, A., Schmidt, G.A., Russell, G., Aleinov, I., Bauer, M., Bauer, S. Bell, N., Cairns, B., Canuto, V., Chandler, M., Cheng, Y., Del Genio, A., Faluvegi, G., Fleming, E., Friend, A., Hall, T., Jackman, C., Kelley, M., Kiang, N.Y., Koch, D., Lean, J., Lerner, J., Lo, K., Menon, S., Miller, R.L., Minnis, P., Novakov, T., Oinas, V., Perlwitz, J.P., Perlwitz, J., Rind, D., Romanou, A., Shindell, D., Stone, P., Sun, S., Tausnev, N., Thresher, D., Wielicki, B., Wong, T., Yao, M. and Zhang, S..: Efficacy of climate forcings, J. Geophys. Res., 110, D18104, doi:10.1029/2005JD005776, 2005.
Hansen, J.E.: Scientific reticence and sea level rise. Environ. Res. Lett., 2, 024002, doi:10.1088/1748-9326/2/2/024002, 2007.
Hansen, J., Sato, M., Ruedy, R., Kharecha, P., Lacis, A., Miller, R., Nazarenko, L.Lo, K., Schmidt, G.A., Russell, G., Aleinov, I., Bauer, S., Baum, E., Cairns, B., Canuto, V., Chandler, M., Cheng, Y., Cohen, A., Del Genio, A.,Faluvegi, G., Fleming, E., Friend, A., Hall, T., Jackman, C., Jonas, J., Kelley, M., Kiang, N.Y., Koch, D., Labow, G., Lerner, J., Menon, S., Novakov, T., Oinas, V., Perlwitz, J.P., Perlwitz, J., Rind, D., Romanou, A., Schmunk, R., Shindell, D., Stone, P., Sun, S., Streets, D., Tausnev, N., Thresher,D. Unger, N., Yao, M., and Zhang, S.: Climate simulations for 1880-2003 with GISS modelE. *Clim. Dyn.*, **29**, 661-696, doi:10.1007/s00382-007-0255-8, 2007a.
Hansen, J., Sato, M., Kharecha, P., Russell, G., Lea, D.W., and M. Siddall, M.: Climate change and trace gases. Phil. Trans. R. Soc. A, 36**5**, 1925-1954, doi:10.1098/rsta.2007.2052., 2007b.
Hansen, J., Sato, M., Ruedy, R., Kharecha, P., Lacis, A., Miller, R., Nazarenko, L.Lo, K., Schmidt, G.A., Russell, G., Aleinov, I., Bauer, S., Baum, E., Cairns, B., Canuto, V., Chandler, M., Cheng, Y., Cohen, A., Del Genio, A.,Faluvegi, G., Fleming, E., Friend, A., Hall, T., Jackman, C., Jonas, J., Kelley, M., Kiang, N.Y., Koch, D., Labow, G., Lerner, J., Menon, S., Novakov, T., Oinas, V., Perlwitz, J.P., Perlwitz, J., Rind, D., Romanou, A., Schmunk, R., Shindell, D., Stone, P., Sun, S., Streets, D., Tausnev, N., Thresher,D. Unger, N., Yao, M., and Zhang, S.: Dangerous human-made interference with climate: A GISS modelE study. *Atmos. Chem. Phys.*, **7**, 2287-2312, doi:10.5194/acp-7-2287, 2007c

Hansen, J., Sato, M., Kharecha, P., Beerling, D., Berner, R., Masson-Delmotte, V., Pagani, M., Raymo, M., Royer, D. and Zachos, J. Target Atmospheric $CO_2$: Where Should Humanity Aim? *Open Atmos Sci J*, 2, 217-231, 2008.
Hansen, J.: Storms of My Grandchildren, New York, Bloomsbury, 304 pp., 2009.
Hansen, J., Ruedy, R., Sato, M., and Lo, K.: Global surface temperature change, Rev. Geophys., 48, RG4004, doi:10.1029/2010RG00035, 2010.
Hansen, J., Sato, M., Kharecha, P., and von Schuckmann, K.: Earth's energy imbalance and implications. *Atmos. Chem. Phys.*, **11**, 13421-13449, doi:10.5194/acp-11-13421-2011, 2011.
Hansen, J., Sato, M., and R. Ruedy, 2012: Perception of climate change. *Proc. Natl. Acad. Sci.*, **109**, 14726-14727, E2415-E2423, doi:10.1073/pnas.1205276109, 2012.
Hansen, J., Kharecha, P., Sato, M., Masson-Delmotte, V., Ackerman, F., Beerling, D., Hearty, P.J., Hoegh-Guldberg, O., Hsu, S.-L., Parmesan, C., Rockstrom, J., Rohling, E.J., Sachs, J., Smith, P., Steffen, K., Van Susteren, L., von Schuckmann, K., and Zachos, J.C.: Assessing "dangerous climate change": Required reduction of carbon emissions to protect young people, future generations and nature, *PLOS ONE*, 8, e81648, doi:10.1371/journal.pone.0081648, 2013a.
Hansen, J.E., Sato, M., Russell, G., and Kharecha, P.: Climate sensitivity, sea level and atmospheric $CO_2$, Phil. Trans. Roy. Soc. A, 371, 20120294, http://dx.doi.org/10.1098/rsta.2012.0294 , 2013b.
Hansen, J., Kharecha, P. and Sato, M.: Climate forcing growth rates: Doubling down on our Faustian bargain. *Environ. Res. Lett.*, **8**, 011006, doi:10.1088/1748-9326/8/1/011006, 2013c.
Hay, C.C., Morrow, E., Kopp, R.E., and Mitrovica, J.X.: Probabilistic reanalysis of twentieth-century sea-level rise, Nature, 517, 481-484, 2015.
Hays, J.D., Imbrie, J., and Shackleton, N.J.: Variations in the Earth's orbit: pacemaker of the ice ages, Science, 194, 1121-1132, 1976.
Hearty, P.J.: Boulder deposits from large waves during the Last Interglaciation on North Eleuthera Island, Bahamas, *Quat. Res.*, 48, 326-338, 1997.
Hearty, P.J.: The geology of Eleuthera Island, Bahamas: A Rosetta stone of Quaternary stratigraphy and sea-level history, *Quat. Sci. Rev.*, 17, 333-355, 1998.
Hearty, P.J., and Kindler, P.: New perspectives on Bahamian geology, San Salvador Island, Bahamas, J. Coastal Res., 9(2), 577-594, 1993.
Hearty, P.J., Neumann, A.C., Kaufman, D.S.: Chevron ridges and runup deposits in the Bahamas from storms late in oxygen-isotope substage 5e, Quatern. Res. 50, 309-322, 1998.
Hearty, P.J., A.C. Neumann: Rapid sea level and climate change at the close of the Last Interglaciation (MIS 5e): evidence from the Bahama Islands, *Quat. Sci. Rev.*, 20, 1881-1895, 2001.
Hearty, P.J., J.T. Hollin, A.C. Neumann, M.J. O'Leary, M. McCulloch: Global sea-level fluctuations during the Last Interglaciation (MIS 5e), *Quat. Sci. Rev.*, 26, 2090-2112, 2007.
Hearty, P.J., and Olson, S.L.: Preservation of trace fossils and models of terrestrial biota by intense storms in mid-last interglacial (MIS 5c) dunes on Bermuda, with a model for development of hydrological conduits, Palaios, 26, 394-405, 2011.
Heinrich, H.: Origin and consequences of cyclic ice rafting in the northeast Atlantic Ocean during the past 130,000 years, Quaternary Res., 29, 142-152, 1988.
Hemming, S.R.: Heinrich events: massive late Pleistocene detritus layers of the North Atlantic and their global climate imprint, Rev. Geophys., 42, RG1005, doi:10.1029/2003RG000128, 2004.
Heuze, C., Heywood, K.J., Stevens, D.P., and Ridley, J.K.: Southern Ocean bottom water characteristics in CMIP5 models, Geophys. Res. Lett., 40, 1409-1414, doi:10.1002/grl.50287, 2013.
Heuze, C., Heywood, K.J., Stevens, D.P., and Ridley, J.K.: Changes in global ocean bottom properties and volume transports in CMIP5 models under climate change scenarios, J. Climate, doi:10.1175/JCLI-D-14-00381.1, in press.
Hu, A., Meehl, G.A., Han, W., and Yin, J.: Transient response of the MOC and climate to potential melting of the Greenland Ice Sheet in the 21st century, Geophys. Res. Lett., 36, L10707, doi:10.1029/2009GL037998, 2009.
Hu, A., Meehl, G.A., Han, W., and Yin, J.: Effect of the potential melting of the Greenland ice sheet on the meridional overturning circulation and global climate in the future, Deep-Sea Res. II, 58, 1914-1926, 2011.
Huhn, O., Rhein, M., Hoppema, M., van Heuven, S.: Decline of deep and bottom water ventilation and slowing down of anthropogenic carbon storage in the Weddell Sea, 1984-2011, Deep-Sea Res.I, 76, 66-84, 2013.
Huybrechts, P., Janssens, I., Poncin, C., and Fichefet, T.: The response of the Greenland ice sheet to climate changes in the 21st century by interactive coupling of an AOGCM with a thermomechanical ice-sheet model, Ann. Glaciol., 35, 409-415, 2002.
Intergovernmental Panel on Climate Change (IPCC): *Climate Change 2007: The Physical Science Basis*, Solomon, S., *et al.* eds., Cambridge University Press, 996 pp., 2007.

Intergovernmental Panel on Climate Change (IPCC): *Climate Change 2013*, Stocker, T., Dahe, Q., Plattner, G.K., *et al.*, eds., Cambridge University Press, 1535 pp., 2013. Also available: http://www.ipcc.ch/report/ar5/wg1/#.UlCweRCvHMM.

Intergovernmental Panel on Climate Change (IPCC): *Climate Change 2014: Impacts, Adaptation, and Vulnerability*, Field, C., Mach, K., Mastrandrea, M., Barros, R., eds., final draft, http://ipcc-wg2.gov/AR5/report/final-drafts/

Irvali, N., Ninnemann, U.S., Galaasen, E.V., Rosenthal, Y., Kroon, D., Oppo, D.W., Kleiven, H.F., Darling, K.F., and Kissel, C.: Rapid switches in subpolar hydrography and climate during the Last Interglacial (MIS 5e), Paleoceanography, 27, PA2207, doi:10.1029/2011PA002244, 2012.

Jackson, L.C., Kahana, R., Graham, T., Ringer, M.A., Woolings, T., Mecking, J.V., and Wood, R.A.: Global and European climate impacts of a slowdown of the AMOC in a high resolution GCM, Clim. Dyn., publ. online 11March, doi10.1007/s00382-015-2540-2, 2015.

Jacobs, S.S., and Giulivi, C.F.: Large multidecadal salinity trends near the Pacific-Antarctic continental margin, J. Clim., 23, 4508-4524, 2010.

Jacobs, S.S., Jenkins, A., Giulivi, C.F., and Dutrieux, P.: Stronger ocean circulation and increased melting under Pine Island Glacier ice shelf, Nature Geosci., 4, 519-523, 2011.

Jenkins, A., and Doake, C.S.M.: Ice-ocean interaction on Ronee Ice Shelf, Antarctica, J. Geophys. Res., 96, 791-813, 1991.

Johns, W.E., Baringer, M.O., Beal, L.M., Cunningham, S.A., Kanzow, T., Bryden, H.L., Hirschi, J.J.M., Marotzke, J., Meinen, C.S., Shaw, B., and Curry, R.: Continuous, array-based estimates of Atlantic Ocean heat transport at 26.5°N, J. Clim., 24, 2429-2449, 2011.

Johnson, G.C., Mecking, S., Sloyan, B.M., and Wijffels, S.E., Recent bottom water warming in the Pacific Ocean, J. Clim, 20, 5365-5375, 2007.

Jouzel, J., Masson-Delmotte, V., Cattani, O., Dreyfus, G., Falourd, S., Hoffmann, G., Minster, B., Nouet, J., Barnola, J.M., Chappellaz, J., Fischer, H., Gallet, J.C., Johnsen, S., Leuenberger, M., Loulergue, L., Luethi, D., Oerter, H., Parrenin, F., Raisbeck, G., Raynaud, D., Schilt, A., Schwander, J., Selmo, E., Souchez, R., Spahni, R., Stauffer, B., Steffensen, J.P., Stenni, B., Stocker, T.F., Tison, J.L., Werner, M., Wolff, E.W.: Orbital and millennial Antarctic climate variability over the past 800,000 years, Science, 317, 793-796, 2007.

Jungclaus, J.H., Haak, H., Esch, M., Roeckner, E., and Marotzke, J.: Will Greenland melting halt the thermohaline circulation?, Geophys. Res. Lett., 33, L17708, doi:10.1029/2006GL026815, 2006.

Kandiano, E.S., Bauch, H.A., and Muller, A.: Sea surface temperature variability in the North Atlantic during the last two glacial-interglacial cycles: comparison of faunal, oxygen isotopic, and Mg/Ca-derived records, Palaeogeography, Palaeoclimatology, Palaeoecology, 204, 145-164, 2004.

Keeling, R.F. and Stephens, B.B.: Antarctic sea ice and the control of Pleistocene climate instability, Paleoceanography, 16, 112-131, 2001.

Keigwin, L.D., and Jones, G.A.: Western North Atlantic evidence for millennial-scale changes in ocean circulation and climate, J. Geophys. Res., 99, 12397-12410, 1994.

Kent, D.V., and Muttoni, G.: Equatorial convergence of India and early Cenozoic climate trends, Proc. Natl. Acad. Sci. USA, 105, 16065-16070, 2008.

Khan, S.A., Kjaer, K.H., Bevis, M., Bamber, J.L., Wahr, J., Kjeldsen, K.K., Bjork, A.A., Korsgaard, N.J., Stearns, L.A., van den Broeke, M.R., Liu, L., Larsen, N.K., and Muresan, I.S.: Sustained mass loss of the northeast Greenland ice sheet triggered by regional warming, Nature C.im. Chan., 16 March, doi:10.1038/nclimate2161, 2014.

Khazendar, A., Schodlok, M.P., Fenty, I., Ligtenberg, S.R.M., Rignot, E., and van den Broeke, M.R.: Observed thinning of Totten Glacier is linked to coastal polynya variability, Nature Commun., 4:2857, doi:10.1038/ncomms3857, 2013.

Kindler, P. and Hearty, P.J.: Carbonate petrology as in indicator of climate and sea-level changes: new data from Bahamian Quaternary units, Sedimentology, 43, 381-399, 1996.

Kleinen, T., Brovkin, V., and Munhoven, G.: Carbon cycle dynamics during recent interglacials, Clim. Past Discuss., 11, 1945-1983, 2015.

Kleiven, H.F., Kissel, C., Laj, C., Ninnemann, U.S., Richter, T.O., and Cortijo, E.: Reduced North Atlantic Deep Water coeval with the glacial Lake Agassiz fresh water outburst, Science, 319, 60-64, 2008.

Kohler, P., Fischer, H., Munhoven, G., and Zeebe, R.E.: Quantitative interpretation of atmospheric carbon records over the last glacial termination, Global Biogeochem. Cycles, 19, GB4020, doi:10.1029/2004GB002345, 2005.

Kopp, R.E., Simons, F.J., Mitrovica, J.X., Maloof, A.C., and Oppenheimer, M.: Probabilistic assessment of sea level during the last interglacial stage, Nature, 462, 863-867, 2009.

Kuhl, N., and Litt, T.: Quantitative time series reconstruction of Eemian temperature at three European sites using pollen data, Veget. Hist. Archaeobot., 12, 205-214, 2003.

Lacis, A.A, Schmidt, G.A., Rind, D., and Ruedy, R.A.: Atmospheric $CO_2$: Principal control knob governing Earth's temperature. *Science*, **330**, 356-359, doi:10.1126/science.1190653, 2010.
Lacis, A.A., Hansen, J.E., Russell, G.L.,Oinas, V. and Jonas, J.: The role of long-lived greenhouse gases as principal LW control knob that governs the global surface temperature for past and future climate change. Tellus B, 65, 19734, doi:10.3402/tellusb.v65i0.19734, 2013.
Lambeck, K. and Chappell, J.: Sea level change through the last glacial cycle, Science, 292, 679-686, 2001.
Lambeck, K., Rouby, H., Purcell, A., Sun, Y., and Sambradge, M.: Sea level and global ice volumes from the Last Glacial Maximum to the Holocene, Proc. Natl. Acad. Sci. USA, 111, 15296-15303, 2014.
Land, L.S., Mackenzie, F.T., and Gould, S.J.: The Pleistocene history of Bermuda, Bull. Geol. Soc. Amer., 78, 993-1006, 1967.
Landais, A., Masson-Delmotte, V., Stenni, B., Selmo, E., Roche, D.M., Jouzel, J., Lambert, F., Guillevic, M., Bazin, L., Arzel, O., Vinther, B., Gkinis, V., and Popp, T.: A review of the bipolar see-saw from synchronized and high resolution ice core water stable isotope records from Greenland and East Antarctica, Quatern. Sci. Rev., 114, 18-32, 2015.
Large, W.G., McWilliams, J.C., and Doney, S.C.: Oceanic vertical mixing: a review and a model with a nonlocal boundary layer parameterization, Rev. Geophys., 32, 363-403, 1994.
Lea, D.W., Martin, P.A., Pak, D.K., and Spero, H.J.: Reconstructing a 350 ky history of sea level using planktonic Mg/Ca and oxygen isotope records from a Cocos Ridge core, Quatern. Sci. Rev., 21, 283-293, 2002.
LeGrande, A.N., Schmidt, G.A., Shindell, D.T., Field, C.V., Miller, R.L., Koch, D.M., Faluvegi, G., and Hoffmann, G.: Consistent simulations of multiple proxy responses to an abrupt climate change event, Proc. Natl. Acad. Sci. USA, 103, 837-842, 2006.
LeGrande, A.N. and Schmidt, G.A.: Ensemble, water isotope-enabled, coupled general circulation modeling insights into the 8.2 ka event, Paleoceanography, 23, PA3207, doi:10.1029/2008PA001610, 2008.
Lehman, S.J., Sachs, J.P., Crotwell, A.M., Keigwin, L.D., and Boyle, E.A.: Relation of subtropical Atlantic temperature, high-latitude ice rafting, deep water formation, and European climate 130,000-60,000 years ago, Quatern. Sci. Rev., 21, 1917-1924, 2002.
Levitus, S., and Boyer, T.P.: World ocean atlas 1994, vol. 4: Temperature, NOAA Atlas NESDIS 4, pp. 177, U.S. Government Printing Office, Washington, D.C., 1994.
Levitus, S., Antonov, J., and Boyer, T.P.: World ocean atlas 1994, vol. 3: Salinity, NOAA Atlas NESDIS 3, pp. 99, U.S. Government Printing Office, Washington, D.C., 1994.
Li, C., Battisti, D.S., Schrag, D.P., and Tziperman, E.: Abrupt climate shifts in Greenland due to displacements of the sea ice edge, Geophys. Res. Lett., 32, L19702, doi:10.1029/2005GL023492, 2005.
Li, C., Battisti, D.S., and Bitz, C.M.: Can North Atlantic sea ice anomalies account for Dansgaard-Oeschger climate signals?, J. Clim., 23, 5457-5475, 2010.
Lisiecki, L.E., and Raymo, M.E.: A Pliocene-Pleistocene stack of 57 globally distributed benthic $\delta^{18}O$ records, Paleoceanography, 20, PA1003, 2005. (http://www.lorraine-lisiecki.com/LR04_MISboundaries.txt)
Lozier, M.S.: Overturning in the North Atlantic, Ann. Rev. Mar. Sci., 4, 291-315, 2012.
Lumpkin, R., and Speer, K.: Global ocean meridional overturning, J. Phys. Oceanogr., 37, 2550-2562, 2007.
Luthi, D., Le Floch, M., Bereiter, B., Blunier, T., Barnola, J.M., Siegenthaler, U., Raynaud, D., Jouzel, J., Fischer, H., Kawamura, K., and Stocker, T.F.: High-resolution carbon dioxide concentration record 650,000-800,000 years before present, Nature, 453, 379-382, 2008.
MacAyeal, D.R.: Binge/purge oscillations of the Laurentide ice-sheet as a cause of the North-Atlantic's Heinrich events, Paleoceanography, 8(6), 775-784, 1993.
Manabe, S. and Stouffer, R.J.: Multiple-century response of a coupled ocean-atmosphere model to an increase of atmospheric carbon dioxide, J. Climate, 7, 5-23, 1994.
Manabe, S. and Stouffer, R.J.: Simulation of abrupt climate change induced by freshwater input to the North Atlantic Ocean, Nature, 378, 165-167, 1995.
Marcott, S.A., Clark, P.U., Padman, L., Klinkhammer, G.P., Springer, S.R., Liu, Z., Otto-Bliesner, B.L., Carlson, A.E., Ungerer, A., Padman, J., He,. F., Cheng, J. and Schmittner, A.: Ice-shelf collapse from subsurface warming as a trigger for Heinrich events, Proc. Natl. Acad. Sci. USA, doi/10.1073/pnas.1104772108, 2011.
Marcott, S.A., Bauska, T.K., Buizert, C., Steig, E.J., Rosen, J.L., Cuffey, K.M., Fudge, T.J., Severinghaus, J.P., Ahn, J., Kalk, M.L., McConnell, J.R., Sowers, T., Taylor, K.C., White, J.W.C., Brook, E.J.: Centennial-scale changes in the global carbon cycle during the last deglaciation, Nature, 514, 616-619, 2014.
Marshall, G.J.: Trends in the Southern Annular Mode from observations and reanalyses, J. Clim., 16, 4134-4143, 2003.
Marshall, J. and Speer, K.: Closure of the meridional circulation through Southern Ocean upwelling, Nature Geosci., 5, 171-180, 2012.

Martin, J.H. and Fitzwater, S.E.: Iron deficiency limits phytoplnnkton growth in the north-east Pacific subarctic, Nature, 331, 341-343, 1988.
Martinez-Garcia, A., Sigman, D.M., Ren, H., Anderson, R., Straub, M., Hodell, D., Jaccard, S., Eglinton, T.I., and Haug, G.H.: Iron fertilization of the subantarctic ocean during the last ice age, Science, 343, 1347-1350, 2014.
Martinson, D.G., Pisias, N.G., Hays, J.D., Imbrie, J., Moore, T.C., and Shackleton, N.J.: Age dating and the orbital theory of the ice ages: development of a high-resolution 0 to 300,000-year chronostratigraphy, Quatern. Res., 27, 1-29, 1987.
Masson-Delmotte, V., Jouzel, J., Landais, A., Stievenard, M., Johnsen, S.J., White, J.W.C., Werner, M., Sveinbjornsdottir, A., and Fuhrer, K.: GRIP deuterium excess reveals rapid and orbital-scale changes in Greenland moisture origin, Science, 309, 118-121, doi10.1126/science.1108575, 2005.
Masson-Delmotte, V., Dreyfus, G., Braconnot, P., Johnsen, S., Jouzel, J., Kageyama, M, Landais, A., Loutre, M.F., Nouet, J., Parrenin, F., Raynaud, D., Stenni, B., and Tuenter, E.: Past temperature reconstructions from deep ice cores: relevance for future climate change, Clim. Past, 2, 145-165, 2006.
Masson-Delmotte, V., Stenni, B., Pol, K., Braconnot, P., Cattani, O., Falourd, S., Kageyama, M., Jouzel, J., Landais, A., Minster, B., Barnola, J.M., Chappellaz, M., Krinner, G., Johnsen, S., Röthlisberger, R., Hansen, J., Mikolajewicz, U., and Otto-Bliesner, B.: EPICA Dome C record of glacial and interglacial intensities. *Quat. Sci. Rev.*, **29**, 113-128, doi:10.1016/j.quascirev.2009.09.030, 2010.
Masson-Delmotte, V., Buiron, D., Ekaykin, A., Frezzotti, M., Gallee, H., Jouzel, J., Krinner, G., Landais, A., Motoyama, H., Oerter, H., Pol, K., Pollard, D., Ritz, C., Schlosser, E., Sime, L.C., Sodemann, H., Stenni, B., Uemura, R., and Vimeux, F.: A comparison of the present and last interglacial periods in six Antarctic ice cores, Clim. Past, 7, 397-423, 2011.
Masson-Delmotte, V., Schulz, M., Abe-Ouchi, A., Beer, J., Ganopolski, A., Gonzalez Rouco, J.F., Jansen, E., Lambeck, K., Luterbacher, J., Naish, T., Osboorn, T., Otto-Bliesner, B., Quinn, T., Ramexh, R. Rojas, M. Shao, X., and Timmermann, A.: Information from paleoclimate Archives. In: Climate Change 2013: The Physical Basis, Contribution of Working Group I to the Fifth Assessment Report of the Intergovernmental Panel on Climate Change [Stocker, T.F., Qin, D., Plattner, G.-K., Tignor, M., Allen, S.K., Boschung, J., Nauels, A., Xia, Y., Bex, V., and Midgley, P.M. (eds.)}, Cambridge Univesity Press, Cambridge, United Kingdom, 2013.
McCulloch, M.T. and Esat, T.: The coral record of last interglacial sea levels and sea surface temperatures, Chem. Geol., 169, 107-129, 2000.
Menviel, L., Joos, F., and Ritz, S.P.: Simulating atmospheric $CO_2$, $^{13}C$ and the marine carbon cycle during the last glacial-interglacial cycle: possible role for a deepening of the mean remineralization depth and an increase in the oceanic nutrient inventory, Quatern. Sci. Rev., 56, 46-68, 2012.
Mercer, J.H.: West Antarctic ice sheet and $CO_2$ greenhouse effect: a threat of disaster, Nature, 271, 321-325, 1978.
Miller, R.L., Schmidt, G.A., Nazarenko, L.S., Tausnev, N., Bauer, S.E., Del Genio, A.D., Kelley, M., Lo, K.K., Ruedy, R., Shindell, D.T., Aleinov, I., Bauer, M., Bleck, R., Canuto, V., Chen, Y.-H., Cheng, Y., Clune, T.L., Faluvegi, G., Hansen, J.E., Healy, R.J., Kiang, N.Y., Koch, D., Lacis, A., LeGrande, A.N., Lerner, J., Menon, S., Oinas, V., Pérez García-Pando, C., Perlwitz, J.P., Puma, M., Rind, D., Romanou, A., Russell, G., Sato, M., Sun, S., Tsigaridis, K., Unger, N., Voulgarakis, A., Yao, M.-S., and Zhang, J.: CMIP5 historical simulations (1850-2012) with GISS ModelE2. *J. Adv. Model. Earth Syst.*, **6**, no. 2, 441-477, doi:10.1002/2013MS000266, 2014.
Morlighem, M., Rignot, E., Mouginot, J., Seroussi, H., and Larour, E.:Deeply incised submarine glacial valleys beneath the Grenland ice sheet, Nature Geosci., 7, 418-422, 2014.
Munk, W. and Wunsch, C.: Abyssal recipes II: energetics of tidal and wind mixing, Deep-Sea Res. I, 45, 1977-2010, 1998.
Neff, W., Compo, G., Ralph, F.M., and Shupe, M.D.: Continental heat anomalies and the extreme melting of the Greenland ice surface in 2012 and 1989, J. Geophys. Res.Atmos., 119, 6520-6536, 2014.
Nerem, R.S., Chanmber, D.P., Choe, C., and Mitchum, G.T.: Estimating mean sea level change from the TOPEX and Jason altimeter missions, Marine Geodesy, 33(S1), 435-446, 2010.
Neumann, A.C., and Hearty, P.J.: Rapid sea-level changes at the close of the last interglacial (substage 5e) recorded in Bahamian island geology, Geology 24, 775-778, 1996.
Neumann, A.C., and MacIntyre, I.: Reef response to sea level rise: keep-up, catch-up or give-up, Proc. 5th International Coral Reef Congress, Tahiti, 3, 105-110, 1985.
Neumann, A.C., and Moore, W.S.: Sea-level events and Pleistocene coral ages in the northern Bahamas, Quatern. Res., 5, 215-224, 1975.
NGRIP (North Greenland Ice Core Project members): High-resolution record of Northern Hemisphere climate extending into the last interglacial period: Nature, 4341, 147-151, 2004.
Ohkouchi, N., Eglinton, T.I., Keigwin, L.D., and Hayes, J.M.:Spatial and temporal offsets between proxy records in a sediment drift, Science, 298, 1224-1227, 2002.
Ohmura, A.: Completing the world glacier inventory, Ann. Glaciology, 50 (53), 144-148, 2009.

Ohshima, K.I., Fukamachi, Y., Williams, G.D., Nihashi, S., Roquet, F., Kitade, Y., Tamura, T., Hirano, D., Herraiz-Borreguero, L., Field, I., Hindell, M., Aoki, S., and Watasuchi, M.: Antarctic bottom water production by intense sea-ice formation in the Cape Darnley polynya, Nature Geosci., 6, 235-240, 2013.

O'Leary, M.J., Hearty, P.J., Thompson, W.G., Raymo, M.E., Mitrovica, J.X., and Webster, J.M.: Ice sheet collapse following a prolonged period of stable sea level during the last interglacial, Nature Geosci., publ. online 28 July, doi:10.1038/NGEO1890, 2013.

Oppo, D.W., McManus, J.F., and Cullen, J.L.: Evolution and demise of the last interglacial warmth in the subpolar North Atlantic, Quaternary Sci. Rev., 25, 3268-3277, 2006.

Orsi, A.H., Johnson, G.C., and Bullister, J.L.: Circulation, mixing, and production of Antarctic bottom water, Progr. Oceanogr., 43, 55-109, 1999.

Paillard, D.: Glacial cycles: toward a new paradigm, Rev. Geophys., 39, 325-346, 2001.

Palaeosens Project members, Rohling, E.J. et al.: Making sense of palaeoclimate sensitivity. *Nature*, **491**, 683-691, doi:10.1038/nature11574, 2012.

Paolo, F.S., Fricker, H.A., and Padman, L.: Volume loss from Antarctic ice shelves is accelerating, Sciencexpress, sciencemag.org/content/early/recent/26March2015/Page8/10.1126/science.aaa0940, 2015.

Parrenin, F., Masson-Delmotte, V., Kohler, P.Raynaud, D., Paillard, D., Schwander, Barbante, C., Landais, A., Wegner, A., and Jouzel, J.: Synchronous change of atmospheric $CO_2$ and Antarctic temperature during the last deglacial warming, Science, 339, 1060-1063, 2013.

Pedro, J.B., Rasmussen, S.O., and van Ommen, T.D.: Tightened constraints on the time-lag between Antarctic temperature and $CO_2$ during the last deglaciation, Clim. Past, 8, 1213-1221, 2012.

Peltier, W.R. and Fairbanks, R.G.: Global glacial ice volume and Last Glacial Maximum duration from an extended Barbados sea level record. Quartern Sci Rev, 25, 3322-3337, 2006.

Petersen, S.V., Schrag, D.P., and Clark, P.U.: A new mechanism for Dansgaard-Oeschger cycles, Paleoceanography, 28, 24-30, 2013.

Pol, K., Masson-Delmotte, V., Cattani, O., Debret, M., Falourd, S., Jouzel, J., Landais, A., Minster, B., Mudelsee, M., Schulz, M., and Stenni, B.: Climate variability features of the last interglacial in the East Antarctic EPICA Dome C ice core, Geophys. Res. Lett., 41, 4004-4012, doi:10.1002/2014GL059561, 2014.

Pollard, D., DeConto, R.M., and Alley, R.B.: Potential Antarctic ice sheet retreat driven by hydrofracturing and ice cliff failure, Earth Planet. Sci. Lett., 412, 112-121, 2015.

Pritchard, H.D., Ligtenberg, S.R.M., Fricker, H.A., Vaughan, D.G., van den Broeke, M.R., and Padman, L.: Antarctic ice-sheet loss driven by basal melting of ice shelves, Nature, 484, 502-505, 2012.

Purkey, S.G., and Johnson, G.S.: Antarctic bottom water warming and freshening: contributions to sea level rise, ocean freshwater budgets, and global heat gain, J. Clim., 26, 6105-6122, 2013.

Rahmstorf, S.: Rapid climate transitions in a coupled ocean-atmosphere model, Nature, 372, 82-85, 1994.

Rahmstorf, S.: Bifurcations of the Atlantic thermohaline circulation in response to changes in the hydrological cycle, Nature, 378, 145-149, 1995.

Rahmstorf, S.: On the freshwater forcing and transport of the Atlantic thermohaline circulation. Clim. Dynam., 12, 799-811, 1996.

Rasmussen, T.L., Oppo, D.W., Thomsen, E., and Lehman, S.J.: Deep sea records from the southeast Labrador Sea: ocean circulation changes and ice-rafting events during the last 160,000 years, Paleoceanography, 18,(1), 1018, doi:10.1029/2001PA000736, 2003.

Rasmussen, S.O., Bigler, M., Blockley, S.P., Blunier, T., Buchardt, S.L., Clausen, H.B., Cvijanovic, I., Dahl-Jensen, D., Johnsen, S.J., Fischer, H., Gkinis, V., Guillevic, M., Hoek, W.Z., Lowe, J.J., Pedro, J.B., Popp, T., Seierstad, I.K., Steffensen, J.P., Svensson, A.M., Vallelonga, P., Vinther, B.M., Walker, M.J.C., Wheatley, J.J., and Winstrup, M.: A stratigraphic framework for abrupt climatic changes during the Last Glacial period based on three synchronized Greenland ice-core records: refining and extending the INTIMATE event stratigraphy, Quatern. Sci. Rev., 106, 14-28, 2014.

Raven, J.A., and Falkowski, P.G.: Oceanic sinks for atmospheric $CO_2$, Plant Cell Environ., 22, 741-755, 1999.

Raymo, M.E.: The timing of major climate terminations, Paleocean. 12, 577-585, 1997.

Rayner, D., Hirschi, J.J.-M., Kanzow, T., Johns, W.E., Wright, P.G., Frajka-Williams, E., Bryden, H.L., Meinen, C.S., Baringer, M.O., Marotzke, J., Beal, L.M., Cunningham, S.A., Monitoring the Atlantic meridional overturning circulation, Deep Sea Res. II, 58, 1744-1753, 2011.

Rignot, E., and Jacobs, S.S.: Rapid bottom melting widespread near Antarctic ice sheet grounding lines, Science, 296, 2020-2023, 2002.

Rignot, E. and Steffen, K.: Channelized bottom melting and stability of floating ice shelves, Geophys. Res. Lett., 35, L02503, doi:10.1029/2007GL031765, 2008.

Rignot, E., Velicogna, I., van den Broeke, M.R., Monaghan, A., and Lenaerts, J.T.M.: Acceleration of the contribution of the Greenland and Antarctic ice sheets to sea level rise, Geophys. Res. Lett., 38, L05503, 2011.

Rignot, E., Jacobs, S., Mouginot, J., and Scheuchl, B.: Ice shelf melting around Antarctica, Science, publ. online 13 June, 10.1126/science.1235798, 2013.
Rignot, E., Mouginot, J., Morlighem, M., Seroussi, H., and Scheuchl, B.: Widespread, rapid grounding line retreat of Pine Island, Thwaites, Smith, and Kohler glaciers, West Antarctica, from 1992 to 2011, Geophys. Res. Lett., 41(10), 3502-3509, 2014.
Rinterknecht, V., Jomelli, V., Brunstein, D., Favier, V., Masson-Delmotte, V., Bourles, D., Leanni, L, Schlappy, R.: Unstable ice stream in Greenland during the Younger Dryas cold event, Geology, 42, 759-762, 2014.
Rintoul, S.: Rapid freshening of Antarctic Bottom Water formed in the Indian and Pacific oceans, Geophys. Res. Lett., 34, L06606, doi:10.1029/2006GL028550, 2007.
Robinson, A., Calov, R., and Ganopolski, A.: Multistability and critical thresholds of the Greenland ice sheet, Nature Clim. Change, publ. online: 11 March 2012, doi:10.1038/NCLIMATE1449, 2012.
Roche, D., Paillard, D., and Cortijo, E.: Constraints on the duration and freshwater release of Heinrich event 4 through isotope modelling, Nature, 432, 379-382, 2004.
Roemmich, D., Church, J., Gilson, J., Monselesan, Sutton, P., and Wijffels, S.: Unabated planetary warming and its ocean structure since 2006, Nature Clim. Chan., 5, 240-245, 2015.
Rohling, E.J., Grant, K., Hemleben, Ch., Siddall, M., Hoogakker, B.A.A., Bolshaw, M., Kucera, M.: High rates of sea-level rise during the last interglacial period, *Nat Geosci*, 1, 38-42, 2008.
Rohling, E.J., Grant, K., Bolshaw, M., Roberts, A., Siddall, M., Hemleben, C., and Kucera, M.: Antarctic temperature and global sea level closely coupled over the past five glacial cycles, Nature Geosci., 2, 500-504, 2009.
Ruddiman, W.F.: The atmospheric greenhouse era began thousands of years ago, Clim. Change, 61, 261-293, 2003.
Ruddiman, W.F.: The Anthropocene, Ann. Rev. Earth Plan.. Sci., doi:10.1146/annurev-earth-050212-123944, 2013.
Russell, G.L., Miller, J.R., and Rind, D.: A coupled atmosphere-ocean model for transient climate change studies, Atmos. Ocean, 33, 683-730, 1995.
Ruth, U., Barnola, J.M., Beer, J., Bigler, M., Blunier, T. Castellano, E., Fischer, H., Fundel, F., Huybrechts, P., Kaufmann, P., Kipfstuhl, S., Lambrecht, A., Morganti, A., Oerter, H., Parrenin, F., Rybak, O., Severi, M., Udisti, R., Wilhelms, F., and Wolff, E.: EDML1: a chronology for the EPICA deep ice core from Dronning Maud Land, Antarctica, over the last 150 000 years, Clim. Past, 3, 549-574, 2007.
Rye, C.D., Naveira Garabato, A.C., Holland, P.R., Meredith, M.P., Norser, A.J.G., Hughes, C.W., Coward, A.C., and Webb, D.J.: Rapid sea-level rise along the Antarctic margins in response to increased glacial discharge, Nature Geosci., published online: 31 August 2014, doi:10.1038/NGEO2230
Sachs, J.P., and Lehman, S.J.: Subtropical North Atlantic temperatures 60,000-30,000 years ago, Science, 286, 756-759, 1999.
Sato, M., J.E. Hansen, M.P. McCormick, and J.B. Pollack: Stratospheric aerosol optical depths, 1850-1990. *J. Geophys. Res.*, **98**, 22987-22994, doi:10.1029/93JD02553, 1993.
Schilt, A., Baumgartner, M., Schwander, J., Buiron, D., Capron, E., Chappellaz, J., Loulergue, L., Schupach, S., Spahni, R., Fischer, H., and Stocker, T.F.: Atmospheric nitrous oxide during the last 140,000 years, Earth Planet. Sci. Lett., 300, 33-43, 2010.
Schmidt, G.A., Ruedy, R., Hansen, J., Aleinov, I., Bell, N., Bauer, M., Bauer, S., Cairns, B., Canuto, V., Cheng, Y., Del Genio, A., Faluvegi, G., Friend, A.D., Hall, T.M., Kelley, M., Kiang, N.Y., Koch, D., Lacis, A.A., Lerner, J., Lo, K.K., Miller, R.L., Nazarenko, L., Oinas, V., Perlwitz, J.P., Perlwitz, J., Rind, D., Romanou, A., Russell, G.L., Sato, M., Shindell, D.T., Stone, P.H., Sun, S., Tausnev, N., Thresher, D., Yao, M.S.: Present day atmospheric simulations using GISS modelE: comparison to in-situ, satellite and reanalysis data, J. Climate, 19, 153-192, 2006.
Schimidtko, S., Heywood, K.J., Thompson, A.F., and Aoki, S.: Multidecadal warming of Antarctic waters, Science, 346, 1227-1231, 2014.
Schmitt, J., Schneider, R., Elsig, J., Leuenberger, D., Lourantou, A., Chappellaz, J., Kohler, P., Joos, F., Stocker, T.F., Leuenberger, M., and Fischer, H.: Carbon isotope constraints on the deglacial $CO_2$ rise from ice cores, Science, 336, 711-714, 2012.
Schmittner, A., Latif, M., and Schneider, B.: Model projections of the North Atlantic thermohaline circulation for the 21st century assessed by observations, Geophys. Res. Lett., 32, L23710, doi:10.1029/2005GL024368, 2005.
Scholz, D., and Mangini, A.: How precise are U-series coral ages?, Cosmochim. Acta, 71, 1935-1948, 2007.
Schulz, M.: On the 1470-year pacing of Dansgaard-Oeschger warm events, Paleoceanography, 17(2), 1014, 10.1029/2000PA000571, 2002.
Shaffer, G., Olsen, S.M., and Bjerrum, C.J.: Ocean subsurface warming as a mechanism for coupling Dansgaard-Oeschger climate cycles and ice-rafting events, Geophys. Res. Lett., 31(24), L24202, doi:`10.1029/2004GL020968, 2004.

Shakun, J.D., Clark, P.U., He, F., Marcott, S.A., Mix, A.C., Liu, Z., OttoBliesner, B., Schmittner, A., and Bard, E.: Global warming preceded by increasing carbon dioxide concentrations during the last deglaciation, Nature, 484, 49-54, 2012.

Sheen, K.L., Naveira Garabato, A.C., Brearley, J.A., Meredith, M.P., Polzin, K.L., Smeed, D.A., Forryan, A., King, B.A., Sallee, J.B., St.Laurent, L., Thurnherr, A.M., Toole, J.M., Waterman, S.N., and Watson, A.J.: Eddy-induced variability in Southern Ocean abyssal mixing on climatic timescales, Nature Geosci., 7, 577-582, 2014.

Shepherd, A., Ivins, E.R., Geruo, A., Barletta, V.R., Bentley, M.J., Bettadpur, S., Briggs, K.H., Bromwich, D.H., Forsberg, R., Galin, N., et al.: A reconciled estimate of ice-sheet mass balance, Science, 338, 1183-1189, 2012.

Sigman, D.M., and Boyle, E.A.: Glacial/interglacial variations in atmospheric carbon dioxide, Nature, 407, 859-869, 2000.

Sigmond, M. and Fyfe, J.C.: The Antarctic ice response to the ozone hole in climate models, 27, 1336-1342, 2014

Sirocko, F., Seelos, K., Schaber, K., Rein, B., Dreher, F., Diehl, M., Lehne, R., Jager, K., Krbetshek, M., and Degering, D.: A late Eemian aridity pulse in central Europe during the last glacial inception, Nature, 436, 833-836, 2005.

Skinner, L.C., Fallon, S., Waelbroeck, Michel, E., and Barker, S.: Ventilation of the deep Southern Ocean and deglacial $CO_2$ rise, Science, 328, 1147-1151, 2010.

Solomon, S., Daniel, J.S., Sanford, T.J., Murphy, D.M., Plattner, G.K., Knutti, R., Friedlingstein, P.: Persistence of climate changes due to a range of greenhouse gases, Proc. Natl. Acad. Sci. USA, 107, 18354-18359, 2010.

Srokosz, M., Baringer, M., Bryden, H., Cunningham, S., Delowrth, T., Lozier, S., Marotzke, J., and Sutton, R.: Past, present, and future changes in the Atlantic meridional overturning circulation, Bull. Amer. Meteorol. Soc., 93, 1663-1676, 2012.

Stenni, B., Buiron, D., Frezzotti, M., Albani, S., Barbante, C., Bard, E., Barnola, J.M., Baroni, M., Baumgartner, M., Bonazza, M., et al.: Expression of the bipolar see-saw in Antarctic climate records during the last deglaciation, Nature Geosci., 4, 46-49, 2011.

Stirling, C.H., Esat, T.M., Lambeck, K., and McCulloch, M.T.: Timing and duration of the last interglacial: evidence for a restricted interval of widespread coral reef growth, Earth Planet. Sci. Lett., 160, 745-762, 1998.

Stocker, T.F.: The seesaw effect, Science, 282, 61-62, 1998.

Stocker, T.F., and Johnsen, S.J.: A minimum thermodynamic model for the bipolar seesaw, Paleoceanography, 18, no. 4, 1087, doi:10.1029/2003PA000920, 2003.

Stocker, T.F., and Wright, D.G.: Rapid transitions of the ocean's deep circulation induced by changes in surface water fluxes, Nature, 351, 729-732, 1991.

Sutterley, T., Velicogna, I., Rignot, E., Mouginot, J., Flament, T., van den Broeke, M., van Wessem, J.M., and Reijmer, C.H.: Mass loss of the Amundsen Sea Embayment of West Antarctica from four independent techniques, Geophys. Res. Lett., 4(23), 8421-8428, 2014.

Swingedouw, D., Braconnot, P., Delecluse, P., Guilyardi, E. and Marti, O.: Quantifying the AMOC feedbacks during a $2\times CO_2$ stabilization experiment with land-ice melting, Clim. Dyn., 29, 521-534, 2007.

Swingedouw, D., Mignot, J., Braconnot, P., Mosquet, E., Kageyama, M., and Alkama, R.: Impact of freshwater release in the North Atlantic under different climate conditions in an OAGCM, J. Climate, 22, 6377-6403, 2009.

Swingedouw, D., Rodehacke, C.B., Olsen, S.M., Menary, M., Gao, Y., Mikolajewicz, and Mignot, J.: On the reduced sensitivity of the Atlantic overturning to Greenland ice sheet melting in projections: a multi-model assessment, Clim. Dyn., published online 26 August doi 10.1007/s00382-014-2270-x, 2014.

Taft, W.H., Arrington, F., Haimoritz, A., MacDonald, C., and Woolheater, C.: Lithification of modern carbonate sediments at Yellow Bank, Bahamas, Bull Marine Sci. Gulf Caribbean, 18, 762-828, 1968.

Talley, L.D.: Closure of the global overturning circulation through the Indian, Pacific, and Southern Oceans, Oceanography, 26, 80-97, 2013.

Tedesco, M., Fettweis, X., Mote, T., Wahr, J., Alexander, P., Box, J., and Wouters, B., Evidence and analysis of 2012 Greenland records from spaceborne observations, a regional climate model and reanalysis data, Cryosphere Disc., 6, 4939-4976, 2012.

Thompson, D.W.J., Solomon, S., Kushner, P.J., England, M.H., Grise, K.M., and Karoly, D.J.: Signatures of the Antarctic ozone hole in Southern Hemisphere surface climate change, Nature Geosci., 4, 741-749, 2011.

Thompson, W.G., Curran, H.A., Wilson, M.A., White, B.: Sea-level oscillations during the last interglacial highstand recorded by Bahamas corals, Nature Geosci., 4, 684-687, 2011.

Thompson, W.G., and Goldstein, S.L.: Open-system coral ages reveal persistent suborbital sea-level cycles, Science, 308, 401-404, 2005.

Thornalley, D.J.R., Barker, S., Becker, J., Hall, I.R., and Knorr, G.: Abrupt changes in deep Atlantic circulation during the transition to full glacial conditions, Paleoceanography, 28, 253-262, 2013.

Toggweiler, J.R.: Variation of atmospheric $CO_2$ by ventilation of the ocean's deepest water, Paleoceanography, 14, 571-588, 1999.

Toggweiler, J.R., Russell, J.L., and Carson, S.R.: Midlatitude westerlies, atmospheric $CO_2$, and climate change during the ice ages, Paleoceanography, 21, PA2005, doi:10.1029/2005PA001154, 2006.
Tormey, B.R.: Run over, run up, and run out: a storm wave origin for fenestral porosity in last interglacial eolianites of the Bahamas, Geological Society of America, 64th Annual Meeting, Session 12, 19-20 MarchTschumi, T., Joos, F., Gehlen, M., and Heinze, C.: Deep ocean ventilation, carbon isotopes, marine sedimentation and the deglacial $CO_2$ rise, Clim. Past, 7, 771-800, 2011.
United States National Climate Assessment (USNCA), http://nca2014.globalchange.gov/, 2014.
Vacher, H.L., and Rowe, M.P.: Geology and hydrogeology of Bermuda, in Geology and Hydrogeology of Carbonate Islands, Vacher, H.L., and Quinn, T. (Eds.), Devel. Sedimentol., 54, 35-90, Elsevier, 1997.
Vaughan, D.G., Bamber, J.L., Giovinetto, M., Russell, J., and Cooper, A.P.R.: Reassessment of net surface mass balance in Antarctica, J. Clim., 12, 933-946, 1999.
Velicogna, I., Sutterley, T.C., and van den Broeke, M.R.: Regional acceleration in ice mass loss from Greenland and Antarctica using GRACE time-variable gravity data, Geophys. Res. Lett., 41, 8130-8137, doi10.1002/2014GL061052, 2014.
Veres, D., Bazin, L., Landais, A., Toye Mahamadou kele, H., Lemieux, B., Parrenin, F., Martinerie, P., Blayo, E., Blunier, T., Capron, E., Chappellaz, J. Rasmussen, S.O., Severi, M., Svensson, A., Vinther, B., and Wolff, E.W., The Antarctic ice core chronology (AICC2012): an optimized multi-parameter and multi-site dating approach for the last 120 thousand years, Clim. Past, 9, 1733-1748, 2013.
Visbeck, M., Marshall, J., Haine, T., and Spall, M.: Specification of eddy transfer coefficients in coarse resolution ocean circulation models, J. Phys. Oceanogr., 27, 381-402, 1997.
Vizcaino, M., Mikolajewicz, U., Groger, M., Maier-Reimer, E., Schurgers, G. and Winguth, A.M.E.: Long-term ice sheet-climate interactions under anthropogenic greenhouse forcing simulated with a complex Earth System Model, Clim. Dyn., 31, 665-690, 2008.
Wanless, H.R., and Dravis, J.J.: Carbonate Environments and Sequences of Calcos Platform. Field Trip Guidebook T374, 28th International Geological Congress, American Geophysical Union, 75 pp., 1989.
Watson, A.J. and Garabato, A.C.N.: The role of Southern Ocean mixing and upwelling in glacial-interglacial atmospheric $CO_2$ change, Tellus, 58B. 73-87, 2006.
Weaver, A.J., Eby, M., Kienast, M., and Saenko, O.A.: Response of the Atlantic meridional overturning circulation to increasing atmospheric $CO_2$: sensitivity to mean climate state, Geophys. Res. Lett., 34, L05708, doi:10.1029/2006GL028756, 2007.
Weber, M.E., Clark, P.U., Kuhn, G., Timmermann, A., Sprenk, D., Gladstone, R., Zhang, X., Lohmann, G., Menviel, L., Chikamoto, M.O., Friedrich, T., and Ohlwein, C.: Millennial-scale variability in Antarctic ice-sheet discharge during the last deglaciation, Nature, 510, 134-138, 2014.
White, B., Curran, H.A., and Wilson, M.A.: Bahamian coral reefs yield evidence of a brief sea-level lowstand during the last interglacial, Carbonates and Evaporites, 13, 10-22, 1998.
Williams, G.D., Meijers, A.J.S., Poole, A., Mathiot, P., Tamura, T., and Klocker, A.: Late winter oceanography off the Sabrina and BANZARE coast (117-128°E), East Antarctica, Deep-Sea Res. II, 58, 1194-1210, 2011.
Wilson, M.A., Curran, H.A., and White, B.: Paleontological evidence of a brief sea-level event during the last interglacial, Lethaia, 31, 241-250, 1998.
Wunsch, C.: What is the thermohaline circulation?, Science, 298, 1179-1180, 2002.
Wunsch, C.: Quantitative estimate of the Milankovitch-forced contribution to observed Quaternary climate change, Quatern. Sci. Rev., 23, 1001-1012, 2004.
Wunsch, C., and Ferrari, R., Vertical mixing, energy, and the general circulation of the oceans, Ann. Rev. Fluid Mech, 36, 281-314, 2004.
Yokoyama, Y., Esat, T.M., and Lambeck, K.: Coupled climate and sea-level changes deduced from Huon Peninsula coral terraces of the last ice age, Earth Planet. Sci. Lett., 193, 579-587, 2001.
Zachos, J., Pagani, M., Sloan, L., Thomas, E., and Billups, K.: Trends, rhythms, and aberrations in global climate 65 Ma to present. *Science*, 292, 686-693, 2001.

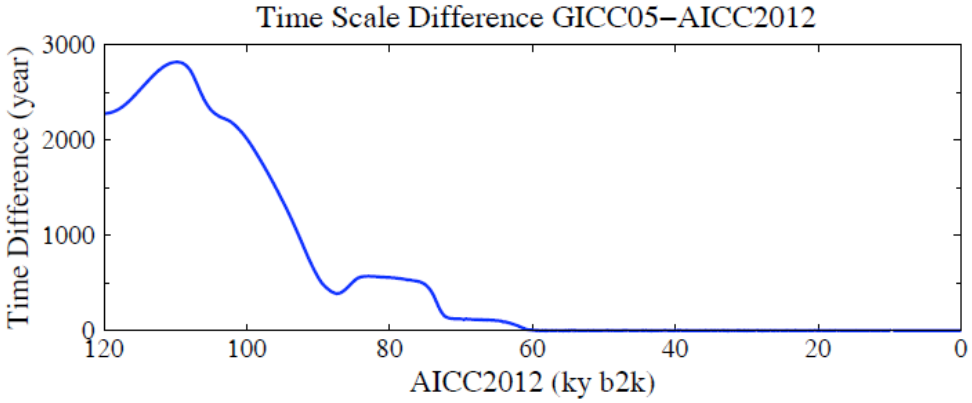


**Fig. S1.** Difference between the GICC2005modelext and AICC2012 time scales (Bazin et al., 2013; Veres et al., 2013; Rasmussen et al., 2014; Seierstad et al., 2014).

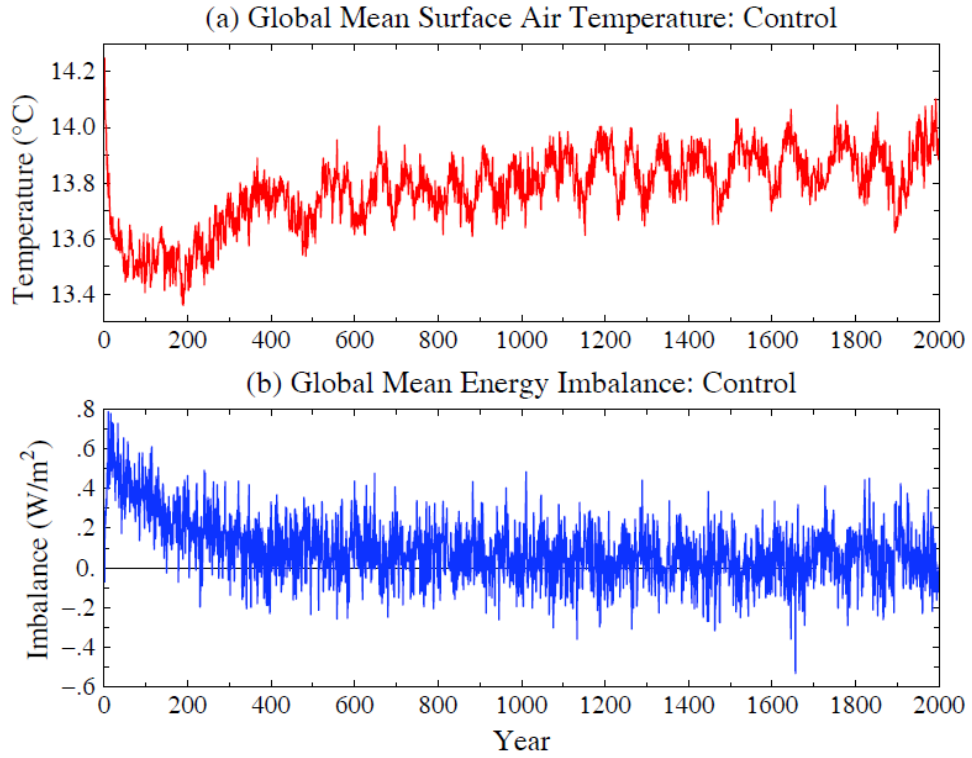


**Fig. S2.** Surface air temperature and planetary energy imbalance in the control run.

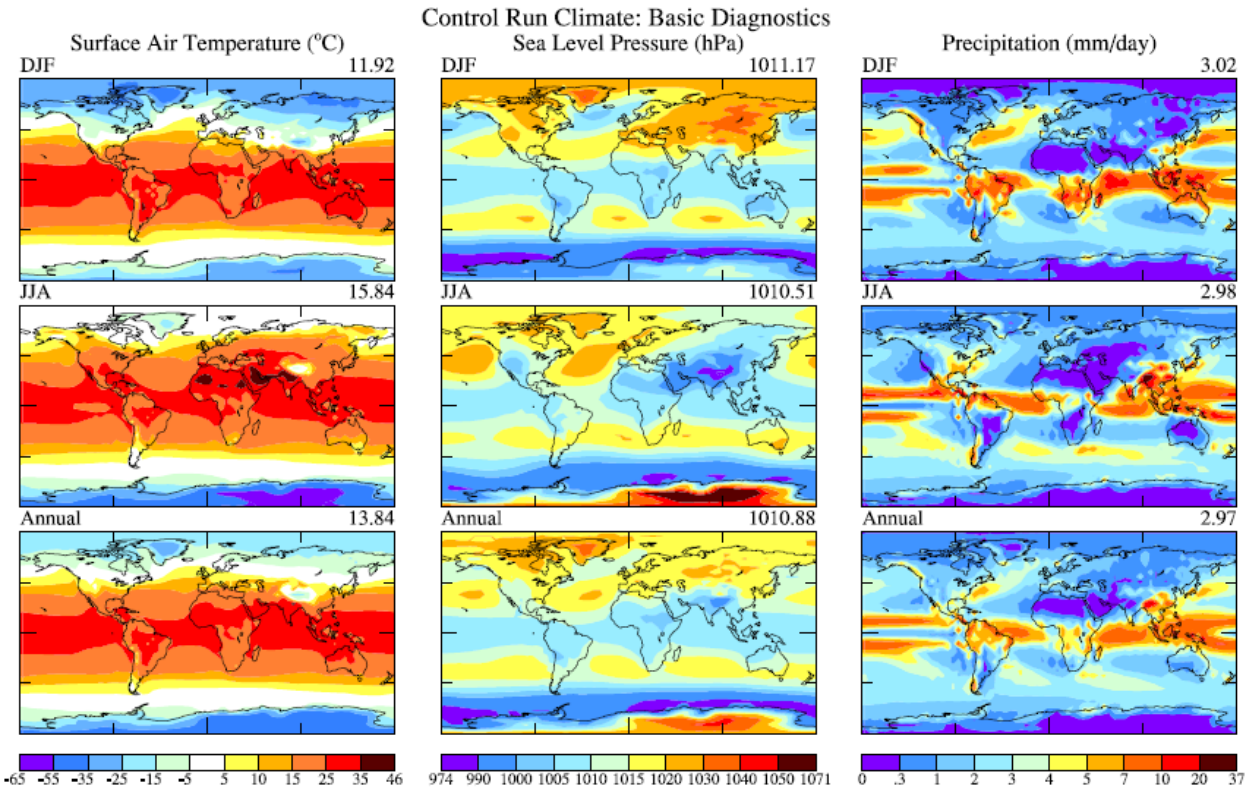


**Fig. S3.** Surface air temperature (left), sea level pressure (center) and precipitation (right) in Dec-Jan-Feb (upper row), JJA (middle row) and annual mean (lower row) in the climate model control run.

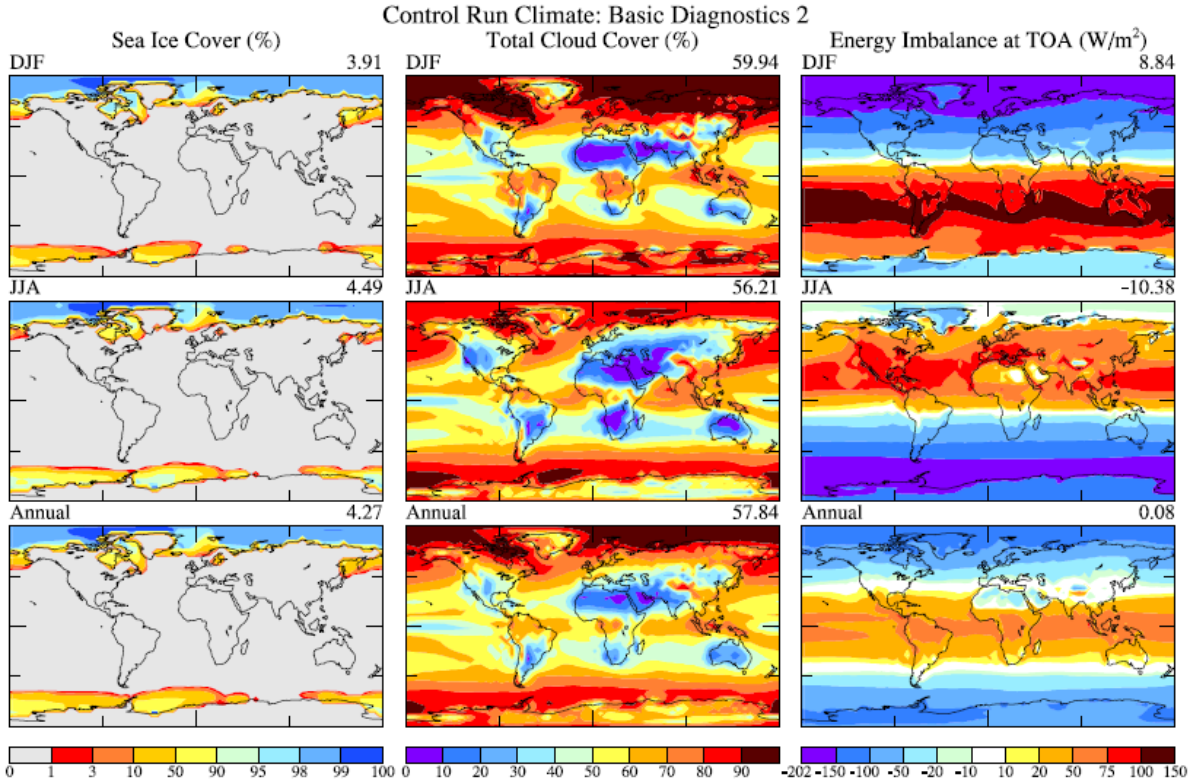


**Fig. S4.** Sea ice cover (left), cloud cover (center) and top of atmosphere energy imbalance (right) in Dec-Jan-Feb (upper row), JJA (middle row) and annual mean (lower row) in climate model control run.

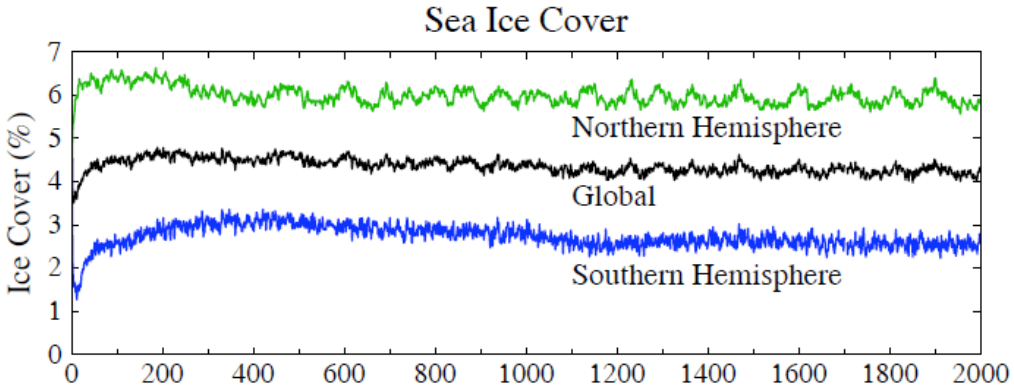


**Fig. S5.** Hemispheric and global sea ice versus time in the control run.

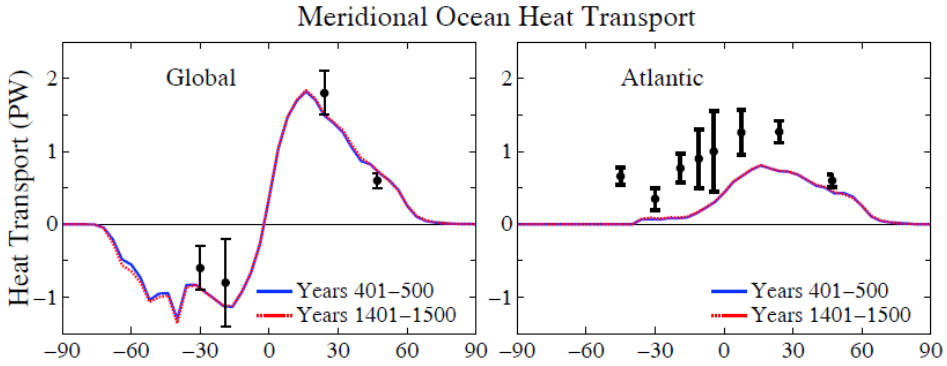


**Fig. S6.** Poleward transport of heat by the ocean in 5th and 15th centuries of the control run. Observational estimates (black dots with error bars) are from Ganachaud and Wunsch (2003).

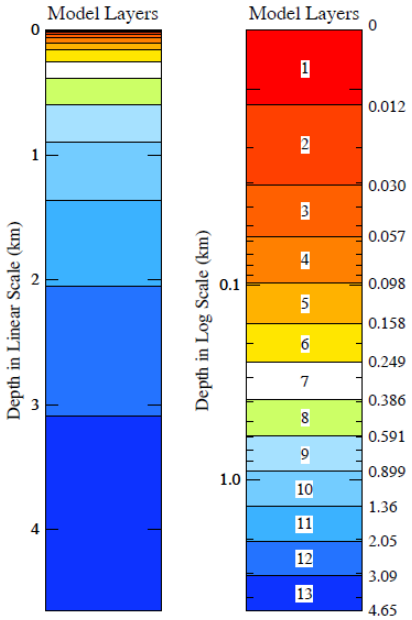


**Fig. S7.** Layer depths in ocean model.

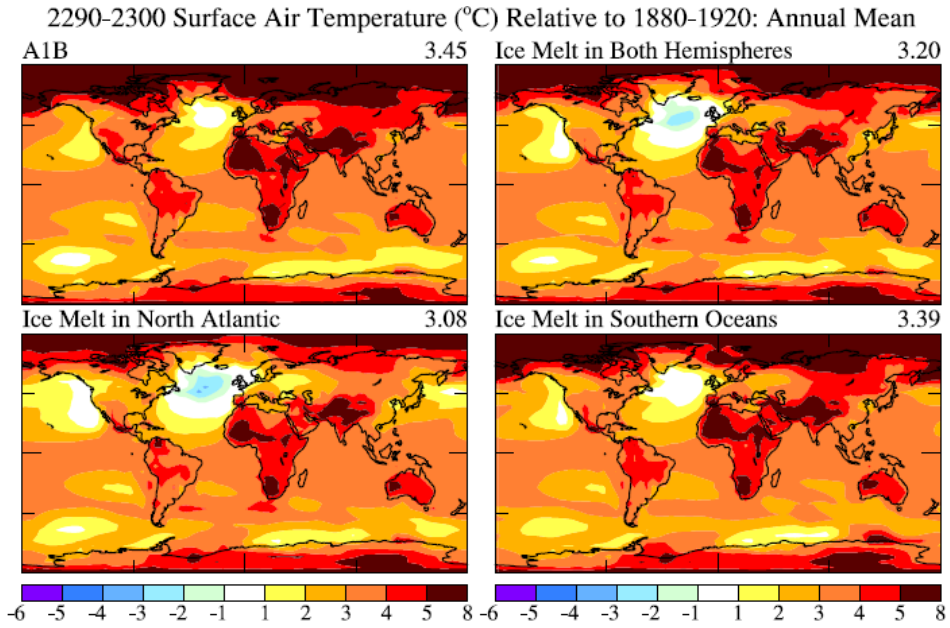


**Fig. S8.** Surface air temperature change relative to 1880-1920 in 2290-2300 for the four climate forcing scenarios shown in Fig. 11.

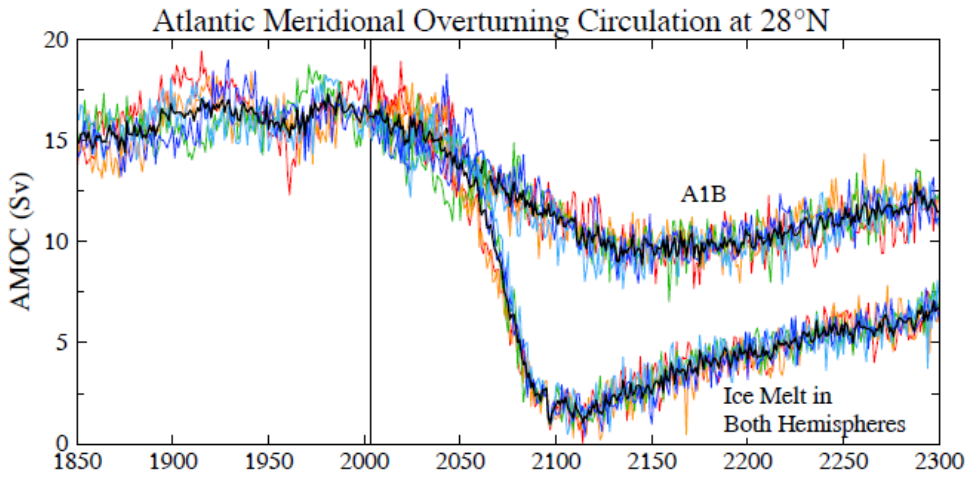


**Fig. S9.** AMOC strength at 28N in five ensemble members and their mean (heavy black line) for the A1B GHG scenario and for that scenario plus ice melt in both hemispheres with 10-year doubling time reaching a maximum 5 m contribution to sea level.

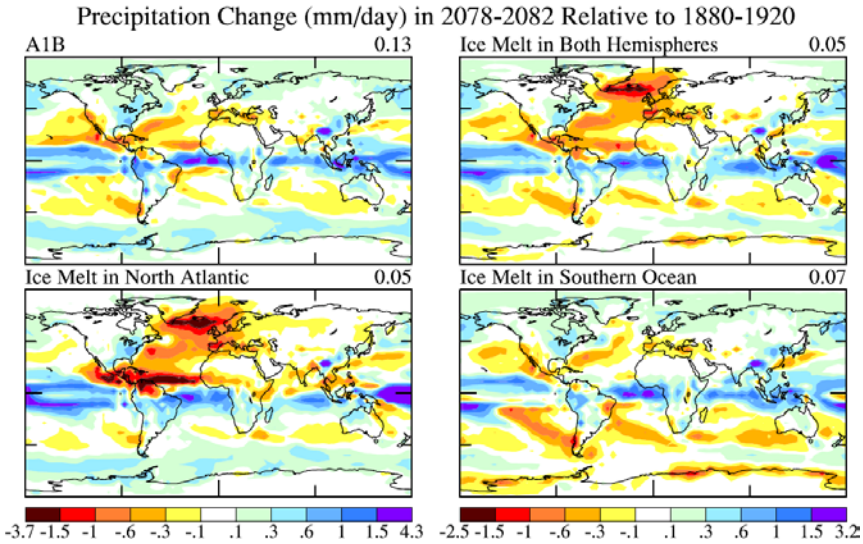


**Fig. S10.** Precipitation change in 2078-2082 for the same four scenarios as in Figs. 9 and 11.

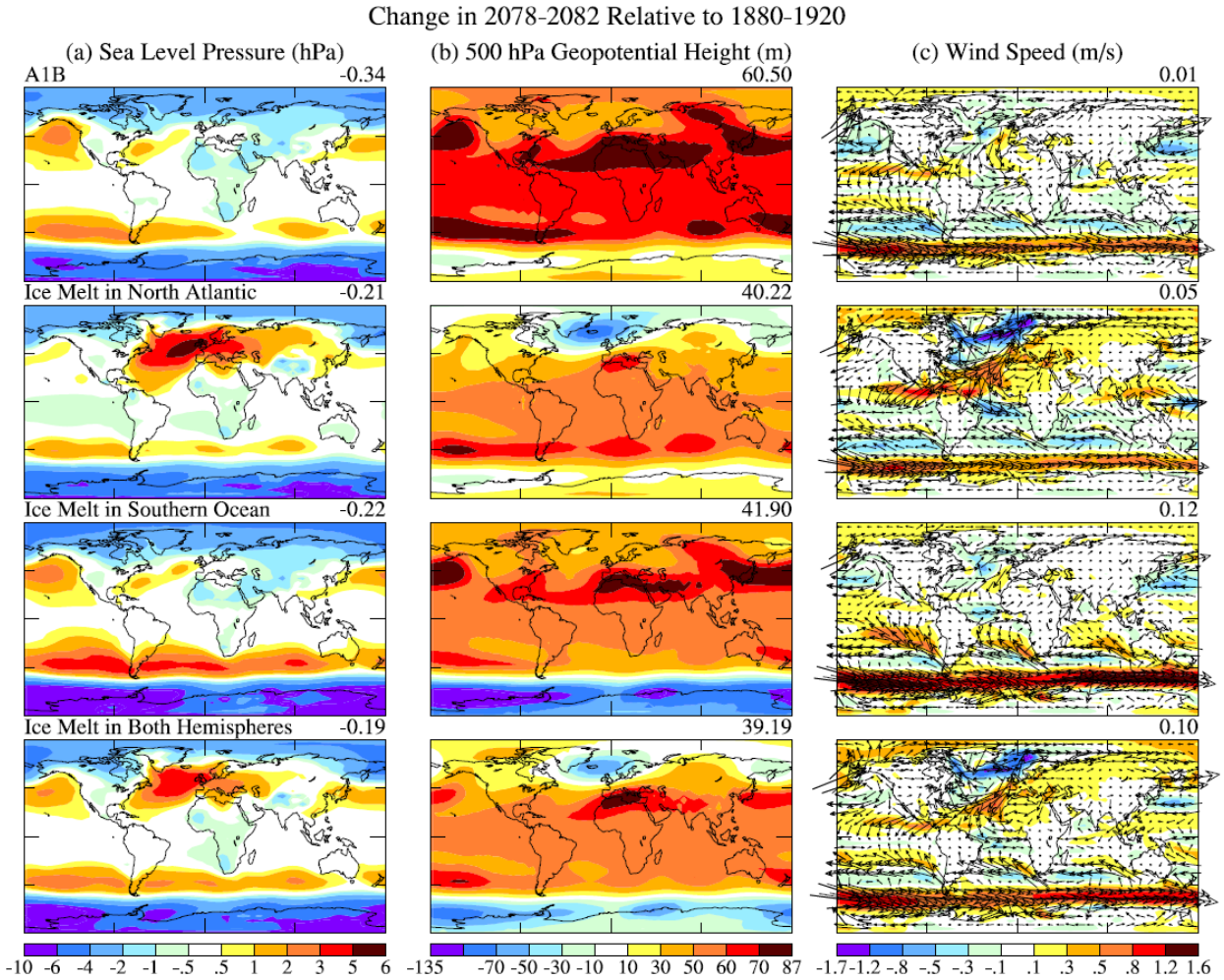


**Fig. S11.** Change in 2078-2082, relative to 1880-1920, of the annual mean **(a)** sea level pressure, **(b)** 500 hPa geopotential height, and **(c)** wind speed, for the same four scenarios as in Fig. 9.

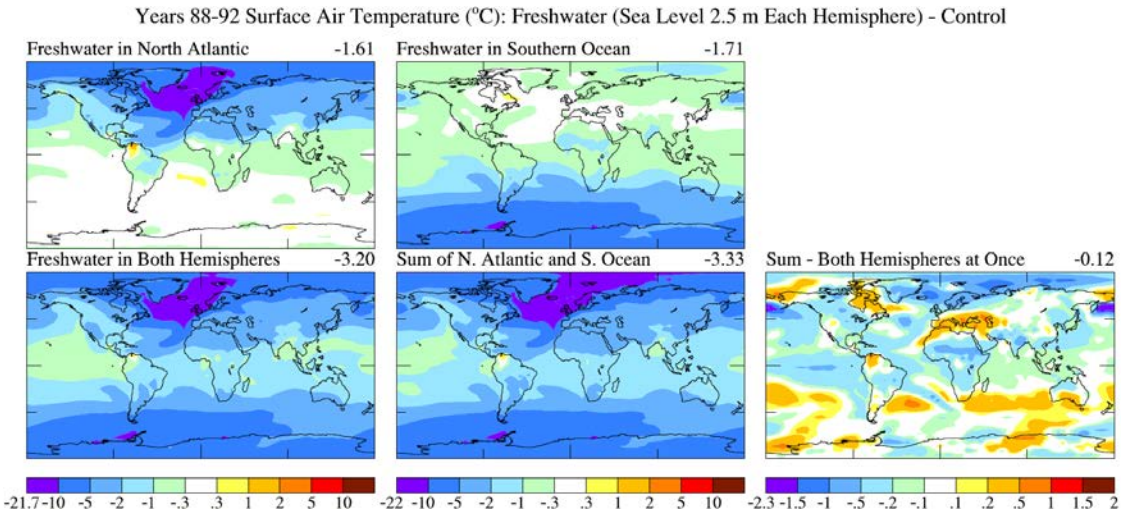


**Fig. S12.** Surface air temperature change in pure freshwater experiments at time of peak cooling (years 88-92) in three experiments with 2.5 m freshwater in each hemisphere. The sum of responses to the hemispheric forcings is compared with the response to forcing in both hemispheres in the bottom row.

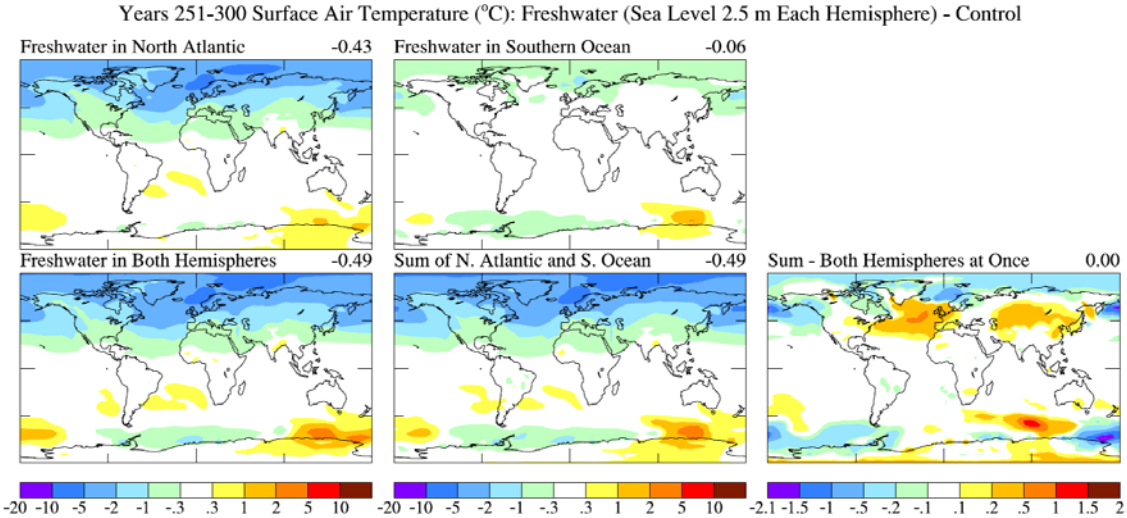


**Fig. S13.** Same as Fig. S12, but for years 251-300.

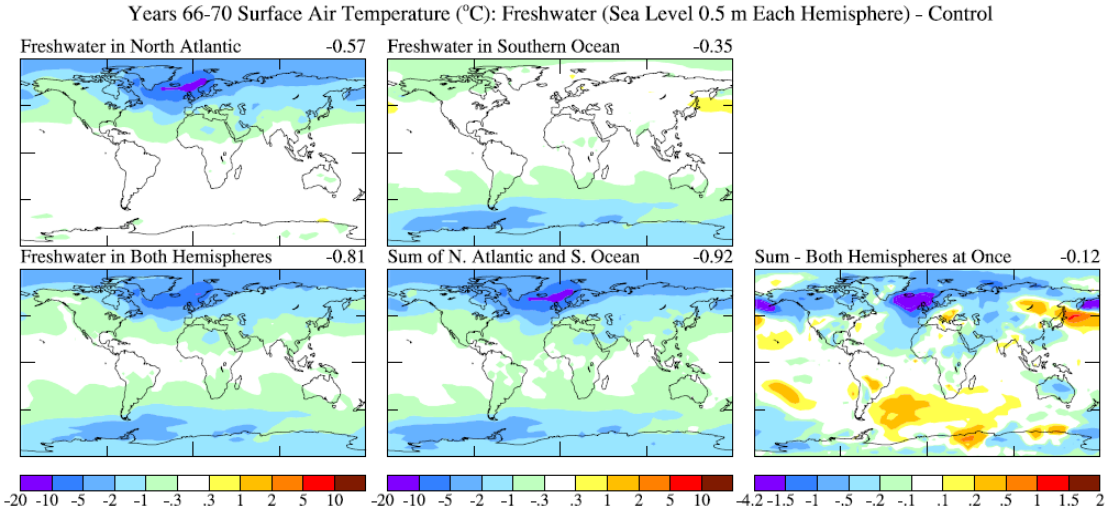


**Fig. S14.** Same as Fig. S12, but for hemispheric freshwater inputs of 0.5 m at years 66-70.

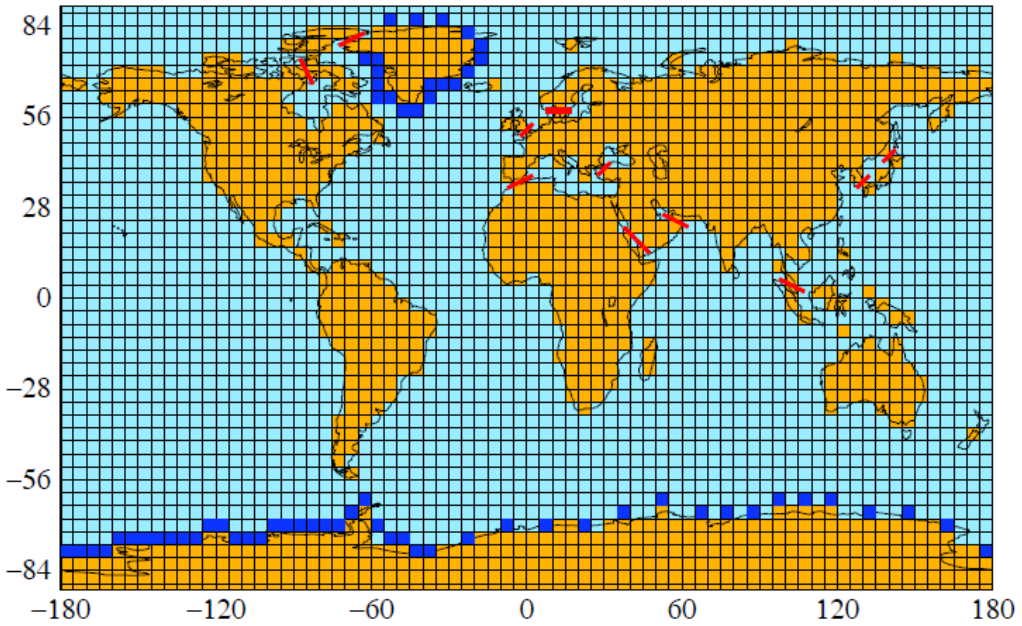


**Fig. S15.** Climate model grid. Dark blue gridoxes are locations of freshwater insertion. Red lines mark the 12 straights connecting ocean gridboxes.

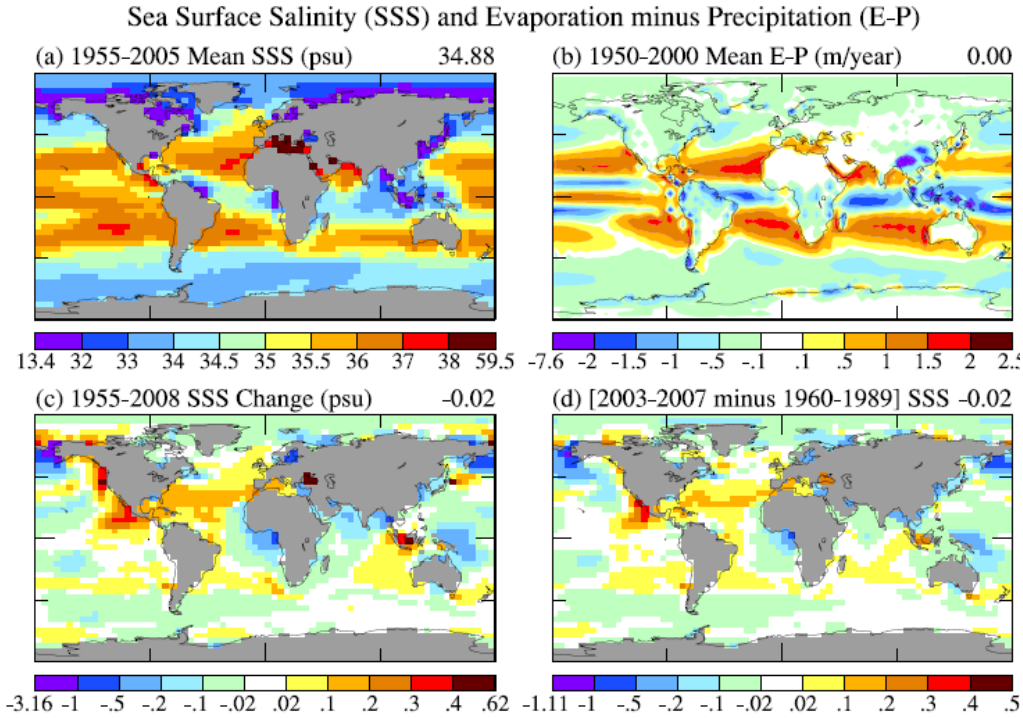


**Fig. S16.** Simulated sea surface salinity (a), evaporation minus precipitation (b), and change of salinity (c, d), the periods being chosen to allow comparison with observations, as discussed in the text.

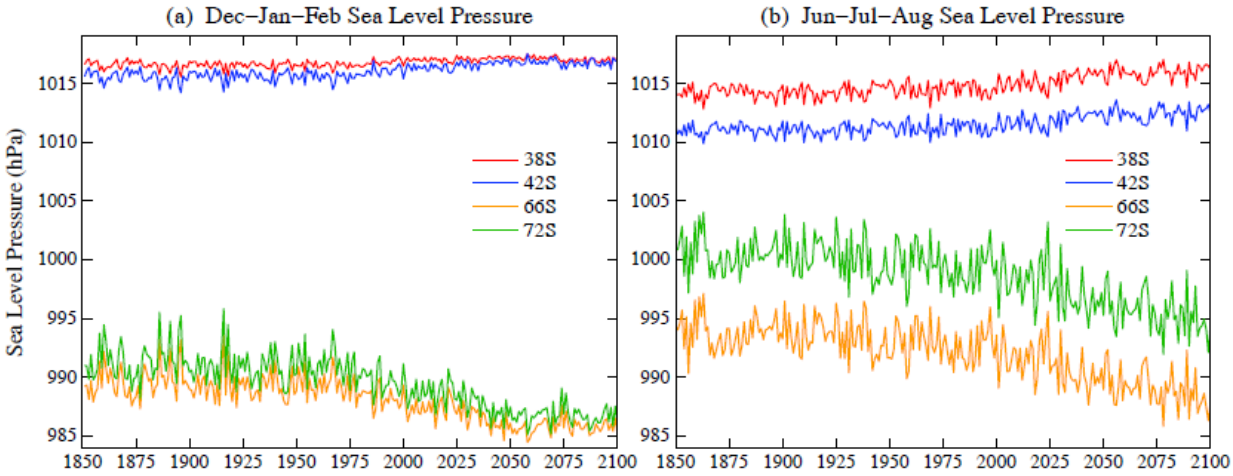


**Fig. S17.** Sea level pressure at four latitudes in (a) Dec-Jan-Feb and (b) Jun-Jul-Aug. The model is driven by the "modified" forcings that include ice melt reaching the equivalent of 1 m sea level by mid-century.

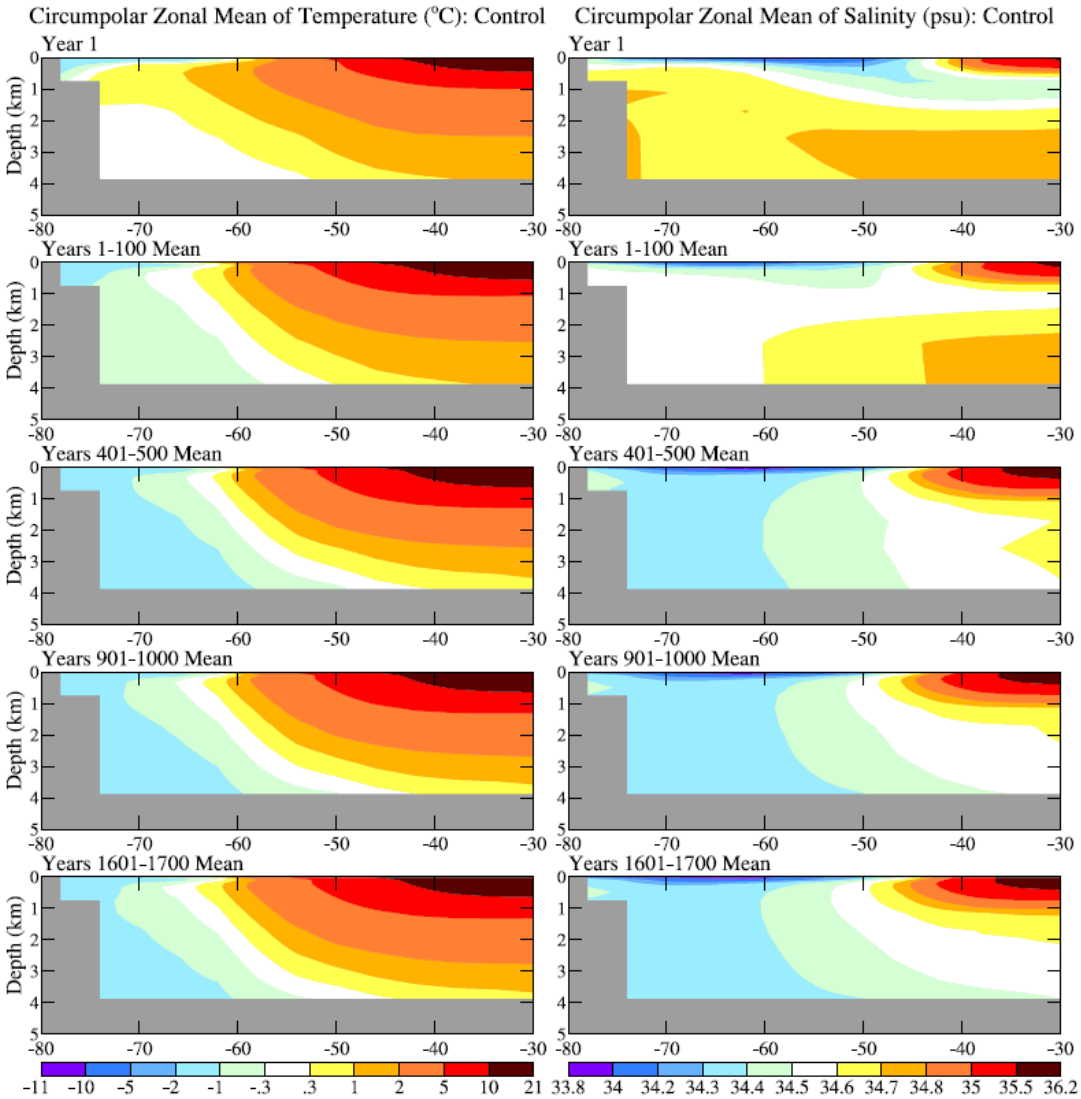


**Fig. S18.** Ocean temperature and salinity in the control run.

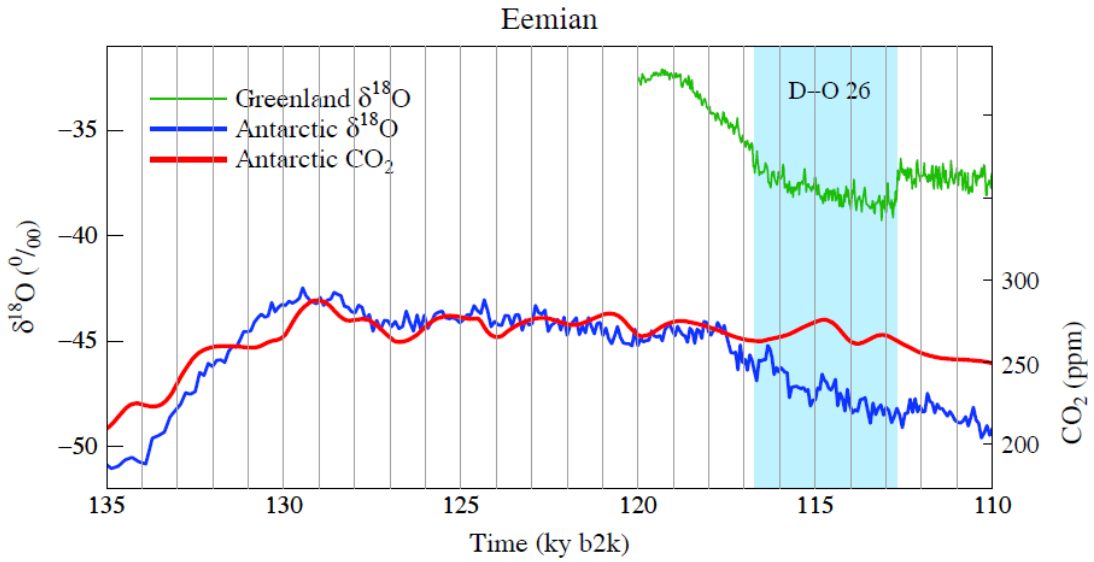


**Fig. S19.** Expansion of data from Fig. 24b,c. $CO_2$ increases during D-O 26 lag Antarctic temperature rises by 1500-2000 years.

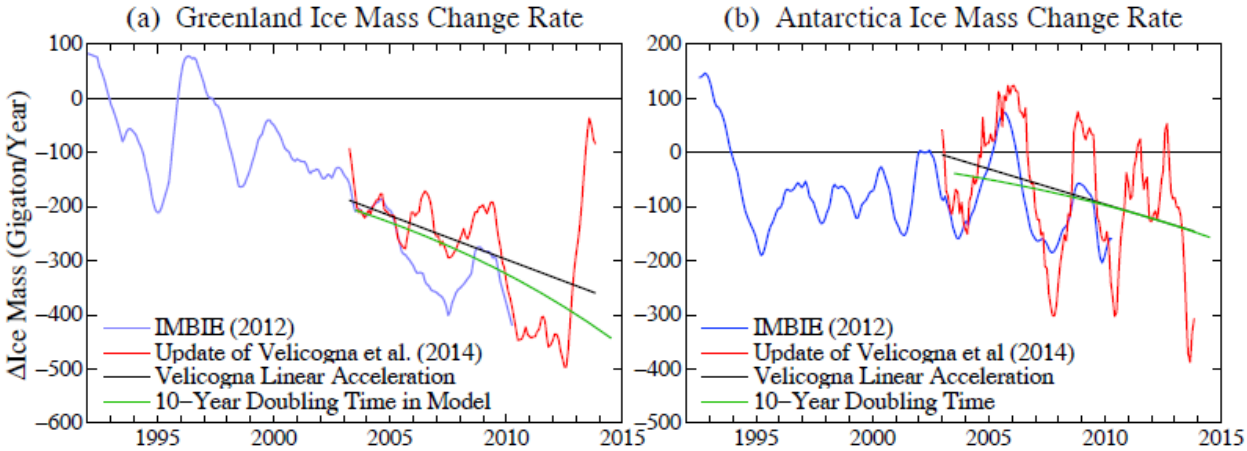


**Fig. S20.** Greenland and Antarctic ice mass change rates. Data from Velicogna et al. (2014) Shepherd et al. (2012), and http://imbie.org/ (IMBIE = Ice Sheet Mass Balance Inter-comparison Exercise).

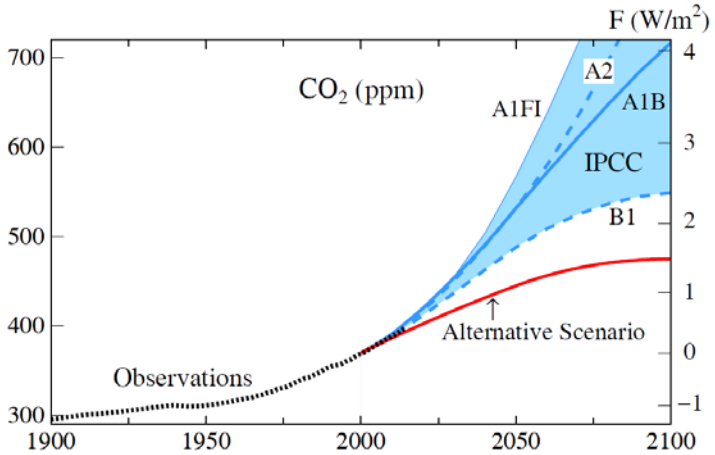


**Fig. S21.** Observed $CO_2$ amount and scenarios for the 21st century (update of Hansen et al., 2007c). The "Alternative Scenario" has peak $CO_2$ 475 ppm in 2100, when global warming reaches 1.6°C relative to 1880-1920.

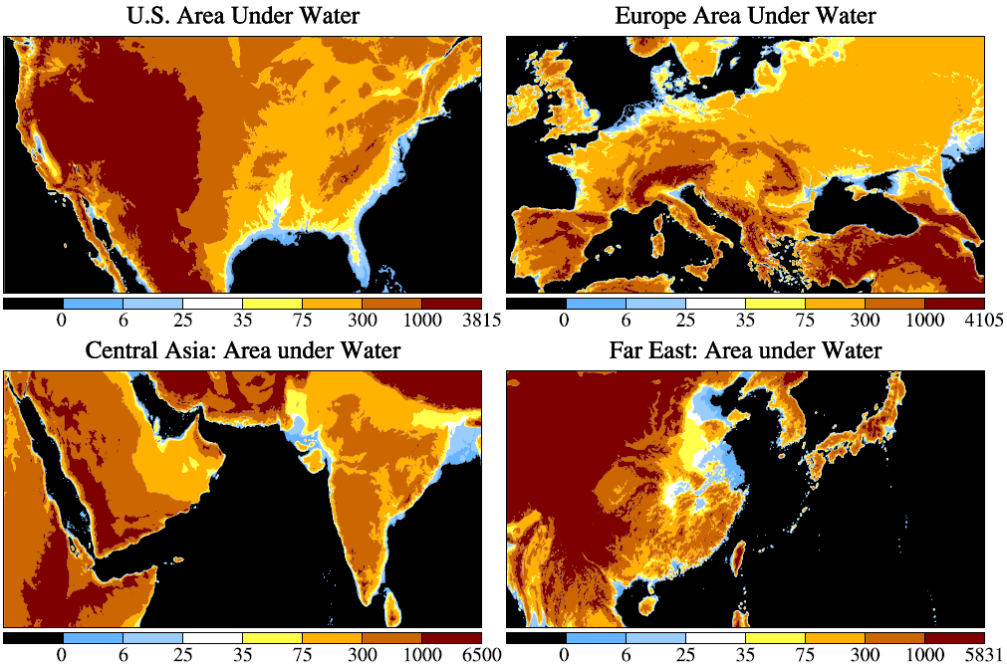


**Fig. S22.** Areas (light and dark blue) that nominally would be under water for 6 and 25 m sea level rise.

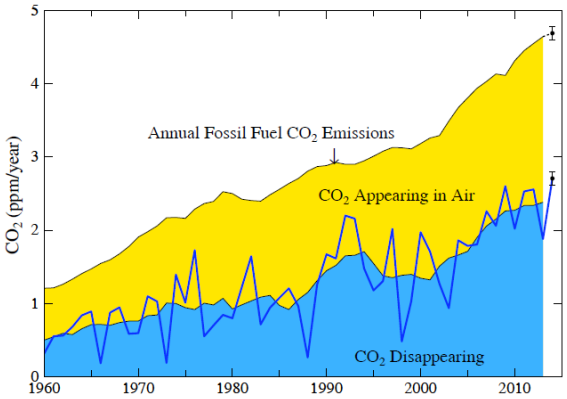


**Fig. S23.** Global fossil fuel $CO_2$ emissions (top curve). Measured $CO_2$ increase in air is the yellow area. The 7-year mean of $CO_2$ going into the ocean, soil and biosphere is blue (5- and 3-year means at the end; dark blue line is annual). 2014 global emissions estimate as 101% ±2% of 2013 emissions. $CO_2$ emissions from Boden et al. (2013) and atmospheric $CO_2$ from P. Tans (www.esrl.noaa.gov/gmd/ccgg/trends) and R. Keeling (www.scrippsco2.ucsd.edu/).

**References**

Boden, T.A., Marland, G., and Andres, R.J.: Global, regional, and national fossil-fuel $CO_2$ emissions, Carbon Dioxide Information Analysis Center, Oak Ridge National Laboratory, U.S. Department of Energy, Oak Ridge, Tenn., USA, doi 10.3334/CDIAC/00001_V2012, 2012.

Ganachaud, A., and Wunsch, C.: Large-scale ocean heat and freshwater transports during the World Ocean Circulation Experiment, J. Clim., 16, 696-705, 2003.

Seierstad, I.K., Abbott, P.M., Bigler, M., Blunier, T., Bourne, A.J., Brook, E., Buchardt, S.L., Buizert, C., Clausen, H.B., Cook, E., Dahl-Jensen, D., Davies, S.M., Guillevic, M., Johnson, S.J., Pedersen, D.S., Popp, T.J., Rasmussen, S.O., Severinghaus, J.P., Svensson, A., Vinther, B.M.: Consistently dated records from the Greenland GRIP, GISP2 and NGRIP ice cores for the past 104 ka reveal regional millennial-scale $\delta^{18}O$ gradients with possible Heinrich event imprint, Quatern. Sci. Rev., 106, 29-46, 2014.